Probabilistic analysis of slope stability in spatially variable soils using Monte Carlo simulation

by

Bo Han

in partial fulfillment of the requirements for the degree of

Master of Science
in Civil Engineering and Geosciences
at the Delft University of Technology,

Supervisor:	Dr. ir. A. P. (Bram) van den Eijnden,	TU Delft
Thesis committee:	Prof. dr. M. A. Hicks,	TU Delft
	Dr. ir. R. C. (Robert) Lanzafame,	TU Delft

Acknowledgment

As the author, I like to sincerely express my thanks to my supervisor Dr. Bram van den Eijnden. It's a great honor to get such an interesting subject and work with him. He would stop whatever he was doing when I walked into his office and discuss the progress with me. His feedback helped me a lot when things were not going so well. Also, I would like to express my sincere gratitude to Prof. Michael Hicks and Dr. Robert Lanzafame for their productive feedback during the meetings we had. Especially during the special quarantine period, I cannot complete this study without all of your help and support.

Furthermore I would like to thank my family and friends. My parents supported me during my years as a student. In the past two years, thanks to my classmates for helping me with my studies. Thanks to my roommates for helping me in life. You are my priceless treasure. My gratitude is beyond words. I will not forget our good memories in Stieltjesweg 28.

Bo Han
February 2021

Abstract

Soil properties are spatially variable due to the natural deposition process. Because of this inherent spatial variability, a slope can actually fail along any potential slip surface. A single value of Factor of safety cannot account for this variation dominated the slope stability problem. Probabilistic analysis considering the spatial variability is a reasonable method to quantify the risk of the slope stability problem. Thus, in order to better simulate this variation, the theory of random field has been widely used in the slope stability problem. However, statistical outcomes derived from the probabilistic analysis will be influenced by how the random fields are generated and how the random field values are assigned to each potential slip surface. In order to investigate the extent of this influence, this study proposed a new probabilistic slope stability analysis method and compared it with the other two methods in terms of accuracy and efficiency.

In this report, three different probabilistic slope stability analysis methods are presented. These methods combined the traditional limit equilibrium method of slices with random fields, which can account for the inherent spatial variability of soil properties. An exponential decaying function is used to describe the correlation structure of this spatial variation. This correlation structure is further expressed by the form of covariance matrix. Since the covariance matrix is a symmetric positive definite matrix, Cholesky decomposition is used to decompose it into the product of two triangular matrices. Because the triangular matrix is more computationally efficient, the two-dimensional random field is generated by multiplying a normal random number vector with the lower triangular matrix derived from Cholesky decomposition.

The main feature of the new proposed probabilistic LEM method in this study is the adoption of linear interpolation in the procedure of random field generation. For convenience' sake, it will be named as 'Random Field - Monte Carlo Simulation method (RF-MCS method)'. Two other MCS methods are also implemented in this study. Since the random field values are directly assigned onto each potential slip circle, they will be named as 'direct Monte Carlo Simulation method (direct MCS method)'. The difference between these two direct MCS methods lies in the normal random number generation for different variables when generate the random fields. Then, Monte Carlo simulation is used to determine the statistical outcomes according to the generated random fields from these different methods.

In this study, two types of slopes were analysed using three MCS methods: undrained slope with only cohesion and c-ϕ slope. The search algorithm ensures that the critical slip circle is selected during the analysis. The system probability of failure considering all potential slip circles is compared with the corresponding probability of failure with respect to the "fixed" critical deterministic slip circle. The differences in the results calculated by the three MCS methods were investigated. The main reason for the difference in the probability of failure P_f from three MCS methods was found out to be the methodology used by the proposed RF-MCS method and direct MCS method to calculate the system probability of failure. This difference implies that how the random fields are generated and how the random

field values are assigned to each potential slip surface can significantly influence the statistical outcomes.

For all three methods, the influences of slope inclination, autocorrelation distance, coefficient variation of strength parameters and cross correlation between strength parameters on the system probability of failure have been investigated by a wide range of parametric studies. In different test scenarios, the results of the RF-MCS method and the direct MCS method shows the same growth trend while large difference still exist. The results indicate sensitivity analysis has nothing to do with using different methods and a combination of three methods is more efficient for future parameter studies.

Key words: slope stability, probabilistic analysis, limit equilibrium method, random fields, spatial variability, Cholesky decomposition, Monte Carlo simulation, system probability of failure

Contents

1 Introduction 1
- 1.1 General . . . 1
- 1.2 Problem definition . . . 1
- 1.3 Research questions . . . 4
- 1.4 Research outline . . . 4

2 Literature review 7
- 2.1 Method of slices . . . 7
  - 2.1.1 Fellenius method . . . 8
  - 2.1.2 Bishop method . . . 9
  - 2.1.3 Spencer method . . . 9
  - 2.1.4 Taylor's analytical method . . . 11
- 2.2 Uncertainty . . . 11
  - 2.2.1 Sources of uncertainty . . . 12
  - 2.2.2 Modeling inherent soil variability . . . 12
  - 2.2.3 Theory of random fields . . . 13
  - 2.2.4 Discretization of random fields . . . 17
- 2.3 Probabilistic analysis methods . . . 19
  - 2.3.1 Monte Carlo simulation . . . 19
- 2.4 System probability of failure . . . 20
- 2.5 Summary . . . 21

3 Probabilistic LEM development and verification 23
- 3.1 Deterministic model . . . 23
  - 3.1.1 Benchmark deterministic analysis 1: a undrained clay slope ($\phi = 0$) . . . 23
  - 3.1.2 Benchmark deterministic analysis 2: a c-ϕ slope . . . 25
- 3.2 Probabilistic model . . . 25
  - 3.2.1 Correlation structure of 2D random field . . . 25
  - 3.2.2 Correlation between different random variables . . . 27
  - 3.2.3 Random field generation for RF-MCS method . . . 28
  - 3.2.4 Estimation of the midpoint value at each slice base . . . 29
  - 3.2.5 Random field generation for direct MCS method . . . 31
- 3.3 Implementation procedure of 3 different methods . . . 31
- 3.4 Benchmark analysis 1: a undrained clay slope ($\phi = 0$) . . . 34
  - 3.4.1 Initial input information . . . 34
  - 3.4.2 Pre-analysis . . . 35
  - 3.4.3 Analysis and results . . . 36
- 3.5 Benchmark analysis 2: a c-ϕ slope . . . 38
  - 3.5.1 Initial input information . . . 38
  - 3.5.2 Pre-analysis . . . 38
  - 3.5.3 Analysis and results . . . 39
- 3.6 Discussion . . . 42

3.7 Summary . . . 42

4 Comparison of 3 different Monte Carlo methods 43
4.1 Comparison based on a undrained clay slope ($\phi = 0$) . . . 43
4.1.1 Initial input information . . . 43
4.1.2 Analysis and results . . . 43
4.2 Comparison based on a c-ϕ slope . . . 48
4.2.1 Initial input information . . . 48
4.2.2 Analysis and results . . . 48
4.3 Discussion . . . 52
4.4 Summary . . . 52

5 Parametric study of 3 different Monte Carlo methods 55
5.1 Study based on a undrained clay slope ($\phi = 0$) . . . 55
5.1.1 Pre-analysis . . . 56
5.1.2 Influence of slope angle . . . 56
5.1.3 Influence of autocorrelation distance . . . 57
5.1.4 Influence of coefficient of variation of strength parameters . . . 59
5.2 Study based on a c-ϕ slope . . . 59
5.2.1 Pre-analysis . . . 61
5.2.2 Influence of slope angle . . . 61
5.2.3 Influence of autocorrelation distance . . . 62
5.2.4 Influence of coefficient of variation of strength parameters . . . 63
5.2.5 Influence of correlation coefficient . . . 64
5.3 Discussion . . . 65
5.4 Summary . . . 65

6 Conclusions and recommendations 67
6.1 Conclusions . . . 67
6.2 Recommendations . . . 68

Bibliography 71

A Appendix 73

List of Symbols

Symbol	Name	[Unit]
P_f	Probability of failure	[-]
β	Reliability index	[-]
FS	Factor of Safety	[-]
FS_{min}	Minimum of Factor of Safety	[-]
μ	Mean	[-]
σ	Standard deviation	[-]
c	Cohesion	[kPa]
ϕ	Friction angle	[°]
γ	Unit weight	[kN/m^3]
β^*	Slope angle	[°]
$\rho_{c\phi}$	Correlation coefficient between c and ϕ	[-]
θ_h	Horizontal autocorrelation distance	[m]
θ_v	Vertical autocorrelation distance	[m]
COV	Coefficient of Variation	[-]
$\mu_{FS_{min}}$	Mean of Factor of Safety	[-]
$\sigma_{FS_{min}}$	Standard deviation of Factor of Safety	[-]
$COV_{FS_{min}}$	Coefficient of Variation of Factor of Safety	[-]
$\vec{\chi}$	Spatial coordinate vector	[-]
$Z(\vec{\chi})$	Standard normal random field	[-]
$H(\vec{\chi})$	Lognormal stationary random field	[-]
$\Psi(.)$	Lognormal transformation function	[-]
μ_{ln}	Mean of logarithm	[-]
σ_{ln}	Standard deviation of logarithm	[-]
Ω	Domain	[-]
COV_X	Coefficient of Variation of random variable X	[-]
Δx	Absolute distance on the horizontal direction	[m]
Δy	Absolute distance on the vertical direction	[m]
$R_{c\phi}$	Correlation matrix between c and ϕ	[-]
$\left[.\right]_{corr.}$	Correlated matrix	[-]
$\left[.\right]_{uncorr.}$	Uncorrelated matrix	[-]
$Chol.$	Cholesky decomposition	[-]
x_{ci}	Horizontal coordinate of the center of slip circle	[m]
y_{ci}	Vertical coordinate of the center of slip circle	[m]
R_i	Radius of slip circle	[m]
$FS_{min,i}$	Minimum of Factor of Safety for realisation i	[-]
N_t	Total number of realisations	[-]
N_f	Number of failure realisations	[-]
$N_{f,i}$	A failure realisation i	[-]
N_p	Number of potential slip circles	[-]
$\boldsymbol{\xi}$	Standard normal random number column vector	[-]

List of Abbreviations

LEM	Limit Equilibrium Method
FEM	Finite-Element Method
FOSM	First-Order Second-Moment Method
FORM	First-Order Reliability Method
MCS	Monte-Carlo Simulation
RFEM	Random Finite-Element Method
RLEM	Random Limit Equilibrium Method
RF-MCS	Random Field-Monte Carlo Simulation
DS-MCS	Direct and Separate-Monte Carlo Simulation
DC-MCS	Direct and Combined-Monte Carlo Simulation
CPU	Central Processing Unit
RAM	Random-Access Memory

Chapter 1

Introduction

1.1 General

As one of the most important issues in the geotechnical engineering, slope stability problem have been widely studied. In the past few decades, various methods have been developed to better analyze this problem. Generally, it can be divided into two different approaches, deterministic and probabilistic analysis. The Limit equilibrium method (LEM) is usually used in the analysis of slope stability problem in the deterministic approach. LEM assumes the sliding surface is circular. It divides the sliding soil mass into multiple vertical slices, and then calculates the factor of safety, FS, which is the ratio of the resisting shear strength to the driving mass load. The circle giving the minimum factor of safety FS_{min} is regarded as the critical deterministic slip surface. Various LEM methods (invented by Bishop, Fellenius, Taylor, Spencer, Janbu, etc.) differ under different assumptions used to render the problem determinate. None of these approximate methods are exact and the result factor of safety FS should be handled with care.

However, it has been widely accepted that a single value of factor of safety FS is somewhat conservative and cannot account for the uncertainties dominated in the geotechnical engineering problems. Therefore, probabilistic slope stability analysis is a better approach which can take account of the uncertainties of soil properties. It calculates the probability of failure P_f, which is considered to be a more reasonable method to quantify the risk of the slope stability problem. In the field of probabilistic analysis, two different approaches, finite-element method (FEM) and LEM, are usually adopted to investigate the slope stability problem. For each approach, several methods have been developed in recent decades. They differ in different assumptions and the ability to deal with complex problems. Generally, it can be divided into four categories: Level I methods (semi-probabilistic design), Level II methods (approximation: first-order second-moment method (FOSM), first-order reliability method (FORM)), Level III methods (numerical integration or Monte-Carlo simulation method (MCS)), Level IV methods (risk-based) (Jonkman et al., 2015). In probabilistic analysis approach, the governing parameters of the soil properties are modeled as random variables which are defined by certain kinds of probability distribution. This study mainly focuses on investigating the slope stability problem in a probabilistic approach.

1.2 Problem definition

How to locate the most critical slip surface that gives the minimum factor of safety FS_{min} is one of the essential issues in the slope stability problem.

Because of the inherent spatial variability of the soil properties that result from the natural deposition process, the slope can actually fail along any potential slip surface. Thus, the slope stability problem can be treated as a system failure that consist of a multitude of failure mechanisms. The overall probability of failure of the slope will depend on the probability of failure concerning each individual failure mechanisms (Chowdhury and Xu, 1995).

There is correlation between each potential slip surface because the slope was analyzed by the same probabilistic analysis method and the same input information for different variables (same mean value, standard deviation and same type of distribution, etc). However, it is difficult to determine the accurate system probability of failure of a slope. Therefore, the probability of failure from the most critical slip surface is considered as a reasonable estimate of the system probability of failure of a slope.

One approach that has been taken by some authors is to perform the deterministic analysis first and locate the critical slip surface. And then carry out probabilistic LEM analysis using the same surface to calculate the probability of failure. However, (Hassan and Wolff, 1999) proved that the critical slip surfaces selected by the deterministic LEM and probabilistic LEM analysis are not always consistent. Similar findings are also reported by (Cho, 2009): the probability of failure calculated using the deterministic critical slip surface are close to the system probability of failure only when the correlation between the limit state function of slip surfaces are very high.

Due to the inherent spatial variability of soil properties, the strength of soil even change within a homogeneous soil layer. However, the mean and standard deviation of the point to point variable cannot accurately characterise this variation. Thus, the theory of random field has been taken into the slope stability problem in order to better model this variation. And it has been commonly used in many recent investigations: ((El-Ramly et al., 2002); (Griffiths and Fenton, 2004); (Low et al., 2007); (Cho, 2007); (Griffiths, Huang, et al., 2009); (Cho, 2009); (Ji et al., 2012); (D.-Q. Li et al., 2014); (Javankhoshdel and Bathurst, 2014); (Javankhoshdel, Luo, et al., 2017)). Figure 1.1 shows the probabilistic slope analysis methods considering spatial variation.

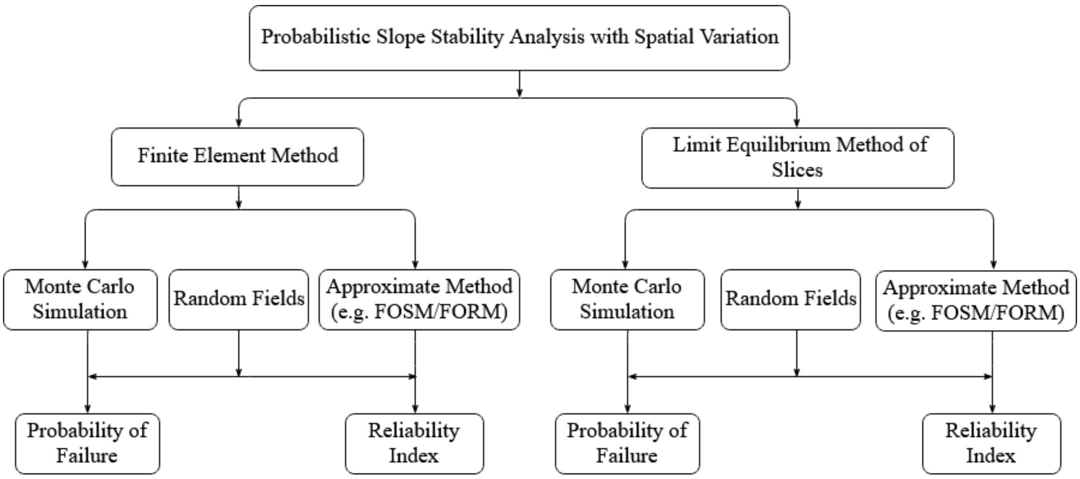

FIGURE 1.1: Probabilistic slope analysis methods considering spatial variation (Modified from (Ji et al., 2012))

(El-Ramly et al., 2002) modeled the inherent soil variability as 1D random fields along the predetermined slip surface. Results from the probabilistic slope analysis showed the probability of failure will be significantly overestimated if the effect of this variation was neglected.

(Griffiths and Fenton, 2004) chosen to use the random finite-element method (RFEM) to perform the probabilistic analysis. Unlike probabilistic LEM analysis, the shape of the critical failure surface is not a perfect circle and the location is not determined beforehand as well. The most critical failure mechanism is searched by the method of strength reduction, which is considered to be more realistic compared with probabilistic LEM method. However, the major drawback of the RFEM is the excessive computational efforts. Because the factor of safety calculated by the strength reduction method is to continuously increase the shear strength to render a limit equilibrium of the slope.

(Low et al., 2007) developed an intuitive spreadsheet model taking account of the spatial variability. The Hasofer–Lind reliability index was calculated by FORM. However, this method cannot work under some extreme conditions and the spatial variability is only modeled along the vertical direction.

(Cho, 2007) performed the probabilistic analysis by adopting the "midpoint method" to discretize the 2D random field combined with MCS. Distribution of the factor of safety has been generated after many times simulations. Results showed that the standard deviation of the factor of safety has been strongly influenced by the spatial variation rather than the mean value of the factor of safety. It also has been found that the skewness of the probability density function of the factor of safety has been affected by varying the horizontal scale of fluctuation.

(Griffiths, Huang, et al., 2009) investigated the influence of slope inclination and correlation coefficient between soil strength parameters using RFEM. Some useful plots are generated by a wide range of parametric studies provided investigators a criterion to decide whether ignoring spatial variation is appropriate for certain soil parameters.

(Cho, 2009) showed the existence of various failure mechanisms of a slope in the process of probabilistic analysis by combining random fields with LEM. Two types of MCS have been performed in the study. One is to calculate the system probability of failure using the search algorithm. The other one only analyze the critical slip surface located by the deterministic analysis and use the probability of failure of this specific surface as the system probability of failure. Results have shown that the difference between these 2 MCS approach are large when there is low correlation between the limit state function of each potential slip surface. Correlation coefficient between different soil parameters also investigated in this study. The probability of failure has a negative relationship with the correlation coefficient between c and ϕ.

(Ji et al., 2012) introduced the concept of interpolated autocorrelation without the limitation of the LEM framework. Results agreed well with the widely used vertical slice discretization of the 2D random field. The finding, the vertical spatial variation has a much more stronger influence on the probability of failure than the horizontal spatial variation, was also verified by this study.

(D.-Q. Li et al., 2014) considered the spatial variability in c and ϕ that increased linearly with depth. (Javankhoshdel and Bathurst, 2014) adopted simple soil conditions to perform a set of probabilistic LEM analysis. Lots of design charts have been generated which can serve as a upper-bound estimate of the factor of safety and the probability of failure. (Javankhoshdel, Luo, et al., 2017) performed probabilistic analysis to compared the results of random limit equilibrium methods (RLEM) under 1D and 2D conditions with the 2D RFEM.

(Cao et al., 2017) carried out direct MCS using the Excel sheet. The results have been compared with those from other commonly used probabilistic analysis methods. For example, FOSM, FORM and commercial software Slope/W, etc. It has been found different analysis methods result in quite different results.

Previous studies have demonstrated the importance of the spatial variability of soil properties. This study aims at combining the limit equilibrium method of slices (LEM) with the random fields which characterize the spatial variability and analyze the slope stability problem in a probabilistic approach.

1.3 Research questions

A new probabilistic LEM method is proposed in this study. Linear interpolation is adopted in the procedure of random field generation. For convenience' sake, it will be named as 'Random Field - Monte Carlo Simulation method (RF-MCS method)'. Two other MCS methods are also implemented in this study. Since the random field values are directly applied on each potential slip circle, they will be named as 'direct Monte Carlo Simulation method (direct MCS method)'. The difference between these two direct MCS methods lies in the random number generation for different variables during the process of Cholesky decomposition.

For example, the strength parameter, cohesion c and friction angle ϕ. For the first direct MCS method, two n-entry vectors of standard normal random numbers for c and ϕ are generated separately by standard normal sampling with $\mu = 0$, $\sigma = 1$. For the other direct MCS method, a $2 * n$-entry vector of standard normal random numbers is generated first. Then, c samples the former n-entries and ϕ samples the latter n-entries. Therefore, the first direct MCS method will be named as Direct and Separate-Monte Carlo Simulation method (DS-MCS method); the other one will be named as Direct and Combined-Monte Carlo Simulation method (DC-MCS method).

The main objective of this study is to ***compare 3 different MCS methods capable of accounting inherent spatial variability of soil properties in probabilistic LEM analysis and evaluate the results from these methods.***

Based on the above, the research questions of this study are formulated as follows:

- How to assign random field values onto each potential slip circle in three different MCS methods?
- How does the proposed RF-MCS method compare with two direct MCS methods in terms of accuracy and efficiency?
- How is the robustness of three different MCS methods in different situations?

In order to answer these questions, a Python program is modified from the code given by Bram van den Eijnden.

1.4 Research outline

The first research question involves the development of the proposed RF-MCS method. After development and verification of the method, the RF-MCS method is compared with direct MCS method. The comparison criterion is the computational time and the probability of failure P_f calculated. The third question deals with parametric studies under a range of different conditions to test the robustness of these 3 different MCS methods.

Thus, the structure of this study can be formulated as:

In Chapter 2, the relevant literatures about deterministic and probabilistic LEM are summarized. The literature study starts with the basic concepts of Fellenius, Bishop, Spencer and Taylor's analytical method. After which, different sources of uncertainties in the slope stability problems are discussed. The Focus is on how to quantify these uncertainties and how to incorporate them into the probabilistic model. General concept of random field and the common used probabilistic analysis methods are elaborated in this chapter. Then, the definition of 'system probability of failure' for different methods is clarified.

The main features of the RF-MCS method are examined in chapter 3. Emphasis is put on the method used for the generation of the random field mesh, the appropriate value for each slice base passing the mesh and the correlation between different slip surface. The investigation on those aspects is based partially on literature review and simulations with the extended Python code. Example analysis is performed using this RF-MCS method and the result is verified using the commercial software D-Geo stability and the work previously did by others.

Chapter 4 involves a comparison between the RF-MCS method with two other direct MCS methods. These three different MCS methods are compared based on benchmark case studies. The comparison is in terms of the yielded results, e.g. the probability of failure P_f calculated and required computational time. Then, What causes the difference in the results from 3 methods has been investigated.

Chapter 5 describes the parametric studies under different conditions to test the robustness of these 3 different MCS methods.

A summary of the work, conclusions on the main findings of the project and recommendations for future research are included in chapter 6.

Chapter 2

Literature review

This chapter introduces the concept of literature that is relevant with this study. It starts with the basic principles in the deterministic analysis. This involves the concept of limit equilibrium methods (LEM) and different LEM approaches. Furthermore, different sources of uncertainty in the slope stability problems are discussed. Emphasis are put on how to quantify these uncertainties and how to incorporate them into a probabilistic model. The use of random fields in combination with LEM is discussed next. Then, the concept of the commonly used Monte Carlo simulation (MCS) methods is elaborated. Finally, the definition of system probability of failure is introduced as well as how three different MCS methods estimate the system probability of failure P_f.

2.1 Method of slices

Most deterministic LEM methods assume a circular slip surface, and then the divide soil above into several vertical slices with a simplifying assumption about the effect of the interslice forces. Different LEM have been developed based on different assumptions to make sure the problem is determinate. Three commonly used methods are introduced here in this study: Fellenius, Bishop and Spencer. Figure 2.1 indicate a typical "slice" method.

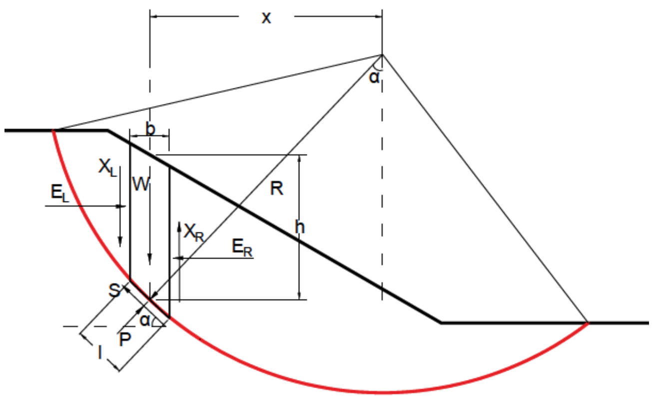

FIGURE 2.1: Visualization of the slope geometry and different forces acting on a slice in LEM

where b, h the width and height of the slice,
R the radius of the circular sliding surface,
x horizontal distance between the center of slice and the center of rotation of the sliding soil mass,
α the angle between the base of the slice and the horizontal direction,
W the self-weight of the slice,
P, S the normal and shear force acting at the base of the slice over a distance of l,
E_L, E_R horizontal forces acting at the left and right side of the slice,
X_L, X_R vertical forces acting at the left and right side of the slice.

By assuming the shear force to be a factor F smaller than the maximum possible shear force and combined with the Mohr-Coulomb failure criteria, the shear force acting at the base of the slice can be expressed as:

$$S = \frac{1}{F}\{c' + (\sigma_n - u)tan\phi'\} \tag{2.1}$$

where c′ cohesion,
σ_n total normal stress,
u pore pressure,
ϕ' internal friction angle.

The total normal stress is σ_n, where

$$\sigma_n = \frac{P}{l} \tag{2.2}$$

Thus, according to equation (2.1), the shear force mobilized is:

$$S = \frac{1}{F}\{c' + (\frac{P}{l} - u)tan\phi'\} \tag{2.3}$$

2.1.1 Fellenius method

The Fellenius method is the oldest and is considered as the simplest among these methods since the factor of safety was calculated by a linear derivation. It is generally assumed that the horizontal forces between each slices can be neglected since they are parallel to the base of the slice (Fellenius, 1936). The remaining forces acting on a slice are the self-weight of the slice W, the normal and shear force acting at the base of the slice P, S. Thus, both horizontal and vertical equilibrium are not satisfied due to this assumption.

The normal force acting at the base of each slice can be determined by summation of all the vertical and horizontal forces.

$$\sum F_v = 0 \qquad W - P\cos\alpha - S\sin\alpha = 0 \tag{2.4}$$

$$\sum F_h = 0 \qquad S\cos\alpha - P\sin\alpha = 0 \tag{2.5}$$

Substituting (2.5) into (2.4) derives the equation of the normal force:

$$P = W\cos\alpha \tag{2.6}$$

Then the factor of safety can be determined by summing the moments about the center of rotation of the sliding mass.

$$\sum M_o = 0 \qquad \sum Wx - \sum SR = 0 \tag{2.7}$$

Substituting (2.3) and (2.6) into (2.7), the equation of factor of safety gives:

$$F = \frac{\sum((P - ul)\tan\phi')R + c'l}{\sum Wx} \tag{2.8}$$

The equation can also be expressed as following if the pore pressure is assumed equal to zero.

$$F = \frac{\sum(W\cos\alpha\tan\phi' + c'l)R}{\sum Wx} \tag{2.9}$$

2.1.2 Bishop method

The simplified Bishop method assumed there are no interslice forces and the resultant forces are horizontal (Bishop, 1955). The horizontal forces are not involved in the computation and only the vertical equilibrium of each slice is satisfied in this method.

$$\sum F_h = 0 \qquad S\cos\alpha - P\sin\alpha - (E_L - E_R) = 0 \tag{2.10}$$

The normal force acting at the base of each slice can be determined by summation of forces in the vertical direction (2.4) and combining the shear force equation (2.3).

$$P = [W - \frac{(c'l - ul\tan\phi')\sin\alpha}{F}]/m_\alpha \tag{2.11}$$

where $m_\alpha = \cos\alpha + \frac{\tan\phi'\sin\alpha}{F}$

Then the factor of safety can be determined by the summation of the moments about the center of rotation of the sliding mass.

$$F = \frac{\sum((P - ul)\tan\phi' + c'l)R}{\sum Wx} \tag{2.12}$$

Substituting (2.3) into (2.12) and neglecting the pore pressure, the equation can then be written as following:

$$F = \frac{\sum((W - \frac{c'l\sin\alpha + c'l}{F})/m_\alpha\tan\phi')R}{\sum Wx} \tag{2.13}$$

2.1.3 Spencer method

The Spencer method makes assumptions that the interslice shear forces has a constant relationship with the normal forces (Spencer, 1967). Thus, vertical, horizontal and driving moment equilibrium are all satisfied on each slice.

$$\tan\theta = \frac{X_L}{E_L} = \frac{X_R}{E_R} \tag{2.14}$$

where θ is the angle between the horizontal direction and the resultant interslice force.

$$\sum F_v = 0 \qquad W - S\sin\alpha - P\cos\alpha + (X_L - X_R) = 0 \tag{2.15}$$

The normal force can be derived by summing the forces in the vertical (2.15) and horizontal (2.10)direction.

$$P = [W + (E_L - E_R)\tan\alpha - \frac{(c'l - ul\tan\phi')\sin\alpha}{F}]/m_\alpha \tag{2.16}$$

Unlike Fellenius and Bishop method, spencer method gives two equations of the factor of safety: the first one is derived by the summation of moments about the center of rotation (2.7), and the result is same as the simplified Bishop methods.

$$F_m = \frac{\sum((P - ul)\tan\phi' + c'l)R}{\sum Wx} \tag{2.17}$$

The other is derived by the summation of forces in the direction parallel to the interslice forces and the second factor of safety equation gives:

$$F_f = \frac{\sum((P - ul)\tan\phi' + c'l)\cos\alpha}{\sum P\sin\alpha} \tag{2.18}$$

Figure 2.2 shows the relationship between F_m and F_f with varying θ. The intersection of the two curves gives the value of the factor of safety (F_1) that satisfies both the force and moment equilibrium.

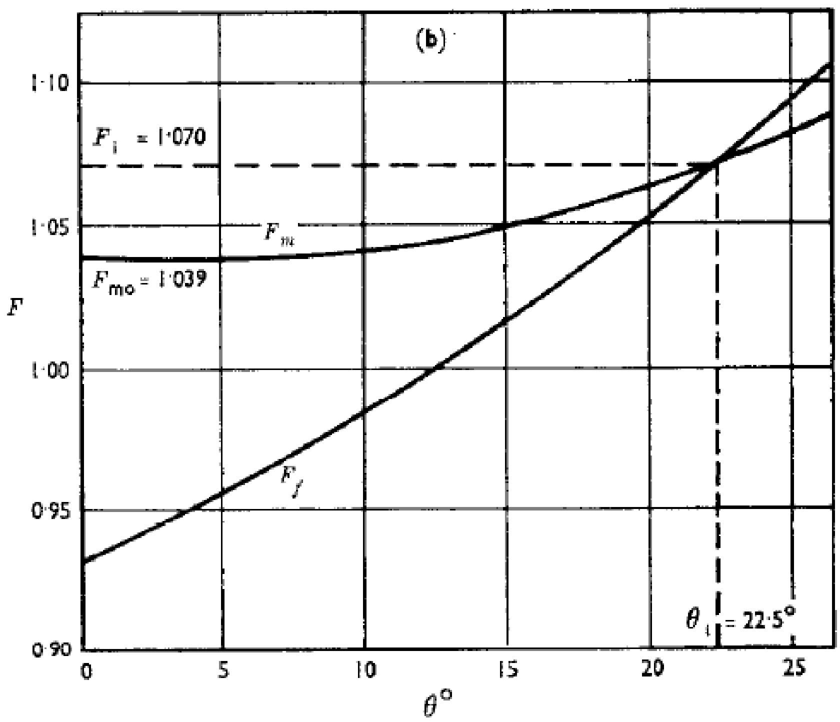

FIGURE 2.2: Variation of two different factor of safety F_m and F_f with θ (Spencer, 1967)

It can observed from the graph that the basis of the accuracy of simplified Bishop method depends on the insensitivity of F_m to variation in θ when this angle is not greater than θ_1.

2.1.4 Taylor's analytical method

(Taylor, 1937) proposed an established solution to deal with the undrained homogeneous slope stability problem after analyzing a series of slopes of different geometries with various combination of soil parameters. The soil strength parameters can be represented by undrained cohesion value c_u, internal friction angle ϕ and unit weight of soil γ, and the slope angle by β^* and slope height by H. The whole combinations of these parameters shown in the Figure 2.3.

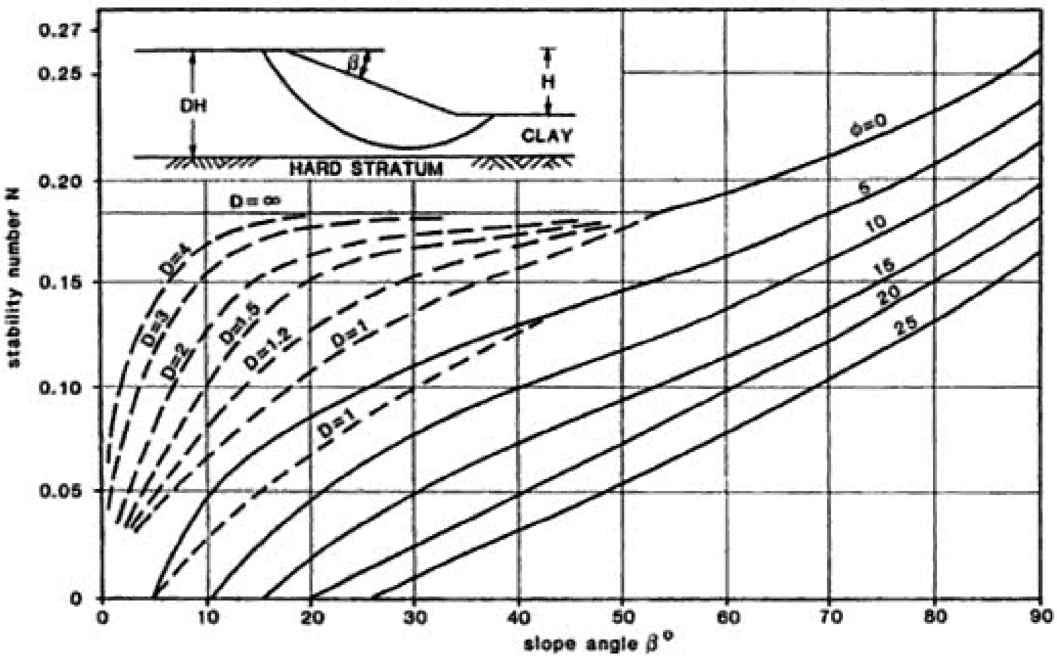

FIGURE 2.3: Stability charts-Taylor's curve (Bromhead, 1992)

The stability of the slope can then be defined by the equation:

$$N_s = \frac{c_u}{F\gamma H} \tag{2.19}$$

where N_s the stability number (a dimensionless parameter).

Therefore, using the set of soil and slope geometry parameters, the corresponding factor of safety can be directly read from the graph:

$$F = \frac{c_u}{N_s\gamma H} \tag{2.20}$$

2.2 Uncertainty

Like other geotechnical problems, slope stability problem also dominated by uncertainty. For example, soil properties vary spatially due to the depositional process and loading history, the statistical uncertainty result from incomplete site investigation data, the bias in the transformation model and correlation structure adpoted, etc. Without rational consideration of the uncertainties, a single factor of safety FS value cannot provide a comprehensive understanding of risk and isn't qualified as a safety indicator. Thus, probabilistic analysis is considered as a better approach which can account for the quantified uncertainties in the calculation process (El-Ramly et al., 2002).

2.2.1 Sources of uncertainty

Many kinds of uncertainties can lead to the overall geotechnical variability. (Phoon and Kulhawy, 1999) distinguished three primary geotechnical sources of uncertainty, as shown in Figure 2.4, the inherent soil variability, measurement error, and transformation uncertainty.

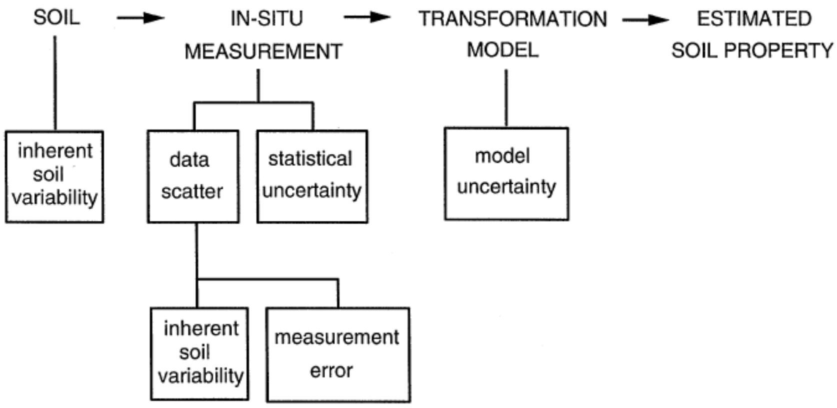

FIGURE 2.4: Uncertainties in geotechnical problems (Kulhawy, 1993)

- The inherent soil variability: results mainly from the natural deposition processes that created and constantly change the in-situ soil mass.
- Measurement error: introduced primarily by testing equipment, testing operator, and the influence of random testing.
- Transformation uncertainty: introduced when the lab or field measurement data are transformed into input information for the geotechnical design. Uncertainty results from empirical data fitting or idealizations and simplifications in the theory.

The above mentioned three sources contribute disproportionally to the general uncertainty for the input parameters of the geotechnical design. They are influenced by the different site conditions, the level of testing control and accuracy of the correlation model. Due to the scope of investigation, this study only take account of the inherent soil variability out of these three sources.

2.2.2 Modeling inherent soil variability

Because of the natural deposition process, all soil properties vary horizontally and vertically. As shown in Figure 2.5. The inherent soil variability can be described by:

$$\xi(z) = t(z) + w(z) \tag{2.21}$$

where z the depth,
ξ the in situ soil property,
$t(z)$ the trend function,
$w(z)$ the fluctuating factor.

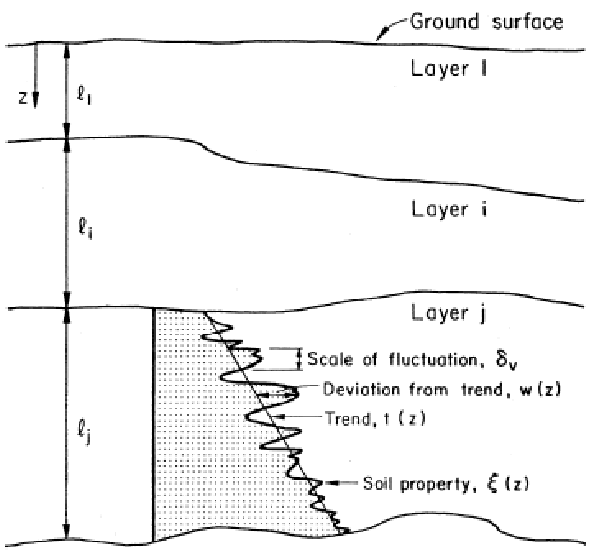

FIGURE 2.5: The inherent soil variability (Phoon and Kulhawy, 1999)

The trend function $t(z)$ is often estimated by regression analysis and a common method to quantify the inherent soil variability is to model the fluctuating factor $w(z)$ as a stationary random field (E. Vanmarcke, 1983).

A soil parameter can be classified as a random variable anywhere within a soil layer, unless it is measured at that specific location. And according to the experimental data of soil properties, the distribution of in-situ soil properties shows resemblance with a number of theoretical distribution functions. In order to transform these data into design use, certain kinds of probability distribution (usually normal or lognormal distribution) are usually adopted to simulate these random variables. And a random variable is correlated with one next to it. Therefore, a random field is actually a collection of random variables at all possible locations within the soil layer.

A random field is called homogeneous (or stationary) under the condition that mean and variance of w keep constant anywhere within the domain of the random field. The correlation between w at two different depths is governed by the relative distance within the random field, rather than their absolute distance.

2.2.3 Theory of random fields

As an important part of probabilistic slope stability analysis, random fields theory has been widely adopted to model the spatial variability of different soil properties. That is, the fluctuating factor, w, can be characterised by the correlation structures using the random fields theory.

The term correlation structure is used for all functions describing the spatial variability of a field. The correlation structure contains information about the scale and shape of the correlation between spatially distributed points within a field and is a function of relative point distance or domain size (Van den Eijnden and Hicks, 2011). Variance function $\Gamma(\Delta z)$ and correlation function $\rho(\Delta z)$ are different correlation structures and contain the same information. These different functions are derived and discussed in this section.

Variance function

Local averaging theory is considered to be a more rational mean to evaluate the slope failure (E. Vanmarcke, 1983). Because:

1. In reality, it is impossible to measure the point to point variation with a soil layer.
2. The average strength over the length of the slip surface is more informative than the point to point strength variation.
3. A slope is more likely to fail with the existence of insufficient average strength over the length of the slip surface than the presence of some weak points within the layer.

The averaged spatial variability of soil properties is likely to be reduced in the process of averaging. Because the fluctuating factor w of the soil properties got removed with the increasing averaging distance Δz, as shown in Figure 2.6. This way, during the process of spatial averaging, the variance of the soil properties is decreased.

Dimensionless variance (reduction) function (Erik H Vanmarcke, 1977) $\Gamma(\Delta z)$ is the ratio between the moving average variance and the original point to point variance. It can measure how much the point to point variance got reduced compared with the moving average variance.

$$\Gamma(\Delta z) = \frac{\sigma^2_{\Delta z}}{\sigma^2} \tag{2.22}$$

where $\sigma^2_{\Delta z}$ the averaging variance over the length Δz ,
σ^2 the original point to point variance.

Figure 2.6 indicates a $1D$ stationary random field. Where $E[X]$ is the mean value and σ^2 is the variance of variable X. The red line indicates the local averages over interval Δz.

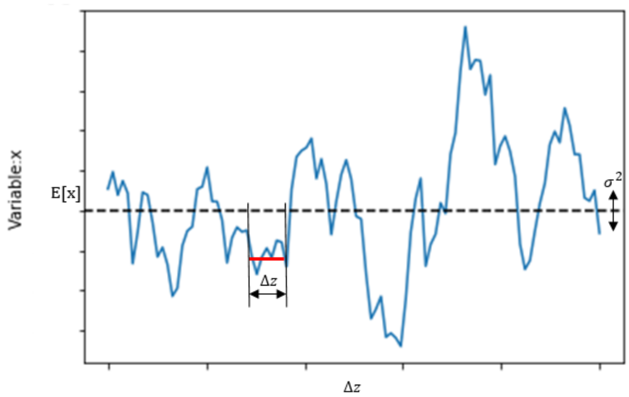

FIGURE 2.6: A visualization of a 1D random field

Correlation function

The correlation function is adopted to defined the correlation between two points at a relative distance Δz within a field. The relationship between the correlation function and the variance function can be expressed as (Erik H Vanmarcke, 1977):

$$\Gamma(\Delta z) = \frac{1}{\Delta z^2} \int_0^{\Delta z} \int_0^{\Delta z} \rho(z_a - z_b) dz_a dz_b \tag{2.23}$$

If an exponential decaying correlation function is considered (Figure 2.7), the variance function $\Gamma(\Delta z)$ can be defined by the ratio of the area under the correlation function (AC) over the averaging distance Δz to the area under AB over the same averaging distance.

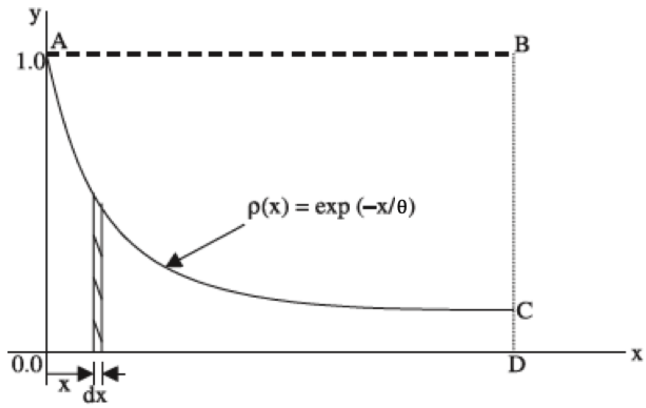

FIGURE 2.7: Exponential decaying correlation function (Sivakumar Babu et al., 2006)

The area under the curve AC over the averaging distance Δz can be calculated by the integral:

$$A = \int_0^{\Delta z} \rho(x) dx = \int_0^{\Delta z} \exp(-\frac{x}{\theta}) dx \tag{2.24}$$

If $-x/\theta = t$, then $dx = -\theta dt$. For $x = 0$, $t = 0$. And for $x = \Delta z$, $t = -\Delta z/\theta$. Thus,

$$A = -\theta \int_0^{-\Delta z/\theta} \exp t dt = \theta[1 - \exp(-\frac{\Delta z}{\theta})] \tag{2.25}$$

Therefore, the variance function can be expressed as:

$$\Gamma(\Delta z) = \begin{cases} 1 & \frac{\Delta z}{\theta} = 0, \\ \frac{\theta}{\Delta z}[1 - \exp(-\frac{\Delta z}{\theta})] & \frac{\Delta z}{\theta} > 0 \end{cases} \tag{2.26}$$

The Markov autocorrelation coefficient function $\rho(\Delta z)$ (2.27) is adopted to characterize soil variability in this study (Figure 2.8):

$$\rho(\Delta z) = \exp(-\frac{|\Delta z|}{\theta}) \tag{2.27}$$

Where θ is the scale of fluctuation.

Thus, the corresponding variance function can be expressed as: (2.28):

$$\Gamma(\Delta z) = \frac{\theta^2}{2\Delta z^2}[\frac{2|\Delta z|}{\theta} + \exp(-\frac{2|\Delta z|}{\theta}) - 1] \tag{2.28}$$

For this commonly used correlation function, the variance function $\Gamma(\Delta z)$ can be estimated as following (E. Vanmarcke, 1983):

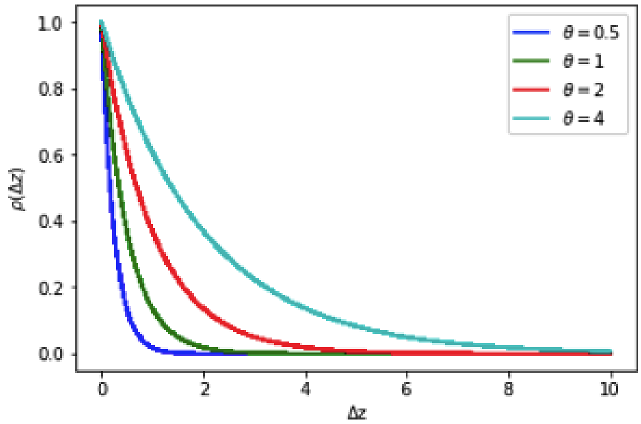

FIGURE 2.8: Exponential decaying correlation function with varying value of θ

$$\Gamma(\Delta z) = \begin{cases} 1 & \Delta z \leq \theta, \\ \frac{\theta}{\Delta z} & \Delta z \geq \theta \end{cases} \tag{2.29}$$

This indicates no variance reduction when the moving average interval Δz equal to θ, $\Gamma(\Delta z) = 1$. And $\Gamma(\Delta z)$ becomes inversely proportional to Δz when it larger than the scale of the fluctuation θ.

Another way to express the correlation function in terms of the the scale of fluctuation is

$$\theta = \lim_{\Delta z \to \infty} \Gamma(\Delta z)\Delta z \tag{2.30}$$

The scale of fluctuation is a measure of variability of soil property over a relative distance. A large value of the scale of fluctuation indicates that the soil property is correlated over a large distance, the soil property vary slowly and the field is more smooth. Conversely, when the scale of fluctuation θ is small, the soil property values change rapidly over small distances, the field tend to be erratic and rough. Figure 2.9 shows exemplary random fields with two different scale of fluctuation θ.

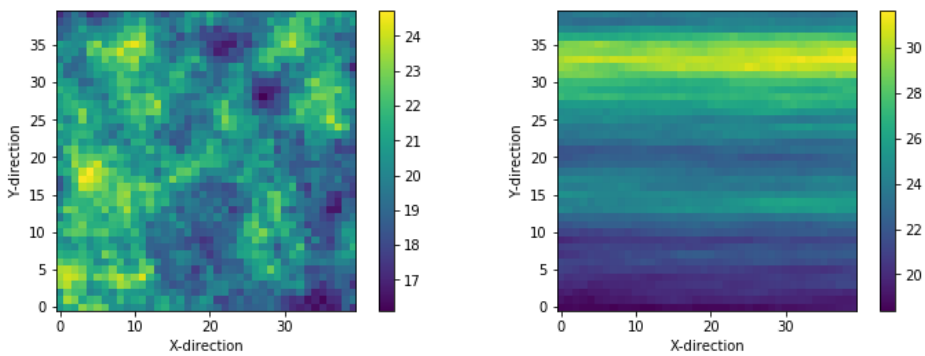

FIGURE 2.9: 2D random fields of X with different scale of fluctuation; low (left) and high (right)

2.2.4 Discretization of random fields

Random fields consist of a list of random variables defined over a continuous domain. However, the numerical solution requires the translation of the continuous parameter fields into discretized form.

Several random field discretization methods have been developed in the past few decadeds. For example, the spatial averaging method, the midpoint method, the shape function method and the covariance matrix decomposition method, etc. Detailed review of these different methods can be found in (C.-C. Li and Der Kiureghian, 1993), (Sudret and Der Kiureghian, 2000).

Considering the number of random field elements and random variables, different methods are more suitable to either FEM or LEM approach. Because of the adoption of LEM approach in this study, only the midpoint method and covariance matrix decomposition method are elaborated here.

The midpoint method The most simplest one among these method is the midpoint method. Each element within the field domain is represented by the value at the centroid of the element domain, as shown in Figure 2.10.

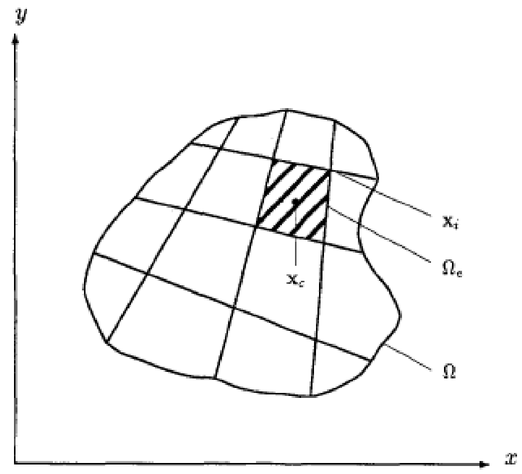

FIGURE 2.10: Random field mesh (C.-C. Li and Der Kiureghian, 1993)

where	X_c	the midpoint value,
	X_i	the node value,
	Ω_e	the element domain,
	Ω	the random field domain.

(Cho, 2007) has found a way to apply this method to probabilistic LEM approach which can describe the inherent spatial variability of the soil properties. Each slice here represents an element domain over a distance Δx, the value at each slice base represents the midpoint value.

This way, the random values within the entire random field domain can be successfully assigned onto each slice. Figure 2.11 shows the midpoint method with same arc length Δx of each slice.

Covariance matrix decomposition

The matrix decomposition method always starts with forming the autocovariance matrix **C**.

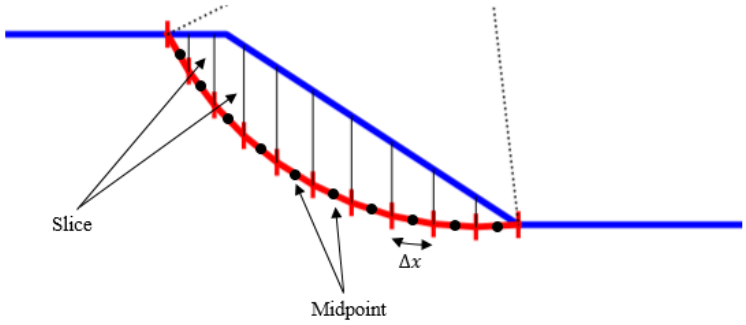

FIGURE 2.11: Schematic viualisation of the midpoint method in the slope stability analysis

The variance of a random variable **X** is the expectation of the squared deviation from the mean of **X**. The variance equals to the square of the standard deviation σ^2. It is also represents the second moment of a distribution s^2, and the covariance of a random variable with itself $var(X)$. It can be expressed by the Eq.2.31:

$$var(X) = \sigma_X^2 = E[(X - E[X])^2] = cov(X) = E[(X - E[X])(X - E[X])^T] \tag{2.31}$$

It also called autocovariance matrix **C** or cross-covariance matrix for a set of data **X** itself. The autocovariance matrix **C** is related to autocorrelation matrix **R** by:

$$\begin{aligned} \mathbf{C} = cov[\mathbf{X},\mathbf{X}] &= E[(\mathbf{X} - E[\mathbf{X}])(\mathbf{X} - E[\mathbf{X}])^T] \\ &= E[(\mathbf{X} - \mu_{\mathbf{X}})(\mathbf{X} - \mu_{\mathbf{X}})^T] = \mathbf{R}\sigma(\mathbf{X})\sigma(\mathbf{X}^T) \end{aligned} \tag{2.32}$$

Where $\mathbf{R} = E[\mathbf{X}\mathbf{X}^T]$, $\mu_{\mathbf{X}} = E[\mathbf{X}]$; **R** is defined by means of the exponential decaying Markov autocorrelation coefficient function $\rho(\Delta z)$ (2.27) in this study, and it can be expressed as follows:

$$\begin{aligned} \mathbf{R} &= \begin{bmatrix} 1 & \frac{E[(X_1-\mu_1)(X_2-\mu_2)]}{\sigma(X_1)\sigma(X_2)} & \cdots & \frac{E[(X_1-\mu_1)(X_n-\mu_n)]}{\sigma(X_1)\sigma(X_n)} \\ \frac{E[(X_2-\mu_2)(X_1-\mu_1)]}{\sigma(X_2)\sigma(X_1)} & 1 & \cdots & \frac{E[(X_2-\mu_2)(X_n-\mu_n)]}{\sigma(X_2)\sigma(X_n)} \\ \vdots & \vdots & \ddots & \vdots \\ \frac{E[(X_n-\mu_n)(X_1-\mu_1)]}{\sigma(X_n)\sigma(X_1)} & \frac{E[(X_n-\mu_n)(X_2-\mu_2)]}{\sigma(X_n)\sigma(X_2)} & \cdots & 1 \end{bmatrix} \\ &= \begin{bmatrix} 1 & \rho_{12} & \cdots & \rho_{1n} \\ \rho_{21} & 1 & \cdots & \rho_{2n} \\ \vdots & \vdots & \ddots & \vdots \\ \rho_{n1} & \rho_{n2} & \cdots & 1 \end{bmatrix} \end{aligned} \tag{2.33}$$

In the probabilistic LEM analysis, the random field domain transformed into n slices after the random field discretization **Z**.

This way, the covariance between any two slices of **Z** can be represented by a $n \times n$ autocovariance matrix **C**:

$$\mathbf{C} = E[\mathbf{Z}\mathbf{Z}^T] \tag{2.34}$$

One of common used covariance matrix decomposition method, Cholesky decomposition can decompose a positive definite covariance matrix into a product of a lower triangular matrix and the transpose of itself.

$$\mathbf{Z} = \mathbf{A}\boldsymbol{\xi} \tag{2.35}$$

Where $\mathbf{A}$ is the $n \times n$ lower triangular matrix with n positive diagonal elements, $\boldsymbol{\xi}$ is a vector with n random numbers sampled by means of standard normal sampling.

Substituting Eq.(2.35) into Eq.(2.34) can derive the expression below:

$$E[\mathbf{Z}\mathbf{Z}^T] = E[\mathbf{A}\boldsymbol{\xi}(\mathbf{A}\boldsymbol{\xi})^T] = E[\mathbf{A}\boldsymbol{\xi}\boldsymbol{\xi}^T\mathbf{A}^T] = \mathbf{A}\mathbf{A}^T = \mathbf{C} \tag{2.36}$$

2.3 Probabilistic analysis methods

In the past few decades, people found ways to apply some commonly used probabilistic analysis methods into slope stability problem. For example, the first order second moment method (FOSM), first order reliability method (FORM), Monte Carlo Simulation (MCS), etc. In order to better understand the implementation of different methods, it first starts with the basic concept of the performance function (limit state function) and the derivation of probability of failure in the slope stability problem.

The performance function $g(X)$ is used to define the limit state ($g(X) = 0$) for a variable X. It separates the failure domain where the slope failed ($g(X) \leq 0$) and the safety domain where the factor of safety of the slope meet the safety requirement($g(X) \geq 0$). Usually, for a single potential slip surface, the performance function can be defined as:

$$g(X) = FS - 1.0 \tag{2.37}$$

This way, the probability of failure of the slope that consist of all the potential slip surfaces can be defined by the joint probability density function integrated over the entire failure domain:

$$P_f = P[g(X \leq 0)] = \int_{g(X \leq 0)} f_X(X)dX \tag{2.38}$$

Where $f_X(X)$ the joint probability density function.

However, it is almost impossible to directly integrate the joint probability density over the failure domain because the limit state function always involves several soil strength parameters in the slope stability problems. And usually it's not just a linear function. Therefore, different probabilistic analysis methods have been developed to approximate this integral.

2.3.1 Monte Carlo simulation

Monte Carlo simulation (MCS) method is commonly used in probabilistic LEM analysis to investigate the slope stability problem. Because the advantage of conceptual simplicity and unrestricted by the complexity of the performance function.

In MCS method, a huge number of sets of random variables are generated first according to the type of their own probability distribution. For each generated set, limit equilibrium method (simplified Biship method) is employed, the performance function is evaluated, statistical analysis is performed to calculate the probability of failure P_f or reliability index β.

For each iteration, the performance function is evaluated to determine whether it exceeded the limit state function or not. The probability of failure P_f can be calculated after this evaluation process is repeated many times:

$$P_f = \frac{1}{N_t} \sum_{n=1}^{N_t} g(X \leq 0) = \frac{1}{N_t} \sum_{n=1}^{N_t} (FS_{min} < 1) \tag{2.39}$$

Where N_t the total number of the iterations during MCS process.

And the reliability index β can then be calculated by the inverse of the cumulative distribution function of the probability of failure P_f:

$$\beta = -\Phi^{-1}[P_f] \tag{2.40}$$

The advantage of the MCS method is not limited to its simple concept. There are various statistical analyses can be performed after the simulation process. For example, the probability density function and cumulative distribution function of the factor of safety, the mean and standard deviation of the factor of safety, etc. Thus, MCS method provides us a more comprehensive understanding of the safety of the slope.

However, the most obvious drawback is that it requires a large amount of computational efforts to reach an acceptable accuracy.

2.4 System probability of failure

(Chowdhury and Xu, 1995) demonstrated the importance of considering the slope stability problem in terms of a system of many potential slip surfaces. The assumption of such a system is a series system. The probability of failure of such a system will be larger than that for any individual slip surface. Therefore, the system probability of failure will depend on each individual modes of failure as well as the correlations between the different failure modes. However, it is difficult to calculate accurately the correlation coefficients between each individual failure modes when the performance function is inexplicit and non-linear.

To simplify the problem, one may consider the slope as a series system (failure occurs if any potential slip circle of the system fails) or a parallel system (the system does not fail unless all potential slip circles fail) or a combination of both. However, the assumption of a series system leads to significantly high failure probability, the assumption of a parallel system leads to extremely low failure probability(Ang and Tang, 1984).

Thus, the slope stability problem in this study is considered as a series system that comprises all potential slip circles with correlations between different potential slip circles.

For RF-MCS method, the system probability of failure is estimated by generating certain amount of potential slip circles first and then performing MCS to calculate the minimum factor of safety FS_{min} among them for each realisation of random field. The P_f can be estimated by dividing the number of failure realisations by the total number of realisations.

For direct MCS method, the critical failure circle is located and the highest value of probability of failure corresponding to that circle is determined simultaneously in one realisation of analysis. This value of probability of failure is regarded as the system probability of failure.

2.5 Summary

This chapter summarises the relevant literature used in this study:

1. The basic concept of limit equilibrium methods (LEM) are introduced first, including three commonly used LEM (Fellenius, Bishop and Spencer) and Taylor's analytical method. The derivation of the factor of safety of each method are illustrated.

2. Three general types of uncertainty in the geotechnical problems are illustrated next. The most important one, the inherent soil variability, and how to model this uncertainty by the theory of random field are introduced next. Relevant techniques used by this study to discretize the random field are presented, namely, the midpoint method and Chokesky decomposition.

3. The definition of system probability of failure is elaborated. Details involved how three different MCS methods estimate the system probability of failure P_f in this study.

Chapter 3

Probabilistic LEM development and verification

This chapter introduces the development and verification of the proposed Random Field - Monte Carlo Simulation method (RF-MCS method). It starts with a basic deterministic analysis model. Then, the relevant concepts used in the probabilistic analysis model, random field generation, the estimation of the midpoint value for each slice base and the correlation between different slip surface, are elaborated. The deterministic and probabilistic model are verified against the results given by (Cho, 2009) and (Jiang et al., 2015).

3.1 Deterministic model

For a slope stability problem, deterministic analysis calculates the factor of safety FS by assuming all the soil mass are homogeneous within the slope geometry domain. In this section, the limit equilibrium methods (LEM) introduced in the previous chapter are employed to calculate the factor of safety. The calculation process of deterministic analysis is implemented in a Python program. The most critical slip surface is selected by the program. The corresponding factor of safety is the minimum factor of safety FS_{min}. The accuracy of the model is verified by the commercial software D-Geo stability (version 18.1) and the results given by (Cho, 2009).

3.1.1 Benchmark deterministic analysis 1: a undrained clay slope ($\phi = 0$)

An example undrained slope is analyzed here using simplified Bishop method under the assumption that there is no external force acting on the slope. The input soil parameters and slope geometry are exactly same with (Cho, 2009). The slope height is $5m$ and the slope angle β^* is 26.56°, as shown in Figure 3.1. The pore pressure is neglected in this study and it keep the same for all the rest analysis. The slope is characterized by homogeneous soil property. The input soil parameters are given in Table 3.1.

Parameter	Value	Unit
Cohesion (c)	23	kPa
Internal friction angle (ϕ)	0	°
Unit weight (γ)	20	kN/m^3

TABLE 3.1: Input soil parameters for deterministic analysis 1

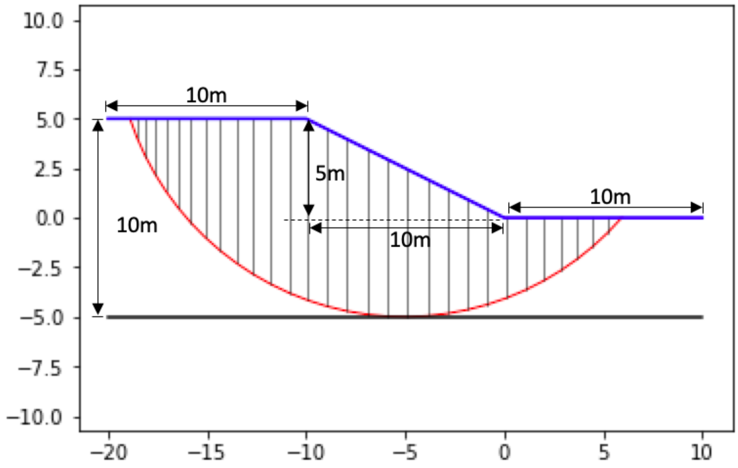

(a:cross-section from Python program)

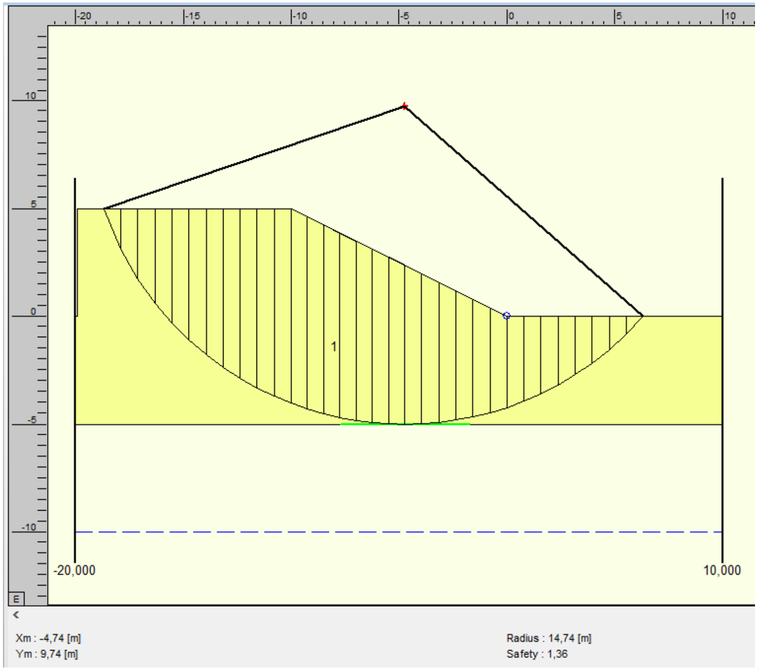

(b:cross-section from D-Geo stability)

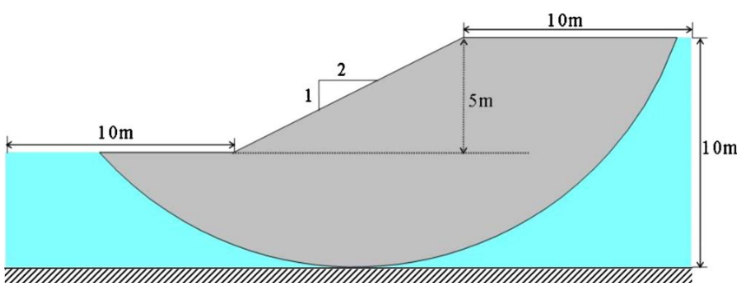

(c:cross-section from (Cho, 2009))

FIGURE 3.1: Example slope geometry 1 (FS_{min}=1.356)

Figure 3.1 (a), (b) show the critical slip surface selected by the Python program and D-Geo stability, respectively. The failure mechanism and the geometry of the circle is identical to the one given by (Cho, 2009).

The minimum factor of safety FS_{min} calculated by the Python program is 1.356, which is the same as the result calculated by D-Geo stability and the result given by (Cho, 2009).

3.1.2 Benchmark deterministic analysis 2: a c-ϕ slope

This second deterministic analysis deals with the problem for a c-ϕ slope. The slope geometry and input soil parameters are still keep the same with (Cho, 2009). The slope height is $10m$ and the slope angle β^* is 45°, as shown in Figure 3.2. The input soil parameters are given in Table 3.2.

Parameter	Value	Unit
Cohesion (c)	10	kPa
Internal friction angle (ϕ)	30	°
Unit weight (γ)	20	kN/m^3

TABLE 3.2: Input soil parameters for deterministic analysis 2

Figure 3.2 (a) shows the critical slip surface selected by the Python program. The failure mechanism and the circle geometry is identical to the one given by (Cho, 2009).

D-Geo stability cannot deal with the slip circle that just cross the toe of the slope, as shown in Figure 3.2 (b). However, this can be achieved by defining the radius of the circle in the Python program so that the circle cut from the toe of the slope.

The minimum factor of safety FS_{min} calculated by the Python program is 1.204, which is the same as the result given by (Cho, 2009).

Therefore, the accuracy of the deterministic Python model can be verified from these 2 deterministic benchmark analysis.

3.2 Probabilistic model

Probabilistic slope stability analysis has been widely adopted in recent study since its ability to take into account of the inherent spatial variability of uncertain soil properties which can be defined by the random field. The general concept of the random field is already elaborated in chapter 2. Therefore, this section focuses more on how to apply these concept into probabilistic analysis.

3.2.1 Correlation structure of 2D random field

The lognormal stationary random field $\underline{H}(\vec{\chi})$ can be generated by applying a transformation $\Psi(.)$. A lognormal random field is adopted here because the lognormal random variable is a nonnegative variable, which can well characterize the physical meaning of certain soil parameters (i.e. c and ϕ).

$$\underline{H}(\vec{\chi}) = \Psi(Z(\vec{\chi})) = \exp(\mu_{lnX} + \sigma_{lnX} Z(\vec{\chi})), \qquad \vec{\chi} \in \Omega \tag{3.1}$$

Where the spatial correlation is taking into considertaion in the standard normal field $Z(\vec{\chi})$. μ_{ln}, σ_{ln} are the mean and standard deviation of the lognormal field, respectively.

$$\mu_{lnX} = ln\mu_X - 0.5\sigma^2_{lnX} \tag{3.2}$$

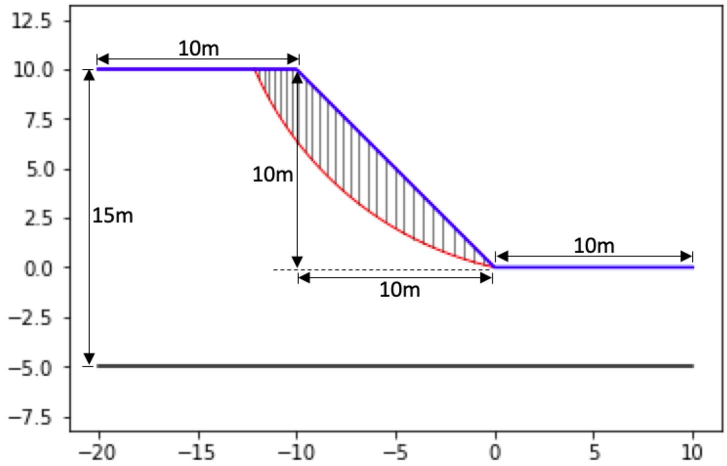

(a:cross-section from Python program)

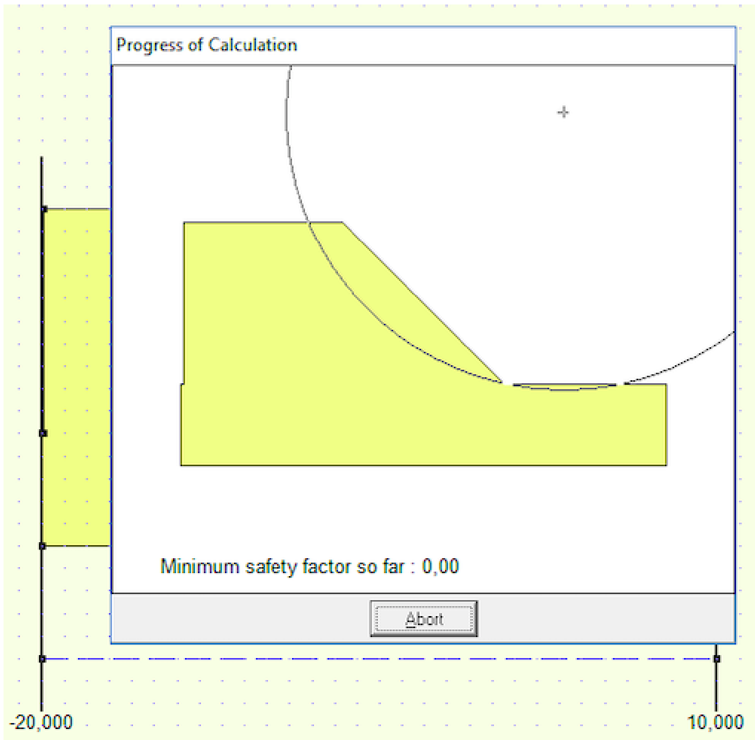

(b:cross-section from D-Geo stability)

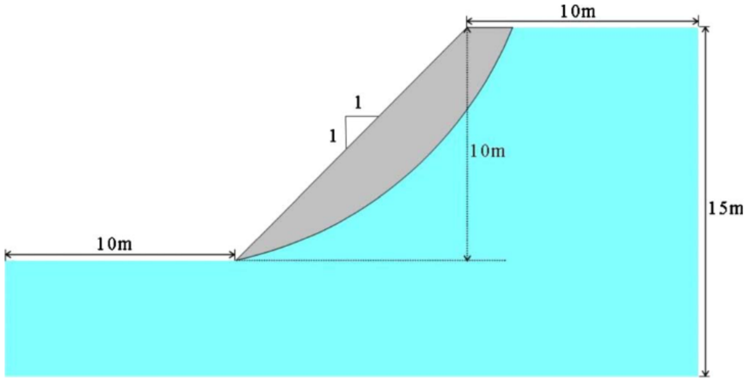

(c:cross-section from (Cho, 2009))

FIGURE 3.2: Example slope geometry 2 (FS_{min}=1.204)

$$\sigma_{lnX} = \sqrt{ln(1 + COV_X^2)} \tag{3.3}$$

$$COV_X = \frac{\sigma_X}{\mu_X} \tag{3.4}$$

The inherent spatial variability of uncertain soil properties in the horizontal and vertical directions can be modeled by a 2D lognormal stationary random field $\underline{H}(x, y)$ with a mean μ_H and standard deviation σ_H, where x, y is the horizontal and vertical coordinate on a bounded domain Ω, $0 \leq x, y \leq L_{x,y}$; L_x and L_y are the lengths of Ω in the horizontal and vertical directions, respectively.

The autocorrelation coefficient function in the in the 2D domain can then be expressed as:

$$\rho_{(x,y)} = \exp\left(- \frac{\Delta x}{\theta_h} - \frac{\Delta y}{\theta_v} \right) \tag{3.5}$$

Where, θ_h and θ_v are the horizontal and vertical autocorrelation distance, respectively. Δx and Δy represent the absolute distance on the horizontal and vertical direction, respectively.

3.2.2 Correlation between different random variables

Despite the spatial correlation of one variable with adjacent locations, correlation exist between different variables X. For example, the cohesion c and the internal friction angle ϕ. To define the correlation between these two random variables, two separate standard normal random fields Z_i^c and Z_i^ϕ are generated both of which are characterized by a normal distribution. Another correlation matrix $R_{c\phi}$ is created to correlate these two random variables.

$$R_{c\phi} = \begin{bmatrix} \rho_{cc} & \rho_{c\phi} \\ \rho_{\phi c} & \rho_{\phi\phi} \end{bmatrix} \tag{3.6}$$

Then the second standard normal random field Z_i^ϕ can be correlated with Z_i^c by Cholesky decomposition of the correlation matrix $R_{c\phi}$.

$$\begin{bmatrix} Z_i^c \\ Z_i^\phi \end{bmatrix}_{corr.} = Chol.(R_{c\phi}) \begin{bmatrix} Z_i^c \\ Z_i^\phi \end{bmatrix}_{uncorr.} \tag{3.7}$$

The magnitude of correlation between these two standard normal random fields Z_i^c and Z_i^ϕ depends on the correlation of each random variable at the same location $\rho_{c\phi}$. Figure 3.3 shows the correlation between two random fields with $\rho_{c\phi}$ = 0.3 and 0.9, respectively. The magnitude of correlation increases with the increasing value of $\rho_{c\phi}$. The right graph below shows the standard normal random field Z_i^ϕ closely follows the trend of Z_i^c with higher value of $\rho_{c\phi}$.

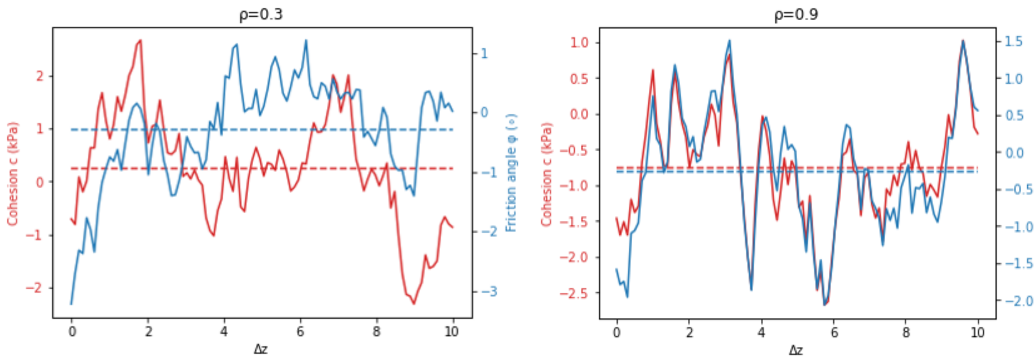

FIGURE 3.3: Two different random fields with different magnitude of correlation; Low correlation (left) and high correlation (right); Dash lines indicate the mean value of the trend

3.2.3 Random field generation for RF-MCS method

For RF-MCS method, in order to create a random field of a certain soil parameter, a rectangular mesh-grid is generated for later to map the random values onto it (Figure 3.4).

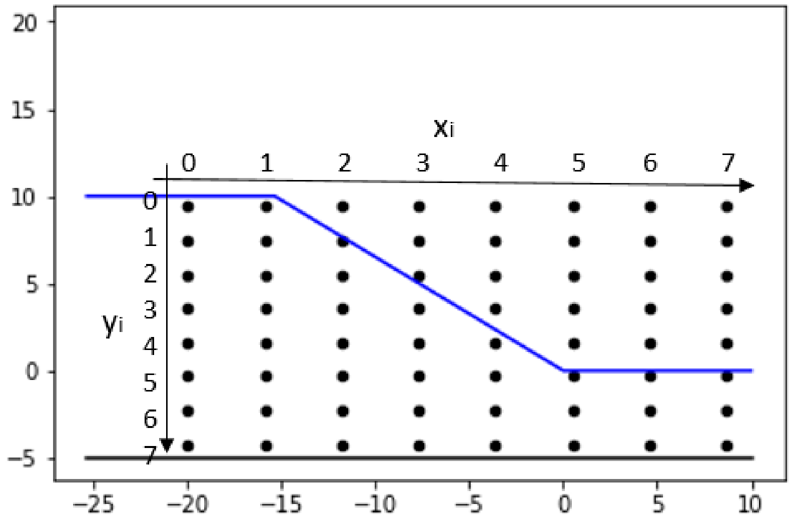

FIGURE 3.4: Generation of the rectangular mesh-grid

A random field can be generated as a list of random values, which can be mapped onto the rectangular mesh-grid. The value of a random variable at one point in the field are correlated with the value within a distance from the point. The mapping procedure of soil parameter, the cohesion c and the internal friction angle ϕ, is shown in Figure 3.5.

The random values of the correlated lognormal variable are assigned to the 2D mesh-grid from the top left corner to the bottom right corner following the arrows shown in Figure 3.4. This way, a random field with point values on the rectangular grid points are generated.

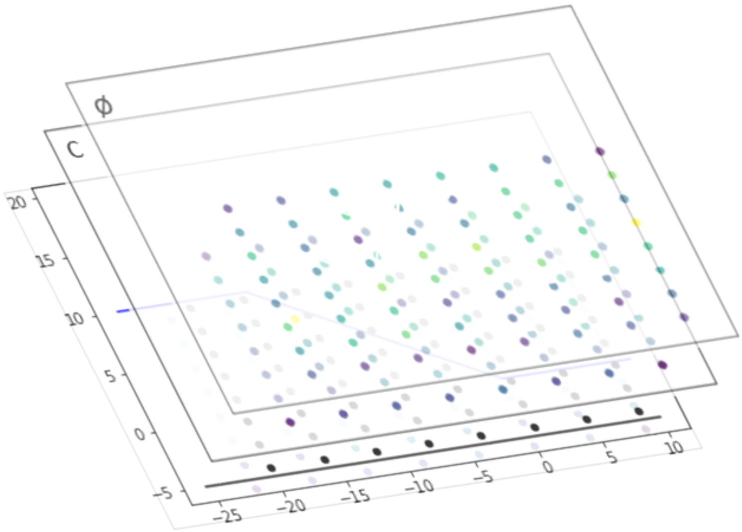

FIGURE 3.5: Schematic visualization of the mapping process

3.2.4 Estimation of the midpoint value at each slice base

The random values should be assigned onto the slip surface after generation of the random field. Figure 3.6 shows a typical slope stability problem with an assumed slip center and slip surface. The colored grid points represent the 2D random field with mapped value, the red plus markers at each slice base represent the midpoint.

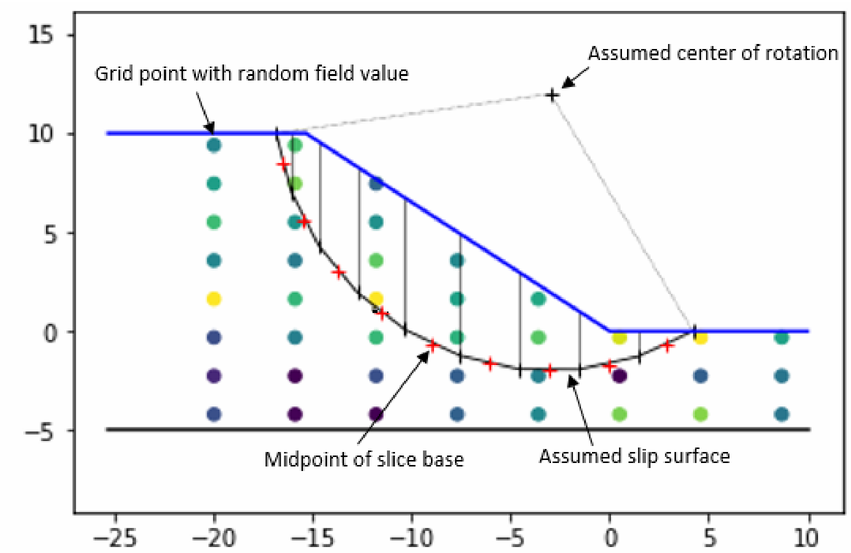

FIGURE 3.6: Cross-section through a soil mass with an assumed slip center and slip circle for RF-MCS

Linear interpolation is adopted in the RF-MCS method to estimate the value at the midpoint of each slice base.

At each midpoint, the values of soil parameter, the cohesion c and the internal friction angle ϕ, are interpolated by the function **RegularGridInterpolator** in the Python program. Then, the factor of safety FS of this single slip surface can be calculated after the interpolation procedure.

Once derived the factor of safety of the single assumed slip circle, same strategy can be extrapolated to a combination of different slip circles, represented by n horizontal coordinates x_{ci}, n vertical coordinates y_{ci} of the center of slip circles and n different radii R_i of the slip circles, as shown in Figure 3.7. The value n for slip circle radius and center coordinates can be different. Therefore, n^3 potential slip circles can be produced in each realisation. The slip circle which gives the lowest factor of safety $FS_{min,i}$ can be selected as the most critical slip surface.

Here, a realisation means one possible analysis that consist of all n^3 potential slip circles. A single realisation could be regarded as a failure realisation $N_{f,i}$, if the lowest factor of safety $FS_{min,i} < 1$. So, the system probability of failure P_f of a slope can be estimated as:

$$P_f = \frac{N_f}{N_t} = \frac{1}{N_t} \sum_{n=1}^{N_t} (FS_{min} < 1) \tag{3.8}$$

Where N_t is the total number of realisations and it equals to the number of random fields generated. N_f is the number of failure realisations.

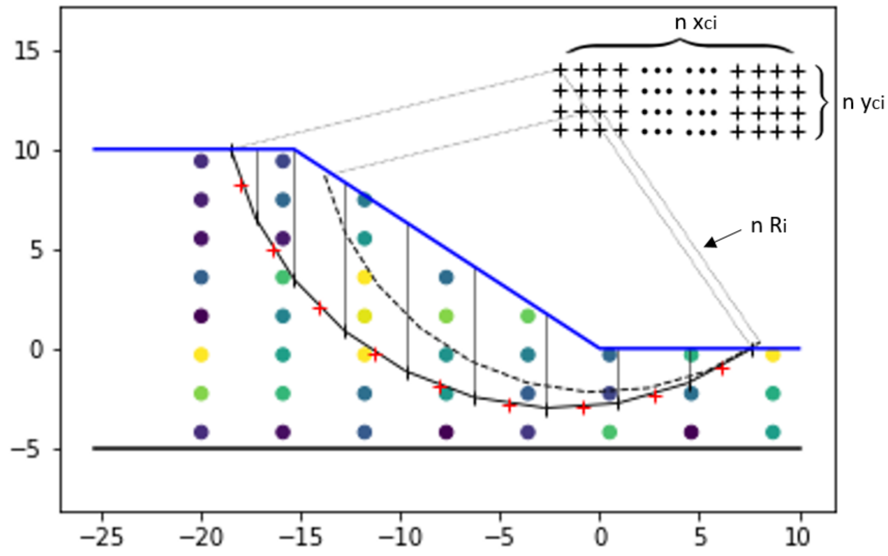

FIGURE 3.7: Schematic visualization of the RF-MCS method

The main features of the proposed RF-MCS method is:

1. The random field only generate once in each realisation which is more realistic compared with two other direct MCS (each potential slip circle was assigned different random fields).

2. The correlation between different slip surfaces is taken into consideration since the mesh-grid values of the random field are correlated and two different soil properties, the cohesion c and the internal friction angle ϕ, are also correlated with each other.

3. The searched critical failure circle can be visualized against the distribution of random field.

3.2.5 Random field generation for direct MCS method

For direct MCS method, the random field is generated and directly assigned onto the midpoint of slice base. Figure 3.8 shows a cross section of a slope with an assumed slip center and slip surface. The correlation structure used in the random field generation process is defined by the coordinate of the midpoint of each slice. And it is modeled by the autocorrelation coefficient function given in equation 3.10.

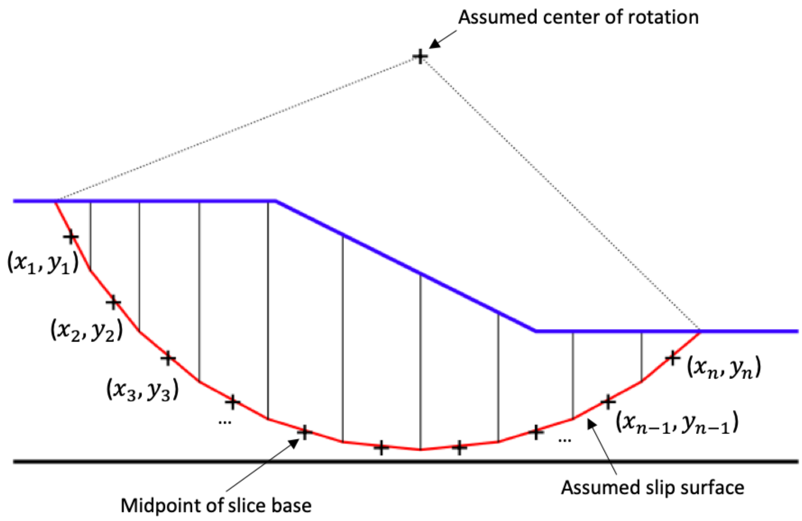

FIGURE 3.8: Cross-section through a soil mass with an assumed slip center and slip circle for direct MCS

For this assumed slip surface, N_t random fields are generated. Then, Monte carlo simulation is performed to calculate N_t Factor of safety FS corresponding to these N_t random fields. The probability of failure of this single circle can be calculated as:

$$P_f = \frac{1}{N_t} \sum_{n=1}^{N_t} (FS < 1) \tag{3.9}$$

This single circle then can be extrapolated to a combination of different slip circles, represented by n horizontal coordinates x_{ci}, n vertical coordinates y_{ci} of the center of slip circles and n different radii R_i of the slip circles (as did in RF-MCS method).

At the end, the system probability of failure of the slope can be derived by selecting the highest single probability of failure among the n^3 potential slip circles.

3.3 Implementation procedure of 3 different methods

The methodology of the 3 methods are elaborated in this section. Figure 3.11 shows flowcharts for the implementation of the RF-MCS method, DS-MCS method and DC-MCS method schematically.

The implementation procedure of DS-MCS method and DC-MCS method will be explained first. In general, it involves four steps and the details of each step are given as follows:

1. Determine the input parameters such as the mean and standard deviation of the soil strength parameters, cross-correlation coefficient between c and ϕ, autocorrelation function used to define the correlation structure, etc) and slope geometry of the soil properties.

2. Generate N_p potential slip circles according to the prescribed domain and the radius. N_p equals to n^3 which represents n horizontal coordinates of slip circle, n vertical coordinates of slip circle, and n radii of slip circle.

3. For each potential slip circle, N_t random fields are generated by normal sampling. A limit equilibrium analysis (simplified Bishop method) is performed and combined with MCS to calculate factor of safety FS, probability of failure P_f for each potential slip circle.

4. Select the circle which gives the highest value of P_f or lowest value of β. The P_f and β are regarded as system probability of failure and system reliability index, respectively. The circle is the most critical failure circle.

The main difference of DS-MCS method and DC-MCS method lies in step 3, the generation random field. Detailed concept of Cholesky decomposition is already explained in chapter 2.2.4.

In DS-MCS method, the standard normal random numbers vector with n-entry $\boldsymbol{\xi}$ is sampled by means of standard normal sampling with $\mu = 0, \sigma = 1$ separately for strength parameter cohesion c and friction angle ϕ, as shown in Figure 3.9.

In DC-MCS method, the standard normal random numbers $\boldsymbol{\xi}$ is sampled once by means of standard normal sampling with $\mu = 0, \sigma = 1$ but generate a $2 * n$-entry vector. Parameter c samples the former n-entries and parameter ϕ samples the latter n-entries, as shown in Figure 3.10.

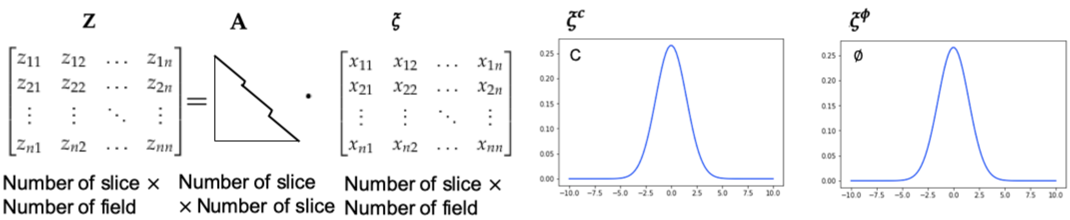

FIGURE 3.9: Random number sampling in DS-MCS method

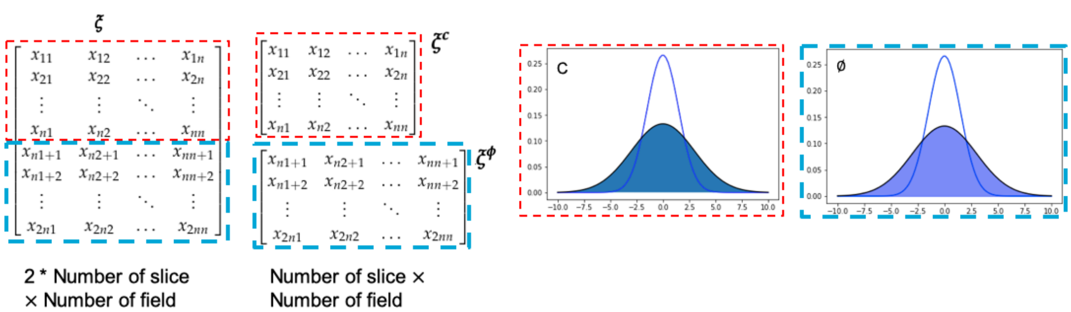

FIGURE 3.10: Random number sampling in DC-MCS method

The implementation procedure of RF-MCS method involves six steps:

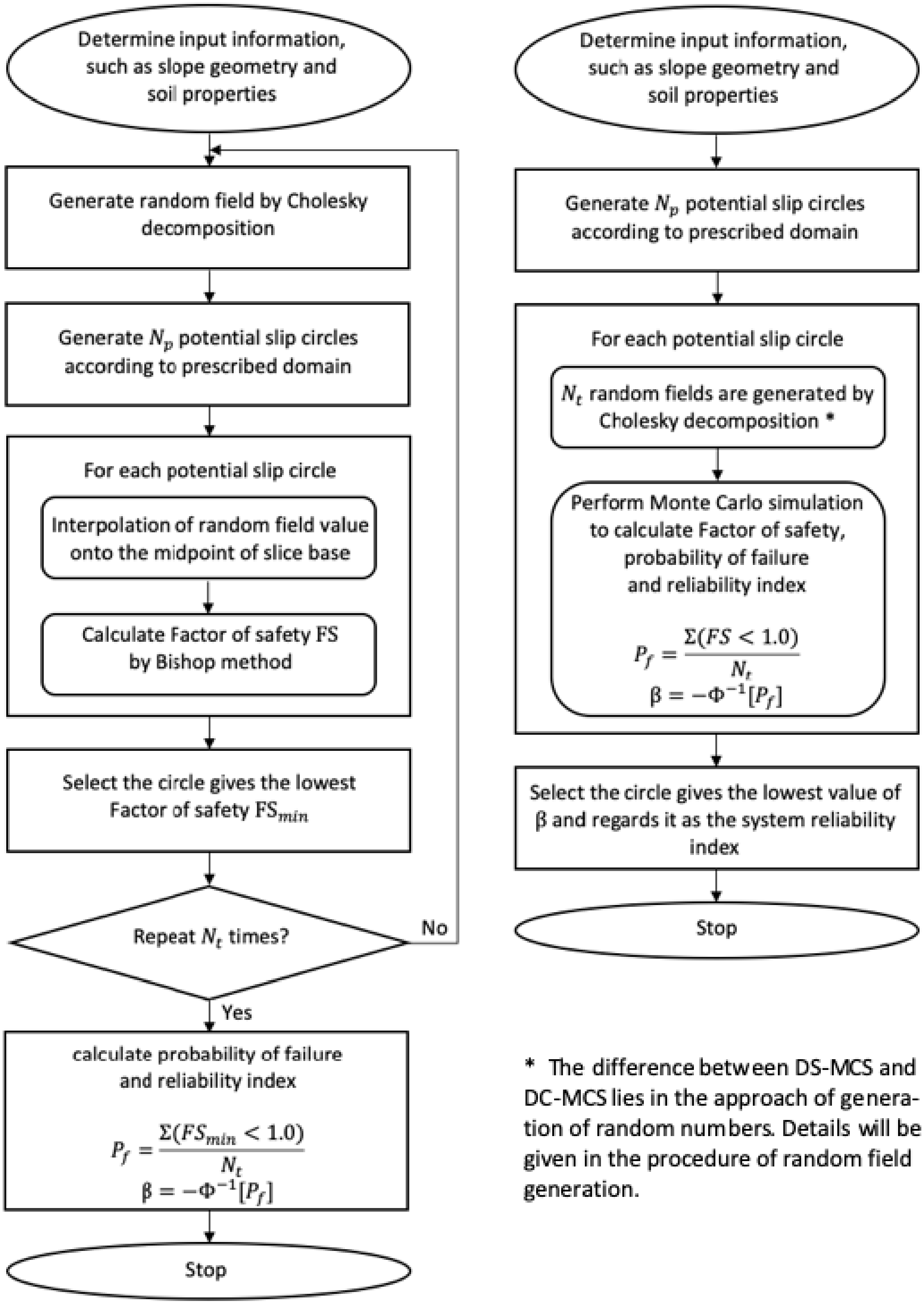

FIGURE 3.11: Flowchart of implementation of the Monte Carlo method; RF-MCS method (left), direct MCS method (right)

1. Determine the input parameters such as the mean and standard deviation of the soil strength parameters, cross-correlation coefficient between c and ϕ, autocorrelation function used to define the correlation structure, etc) and slope geometry of the soil properties.

2. Generate a random field by Cholesky decomposition.

3. Generate N_p potential slip circles according to the prescribed domain and the radius. N_p equals to n^3 which represents n horizontal coordinates of slip circle, n vertical coordinates of slip circle, and n radii of slip circle.

4. For each potential slip circle, perform linear interpolation to map the random field value onto the midpoint of slice base. Perform a limit-equilibrium analysis (simplified Bishop method) to calculate factor of safety FS.

5. Select the circle which gives the lowest value of factor of safety FS_{min}.

6. Calculate the probability of failure P_f and reliability index β after repeat N_t times. The P_f and β are regarded as system probability of failure and system reliability index, respectively.

3.4 Benchmark analysis 1: a undrained clay slope ($\phi = 0$)

This section uses the proposed RF-MCS method to analyze a undrained clay slope. A benchmark probabilistic analysis is performed here aims to verify the probabilistic model against the work did by (Cho, 2009) which demonstrate the advantages of the probabilistic analysis of slope stability problem.

3.4.1 Initial input information

The geometry of this undrained slope is keep the same as the one used in the first deterministic analysis (Figure 3.1). The slope height is H = 5 m and the slope angle is 26.56°. The unit weight of the soil is γ = 20 kN/m^3. The domain of potential slip circle is defined as: (x $\in$ [-10,0]; y $\in$ [5,15]) and the domain of random field is defined as: (x $\in$ [-20,10]; y $\in$ [-5,5]) (Figure 3.12). The number of circle is 10*10*10. The number of slice division is 30. The strength parameter cohesion c is lognormally distributed. According to (El-Ramly et al., 2002), the reasonable horizontal autocorrelation distance fluctuate between 10 $\sim$ 40m, and 1 $\sim$ 3 m in the vertical direction. Thus, $\theta_h = 20m$, $\theta_v = 2m$ are adopted in this study. All the other input soil and domain parameters are given in Table 3.3.

The autocorrelation function in this benchmark analysis is given below and it keeps the same for all the following analysis in this report:

$$\rho_{(x,y)} = \exp\left(- \frac{\Delta x}{\theta_x} - \frac{\Delta y}{\theta_y} \right) \tag{3.10}$$

Parameter	Value	Unit
Slope angle (β^*)	26.56	($\circ$)
Cohesion (c)(COV=0.3)	23	(kPa)
Density of random field mesh	60*60	(-)
Horizontal autocorrelation distance (θ_h)	20	(m)
Vertical autocorrelation distance (θ_v)	2	(m)

TABLE 3.3: Initial parameters for benchmark analysis 1

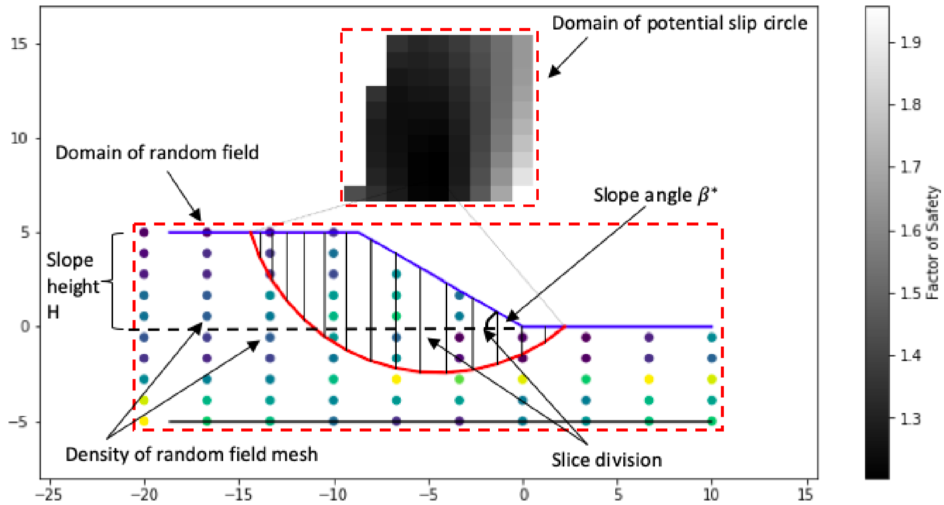

FIGURE 3.12: Indication of some input information

3.4.2 Pre-analysis

This section aims to identify the influence of the slice division and the number of potential slip circles used in the inital input information for the analysis. A sensitivity analysis is performed to investigate this influence. All the other parameters are keep constant as indicated in the previous section, the only variable here is the number of slice and and the number of potential slip circles, respectively. 50,000 random fields have been generated for each analysis.

Number of slice division	P_f	$\mu_{FS_{min}}$	$\sigma_{FS_{min}}$	$COV_{FS_{min}}$
30	0.0385	1.3396	0.2116	0.1579
40	0.0374	1.3400	0.2112	0.1576
50	0.0372	1.3418	0.2116	0.1577

TABLE 3.4: Results from sensitivity analysis of slice division

Number of slip circle	P_f	$\mu_{FS_{min}}$	$\sigma_{FS_{min}}$	$COV_{FS_{min}}$
8^3	0.0375	1.3433	0.2127	0.1584
10^3	0.0385	1.3396	0.2116	0.1579
12^3	0.0394	1.3361	0.2107	0.1577

TABLE 3.5: Results from sensitivity analysis of number of slip circle

Table 3.4 summarises the results from the sensitivity analysis of slice division. The largest difference of the derived probability of failure is 3.5%. Table 3.5 summarises the results from the sensitivity analysis of number of slip circle. The largest difference of the derived probability of failure is 5%.

Because the computational time suffers from the increasing number of slice and the number of slip circle. Under the condition that the adequate accuracy can be guaranteed, the slice division is set to be 30 and the number of slip circle is chosen as 10^3 for the following analysis.

3.4.3 Analysis and results

Figure 3.13 shows four realizations of random field obtained by the RF-MCS method. The darker area represent a smaller soil parameter value while the lighter area represent a larger soil parameter value. Various failure mechanisms can be observed. Some failure surfaces go deep or even touch the base of the slope. Some are relatively shallow and go across the toe. Another phenomenon is that the failure surface always pass through the weaker area in the slope. The inherent spatial variability caused various failure mechanisms can not be demonstrated by the deterministic analysis.

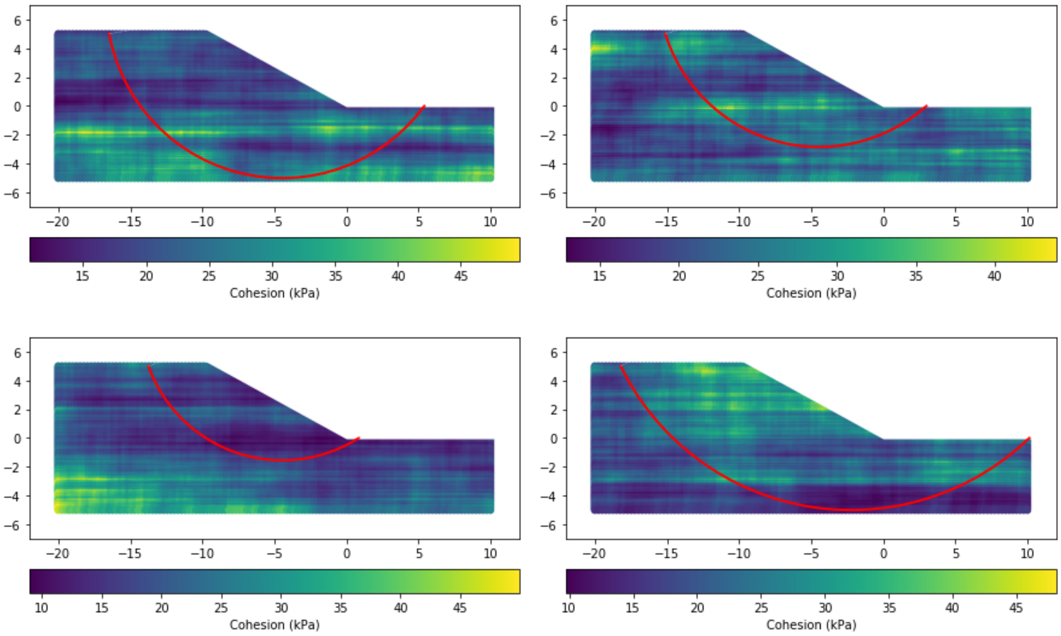

FIGURE 3.13: Typical realizations of random fields (θ_h=20 m,θ_v=2 m)

Table 3.6 summaries the simulation results from this benchmark probabilistic analysis and results reported by (Cho, 2009) and (Jiang et al., 2015). Here, simulation result indicates the minimum number of realisations that could yield a converged result. The last column k in the table indicate the relative difference of probability of failure P_f from different studies. It is derived by the P_f from 2 other studies divided by the P_f from this study.

The relative difference of probability of failure P_f is almost twice smaller than the result given by (Cho, 2009) and (Jiang et al., 2015). The difference might result from the different method adopted to generate the random field (Karhunen-Loève Expansion were adopted by (Cho, 2009) and (Jiang et al., 2015)).

Method	P_f	Source	k
RF-MCS + Cholesky decomposition (50,000)	3.85×10^{-2}	This study	-
MCS + KL expansion (100,000)	7.6×10^{-2}	(Cho, 2009)	1.97
MCS + LHS (1,000)	8.3×10^{-2}	(Jiang et al., 2015)	2.16

TABLE 3.6: Influence of autocorrelation distance on the statistical response 1

In order to further verify the RF-MCS method in this study, the critical failure surface selected by the deterministic analysis was reanalysed by this RF-MCS probabilistic analysis approach.

Figure 3.14 indicates the convergence of the simulation. The blue dash line in the figure indicate the result from the fixed slip circle selected by the deterministic analysis previously in section 3.1.1. Even though the same slope was analyzed using the same proposed RF-MCS method, the system probability of failure of the slope is 0.0385 which is significantly greater than the one calculated from the fixed deterministic critical surface (0.0148).

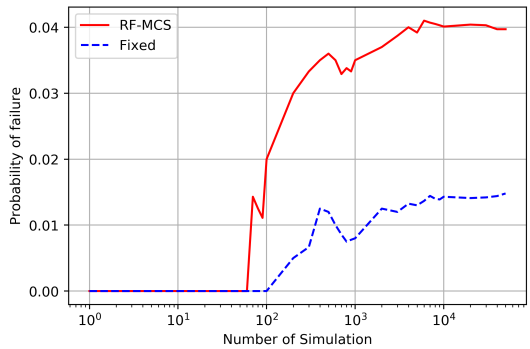

FIGURE 3.14: Probability of failure derived from 2 approaches

Figure 3.15 shows the probability density function and the cumulative distributions of the factor of safety derived from the two approaches.

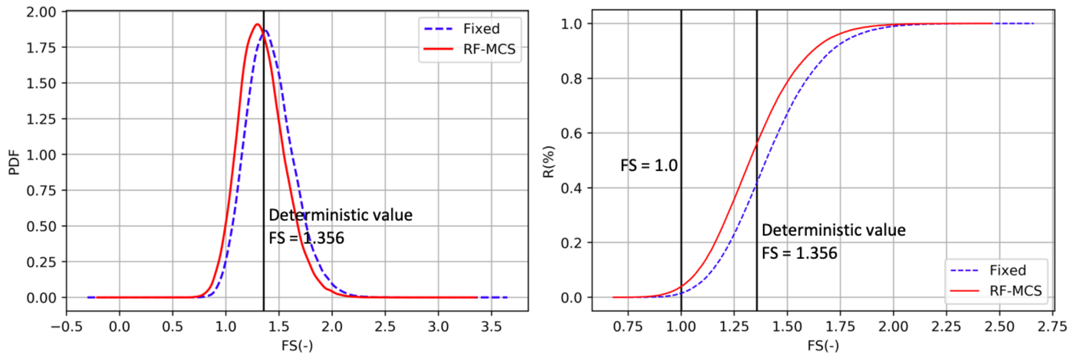

FIGURE 3.15: Probability density function (left) and cumulative distribution of the factor of safety (right)

Large difference can be found from the results derived by two different approaches. This is because the correlation between different failure surfaces are quite low and the accuracy of the probability of failure approximated by the fixed critical surface can only be guaranteed when the correlation between different surfaces is very high

(Cornell, 1967). This phenomenon is the same as the work done by (Cho, 2009) which can verify the RF-MCS method from another angle.

3.5 Benchmark analysis 2: a c-ϕ slope

A c-ϕ slope is analyzed in this section by RF-MCS method so that the model can be further verified.

3.5.1 Initial input information

The geometry of this c-ϕ slope is keep the same as the one used in the second deterministic analysis (Figure 3.2). The slope height is H = 10 m and the slope angle is 45°. The unit weight of the soil is γ = 20 kN/m^3. The domain of potential slip circle is defined as: (x $\in$ [-1,9]; y $\in$ [10,20]) and the domain of random field is defined as: (x $\in$ [-20,10]; y $\in$ [-5,10]). The number of circle is 10*10*10. The soil strength parameter cohesion c and friction angle ϕ are lognormally distributed. The correlation coefficient $\rho_{c\phi}$ is chosen as -0.5. A negative correlation coefficient indicates that negative relationship exist between the cohesion and friction angle. That is, increasing the cohesion value will decrease the value of friction angle and vice versa.

All the other input soil and domain parameters are given in Table 3.7.

Parameter	Value	Unit
Slope angle (β^*)	45	($\circ$)
Cohesion (c)(COV=0.3)	10	(kPa)
Friction angle (ϕ)(COV=0.2)	30	($\circ$)
Density of random field mesh	60*60	(-)
Horizontal autocorrelation distance (θ_h)	20	(m)
Vertical autocorrelation distance (θ_v)	2	(m)

TABLE 3.7: Initial parameters for benchmark analysis 2

3.5.2 Pre-analysis

As did in the previous section, a sensitivity analysis was performed first to test the influence of the slice division and the number of slip circle. 50,000 random fields have been generated for each analysis.

Number of slice division	P_f	$\mu_{FS_{min}}$	$\sigma_{FS_{min}}$	$COV_{FS_{min}}$
30	0.0055	1.2269	0.0967	0.0788
40	0.0054	1.2261	0.0965	0.0787
50	0.0051	1.2272	0.0973	0.0793

TABLE 3.8: Results from sensitivity analysis of slice division

Number of slip circle	P_f	$\mu_{FS_{min}}$	$\sigma_{FS_{min}}$	$COV_{FS_{min}}$
8^3	0.0055	1.2275	0.0974	0.0793
10^3	0.0055	1.2269	0.0967	0.0788
12^3	0.0059	1.2262	0.0972	0.0792

TABLE 3.9: Results from sensitivity analysis of number of slip circle

Table 3.8 summarises the results from the sensitivity analysis of slice division. Table 3.9 summarises the results from the sensitivity analysis of number of slip circle. In both cases, the largest difference of the derived probability of failure is 7%, which is still within the acceptable level ($\pm$10%). Therefore, the slice division is set to be 30 and the number of slip circle is chosen as 10^3 for the following analysis for the c-ϕ slope.

3.5.3 Analysis and results

Figure 3.16 shows three realizations of random field obtained by the RF-MCS method. Notice that negative relationship exist between the cohesion and the friction angle. (The darker area displayed in the cohesion diagram correspond with the lighter area shown in the friction angle diagram). And the failure surfaces always go across the toe of the slope.

Table 3.10 summaries the simulation results from this benchmark probabilistic analysis and the results reported by (Cho, 2009) and (Jiang et al., 2015). The last column *k* in the table indicate the relative difference of probability of failure P_f from different studies. It is derived by the P_f from 2 other studies divided by the P_f from this study.

The slight difference of probability of failure P_f might result from the different method adopted to generate the random field (Karhunen-Loève Expansion were adopted by (Cho, 2009) and (Jiang et al., 2015)).

Method	P_f	Source	k
RF-MCS + Cholesky decomposition (50,000)	5.5×10^{-3}	This study	-
MCS + KL expansion (100,000)	3.9×10^{-3}	(Cho, 2009)	0.71
MCS + LHS (10,000)	4.4×10^{-3}	(Jiang et al., 2015)	0.80

TABLE 3.10: Influence of autocorrelation distance on the statistical response 2

Figure 3.17 indicates the convergence of the simulation. The blue dash line in the figure indicate the result from the fixed slip circle selected by the deterministic analysis previously in section 3.1.2. The proposed RF-MCS method calculated similar results for the system probability of failure (0.0055) and the P_f from the fixed deterministic critical surface (0.0042) (Figure 3.17).

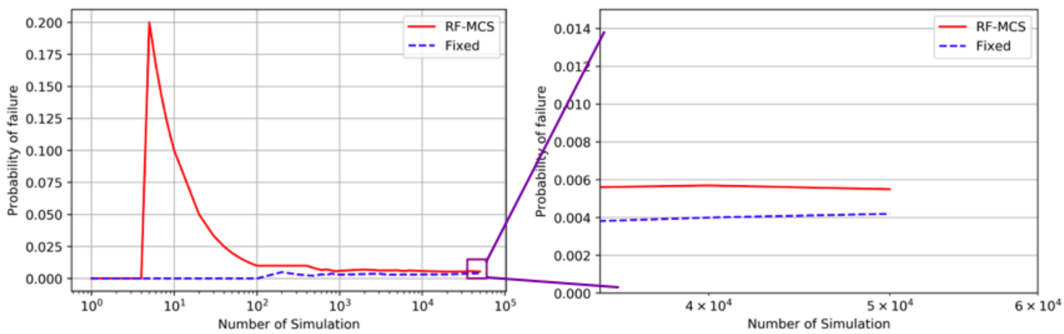

FIGURE 3.17: Probability of failure derived from 2 approaches

Figure 3.18 shows the probability density function and the cumulative distributions of the factor of safety derived from the two approaches.

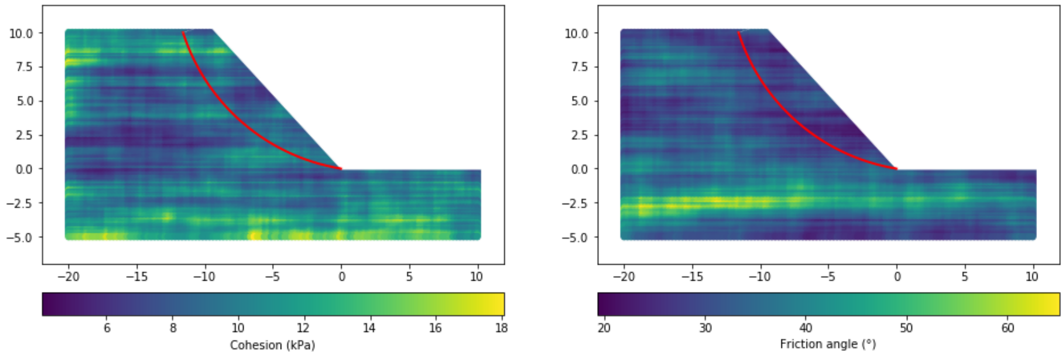

(a)

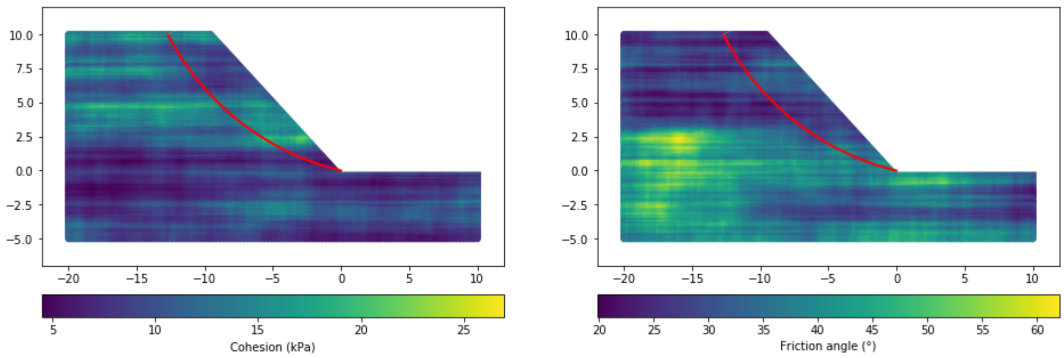

(b)

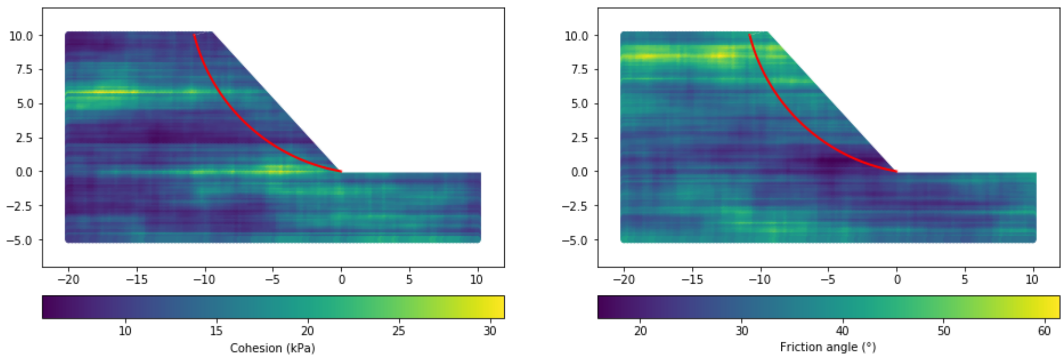

(c)

FIGURE 3.16: Typical realizations of random fields (ρ=-0.5, θ_h=20 m,θ_v=2 m)

Because the correlation between different failure surfaces are quite high (almost all the slip surfaces go across the toe and stay above the base of the slope, as shown in Figure 3.16), the results from the fixed deterministic critical surface are very close to the system analysis results by RF-MCS method.

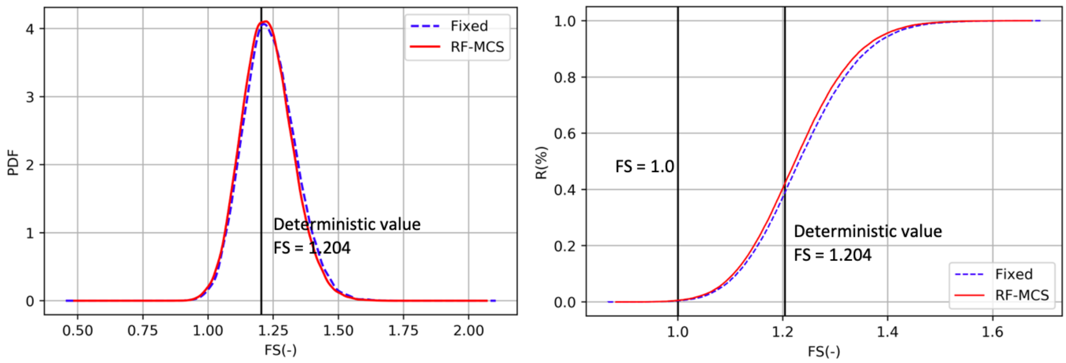

FIGURE 3.18: Probability density function (left) and cumulative distribution of the factor of safety (right)

Table 3.11 summarised the study of the effect of varying the cross correlation coefficient between c and ϕ.

$\rho_{c\phi}$	Deterministic	$\mu_{FS_{min}}$	$\sigma_{FS_{min}}$	$COV_{FS_{min}}$
-0.7	1.204	1.2284	0.0790	0.0643
-0.5	1.204	1.2269	0.0967	0.0788
-0.25	1.204	1.2265	0.1159	0.0945
0	1.204	1.2217	0.1330	0.1089
0.25	1.204	1.2229	0.1462	0.1196
0.5	1.204	1.2169	0.1577	0.1296

TABLE 3.11: Influence of correlation coefficient on the statistical response

Figure 3.19 shows the probability density functions and the cumulative distributions of the factor of safety.

The narrower trend of the probability density function can be observed when cross correlation coefficient values decreased. This trend is also the same as the finding reported by (Cho, 2009) which can also verify the RF-MCS method from another point of view.

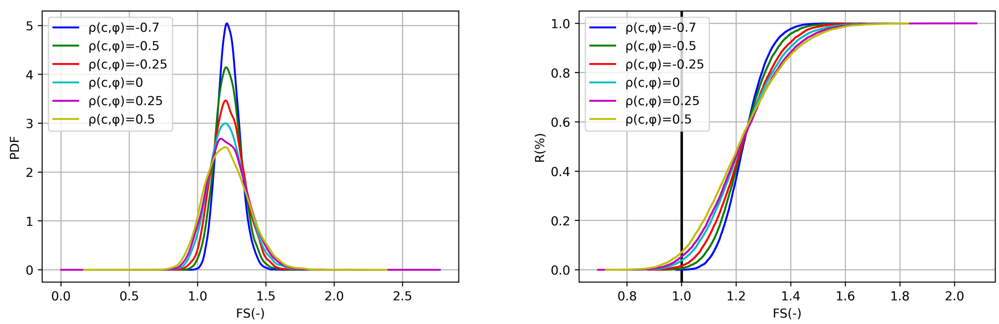

FIGURE 3.19: Distribution of F_{min} for correlation coefficient; PDF (left) and CDF (right)

3.6 Discussion

As one of the main features of this new proposed RF-MCS method, the combination of LEM and random fields allows us to visualise various failure mechanisms against the distribution of random fields. Various failure mechanisms caused by the inherent spatial variability of soil properties can not be manifested by the deterministic analysis. Instead of analyzing the fixed deterministic critical failure circle, the program can locate the probabilistic critical failure circle by the search algorithm. The degree of variation of different failure mechanisms depends on the correlation between different potential slip surfaces. When the correlation is low, different failure mechanisms will change greatly (as indicated in the slope with only cohesion). When the correlation is high, different failure mechanisms behave similarly to each other (as indicated in the c-ϕ slope).

3.7 Summary

This chapter verified the Python program of this proposed RF-MCS method. The verification of the deterministic model is performed by the commercial software D-Geo stability and the results given by (Cho, 2009). The verification is based on the critical failure surface located and the corresponding factor of safety derived.

- For the slope with only cohesion, the geometry of the critical slip surface selected by 3 programs and the corresponding factor of safety are the same.
- For the c-ϕ slope, D-Geo stability cannot locate the critical slip surface due to the circle just cross the toe and go deep to the base of the slope. But the results from the Python program are consistent with that given by (Cho, 2009).

Therefore, the accuracy of the deterministic model can be guaranteed.

The verification of the probabilistic model is mainly based on the results given by (Cho, 2009) and (Jiang et al., 2015) who performed the investigation using similar methods. The verification is based on the calculated system probability of failure of the slope.

- Difference of results exist for both the slope with only cohesion and the c-ϕ slope. The difference might result from different methods used to generate the random field. This study used Cholesky decomposition with standard normal sampling method. But the study did by two other authors adopted KL expansion with Latin hypercube sampling method.
- However, some other findings from this probabilistic model are consistent with that from (Cho, 2009). That is, the probability of failure from a single slip surface can represent the system probability of failure of a slope only under the condition that the correlation between them are high enough. Similar results also have been found from the parametric study of the correlation coefficient for c-ϕ.

Thus, these findings can verify the probabilistic model.

Chapter 4

Comparison of 3 different Monte Carlo methods

The proposed RF-MCS method will be compared with Direct and Separate-Monte Carlo Simulation method (DS-MCS method) and Direct and Combined-Monte Carlo Simulation method (DC-MCS method) after the verification in the last chapter. The demonstration of the difference of these 3 methods will be elaborated theoretically and numerically.

4.1 Comparison based on a undrained clay slope ($\phi = 0$)

This section uses the proposed RF-MCS method and direct MCS method to analyze a undrained clay slope. Results are compared after the simulation process. The criterion of comparison of 3 MCS methods are the calculated probability of failure P_f and computational time needed for each method.

4.1.1 Initial input information

The slope and all the other input soil and domain parameters are keep constant as the benchmark analysis have done previously in section 3.4.1. Figure 4.1 gives the example analysis result from 3 MCS methods (Only one figure is shown for DS-MCS method and DC-MCS method since the visualisation of DS-MCS method and DC-MCS method is almost the same).

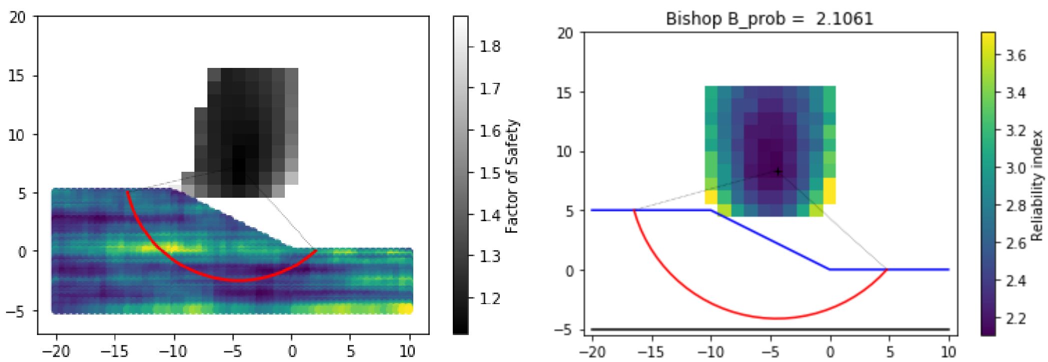

FIGURE 4.1: Schematic visualisation of the calculation from 3 MCS methods; RF-MCS method (left) and direct MCS method (right)

4.1.2 Analysis and results

Figure 4.2 shows the convergence of the simulation from 3 MCS methods. Table 4.1 summarised the results from 3 MCS methods. The last column k in the table indicate the relative difference of probability of failure P_f from different methods. It is calculated by the P_f from RF-MCS method divided by the P_f from DS-MCS method and DC-MCS method.

50,000 random fields have been generated for each MCS methods. Results have shown the overall probability of failure calculated by the RF-MCS method is more than twice as large as the P_f calculated by DS-MCS method and DC-MCS method. The RF-MCS method requires much longer computational time than direct MCS method. The computer used for the calculation is MacBook Air (2017) with 1.8 GHz dual-Core i5 CPU and 8GB of RAM.

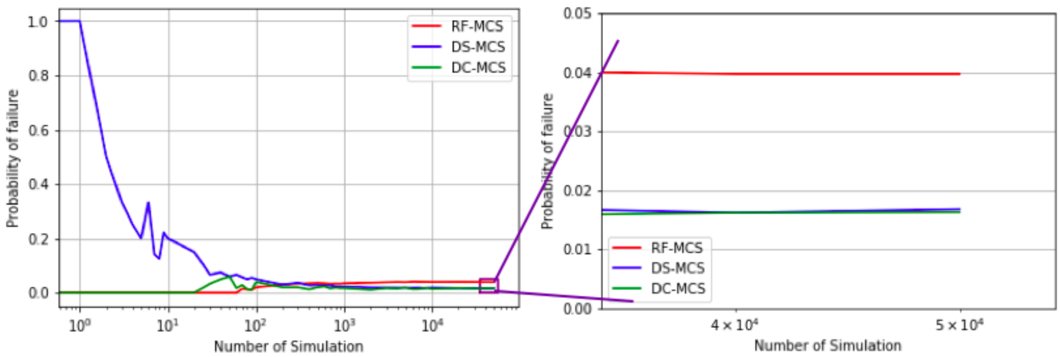

FIGURE 4.2: Convergence of probability of failure from 3 different methods

Method	P_f(-)	Computational time t(s)	k(-)
RF-MCS (50,000)	3.85×10^{-2}	0.95*50,000	-
DS-MCS (50,000)	1.68×10^{-2}	282	2.36
DC-MCS (50,000)	1.63×10^{-2}	135	2.44

TABLE 4.1: Results of 3 different methods

The effect of varying the number of slice division was investigated then and the results are shown in Figure 4.3. Table 4.2 summarised the results from 3 MCS methods. The column k1, k2 in the table are calculated by the P_f from RF-MCS method divided by the P_f from DS-MCS method and DC-MCS method, respectively. It can be observed the overall probability of failure calculated from 3 MCS methods are not largely influenced by the number of slice division. Therefore, the number of slice division is chosen to be 30 for all the following analysis in this section.

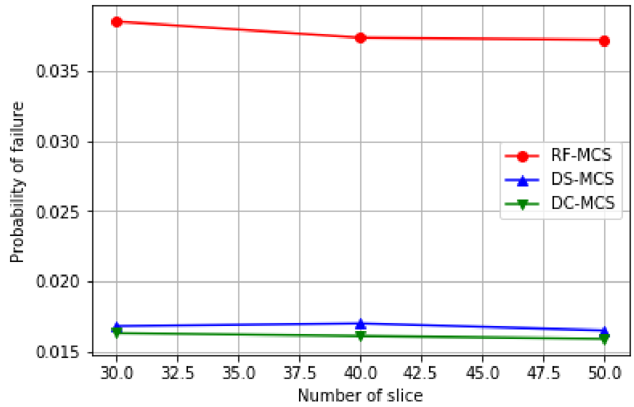

FIGURE 4.3: Influence of slice division on probability of failure from 3 different methods

Slice division	RF-MCS	DS-MCS	DC-MCS	k1(-)	k2(-)
30	0.0385	0.0168	0.0163	2.29	2.36
40	0.0374	0.017	0.0161	2.20	2.32
50	0.0372	0.0165	0.0159	2.25	2.34

TABLE 4.2: Influence of slice division on the results of 3 different methods

For RF-MCS method, the random values at the midpoint of each slice base are derived by linear interpolation. Because the extreme values at both tails of the distribution are removed during the interpolation procedure due to the averaging effect. This could be one of the reasons that causes the difference of the overall probability of failure.

Therefore, to demonstrate the value change during the interpolation procedure, the critical deterministic failure circle was reanalysed here. The basic geometry and all the other input soil and domain parameters are keep constant. The mesh density of the random field is 60×60.

Figure 4.4 shows the distribution of the cohesion value before and after the interpolation procedure. The result was derived after only 1 realisation. The sampling range of the distribution became narrower after the interpolation procedure (C.-C. Li and Der Kiureghian, 1993).

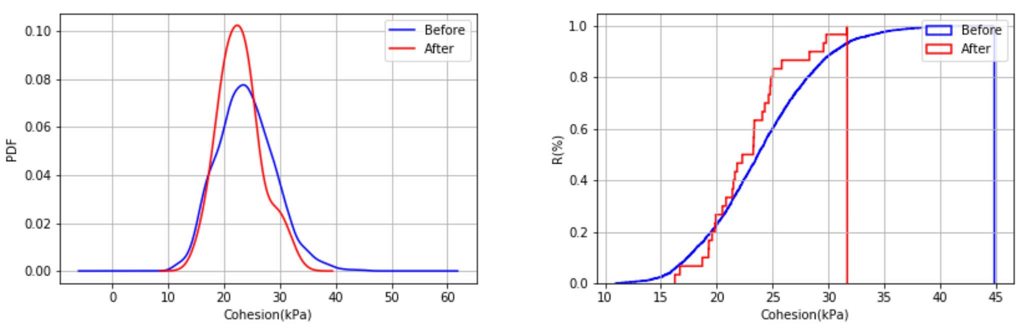

FIGURE 4.4: Distribution of Cohesion before and after interpolation; PDF (left) and CDF (right)

Then, this same critical deterministic failure circle was reanalysed by varying the density of mesh points. Figure 4.5 shows the distribution of the cohesion values from RF-MCS method for different density of the mesh points after the interpolation procedure. The distributions are compared with that from DS-MCS method and DC-MCS method. The result was derived after only 1 realisation. It can be observed that:

- The distributions of the cohesion values from RF-MCS method didn't follow the "perfect" lognormal distribution after the interpolation procedure.
- The distributions of the cohesion values from DS-MCS method and DC-MCS method are wider than that from RF-MCS method.
- The sampling range of the distribution from the RF-MCS method increased with the increasing density of the mesh points.

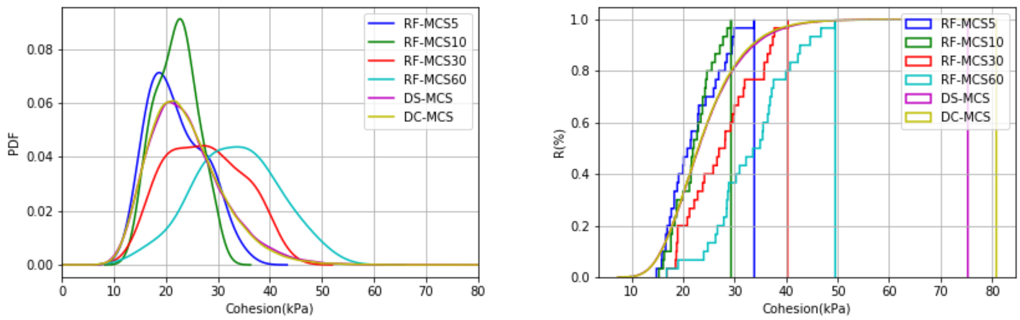

FIGURE 4.5: Distribution of Cohesion comparison; PDF (left) and CDF (right)

The effect of varying the density of mesh points was investigated at last. The results are shown in Figure 4.6. Table 4.3 summarised the statistical results. It can be observed the overall probability of failure calculated by RF-MCS method has positive relationship with the density of the mesh points.

Mesh density of RF-MCS	P_f(-)	$\mu_{FS_{min}}$	$\sigma_{FS_{min}}$	$COV_{FS_{min}}$
$5 * 5$	2.89×10^{-2}	1.3732	0.2214	0.1612
$10 * 10$	3.24×10^{-2}	1.3566	0.2144	0.1580
$30 * 30$	3.60×10^{-2}	1.3424	0.2105	0.1568
$60 * 60$	3.85×10^{-2}	1.3396	0.2116	0.1579

TABLE 4.3: Influence of mesh density on the statistical response

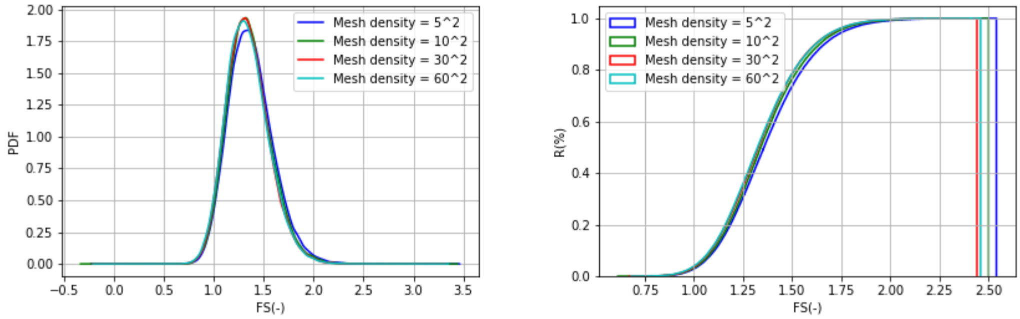

FIGURE 4.6: Distribution of F_{min} for mesh density; PDF (left) and CDF (right)

After demonstration of the influence of the mesh density of RF-MCS method, another finding about the system probability of failure from direct MCS method can be drawn.

For direct MCS method, the critical failure circle selected by probabilistic approach and deterministic approach is almost same (Table 4.4). This is different from RF-MCS method (the critical failure circle varies in each realisation when the correlation among different potential slip circle is low).

And the system probability of failure calculated by the search algorithm in probabilistic approach is also close to the probability of failure calculated from the fixed deterministic critical failure circle by probabilistic approach (Table 4.5). Figure 4.7 shows the convergence of the probability of failure by DS-MCS method and DC-MCS method from 2 different approaches.

Critical failure circle	x coordinate (m)	y coordinate (m)	radius (m)
Deterministic	-5.556	9.444	14.444
Probabilistic (DS-MCS)	-4.444	9.444	13.999
Probabilistic (DC-MCS)	-5.556	9.444	14.444

TABLE 4.4: Critical failure circle selected by direct MCS

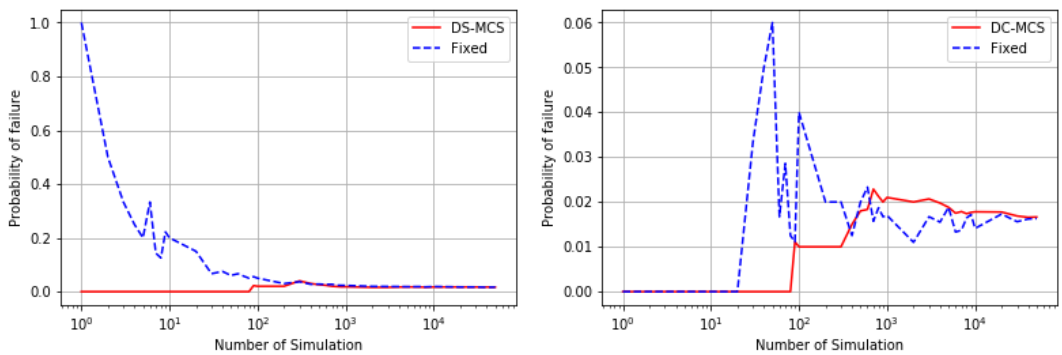

FIGURE 4.7: Probability of failure derived from 2 approaches; DS-MCS (left) and DC-MCS (right)

Approach	RF-MCS	DS-MCS	DC-MCS
Search (50,000)	3.85×10^{-2}	1.68×10^{-2}	1.63×10^{-2}
Fixed (50,000)	1.48×10^{-2}	1.68×10^{-2}	1.66×10^{-2}

TABLE 4.5: Probability of failure from different approach

It can be noticed that the system probability of failure calculated by the search algorithm from DC-MCS method (0.0163) is even smaller than the probability of failure calculated by the single fixed deterministic critical failure cirlce (0.0166). This finding is different from the result by RF-MCS method (the system probability of failure is larger than the probability of failure from the fixed deterministic critical failure circle). It can demonstrate that different definition of the system probability of failure can yield different results.

4.2 Comparison based on a c-ϕ slope

A c-ϕ slope was analysed in this section using the proposed RF-MCS method, DS-MCS method and DC-MCS method. Results are compared after the simulation process. The criterion of comparison of 3 MCS methods are the calculated probability of failure P_f and computational time needed for each method.

4.2.1 Initial input information

The slope and all the other input soil and domain parameters are keep constant as the benchmark analysis have done previously in section 3.5.1. Figure 4.8 shows the example analysis result from 3 MCS methods (Only one figure is shown for DS-MCS method and DC-MCS method since the visualisation of DS-MCS method and DC-MCS method is almost the same).

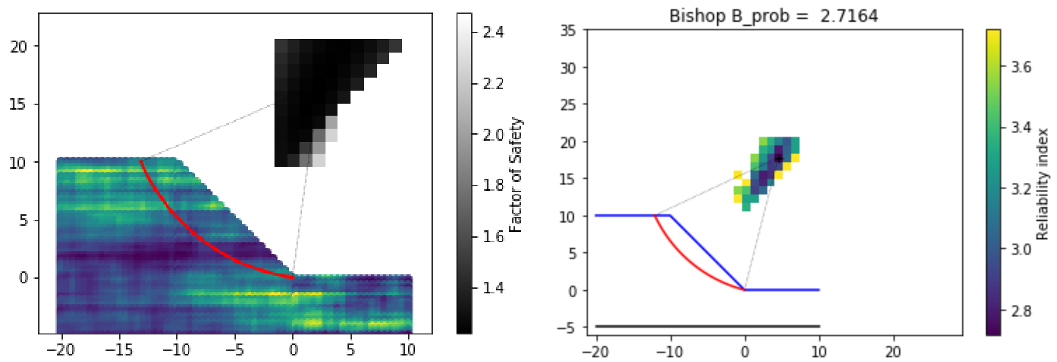

FIGURE 4.8: Schematic visualisation of the calculation from 3 MCS methods; RF-MCS method (left) and direct MCS method (right)

4.2.2 Analysis and results

Figure 4.9 shows the convergence of the simulation from 3 MCS methods. Table 4.6 summarised the results from 3 MCS methods. The last column k in the table indicate the relative difference of probability of failure P_f from different methods. It is calculated by the P_f from RF-MCS method divided by the P_f from DS-MCS method and DC-MCS method.

50,000 random fields have been generated for each MCS methods. Results have shown the overall probability of failure calculated by the RF-MCS method is more than twice larger than the P_f calculated by DS-MCS method and DC-MCS method. The computational time needed for RF-MCS method is way more longer than DS-MCS method and DC-MCS method.

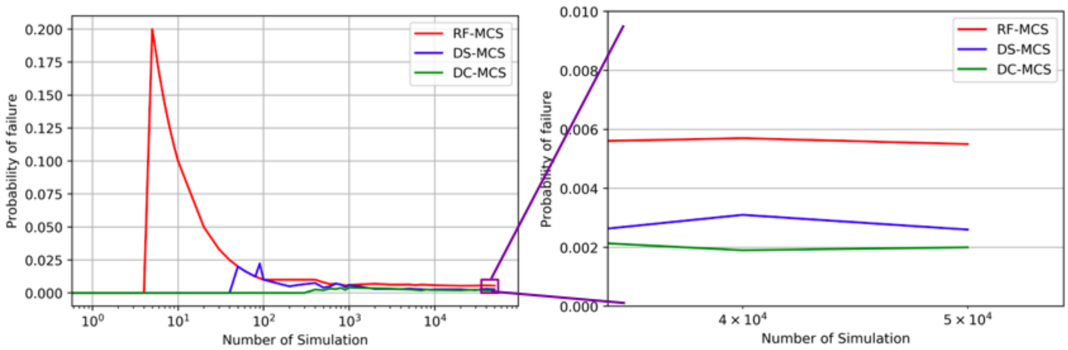

FIGURE 4.9: Convergence of probability of failure from 3 different methods (ρ = -0.5)

Method	P_f(-)	Computational time t(s)	k(-)
RF-MCS (50,000)	5.5×10^{-3}	0.95*50000	-
DS-MCS (50,000)	2.3×10^{-3}	420	2.39
DC-MCS (50,000)	2.0×10^{-3}	414	2.75

TABLE 4.6: Results of 3 different methods

The effect of varying the number of slice division was investigated and the results are shown in Figure 4.10. Table 4.7 summarised the results from 3 MCS methods. The column k1, k2 in the table are calculated by the P_f from RF-MCS method divided by the P_f from DS-MCS method and DC-MCS method, respectively. It can be observed the overall probability of failure calculated from 3 MCS methods are not largely influenced by the number of slice division.

Slice division	RF-MCS	DS-MCS	DC-MCS	k1(-)	k2(-)
30	0.0055	0.0023	0.0020	2.35	2.75
40	0.0054	0.0021	0.0020	2.57	2.70
50	0.0051	0.0022	0.0022	2.32	2.32

TABLE 4.7: Influence of slice division on the results of 3 different methods

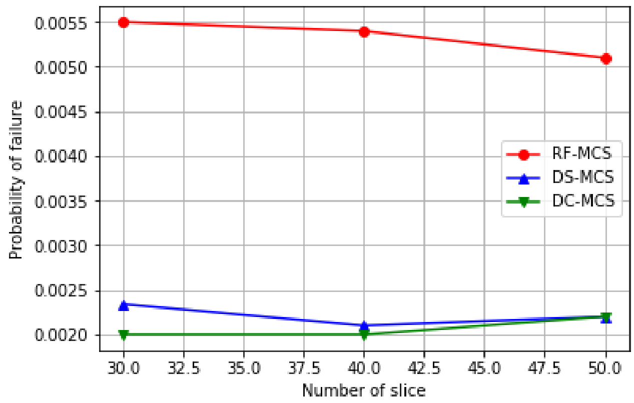

FIGURE 4.10: Influence of slice division on probability of failure from 3 different methods

In order to further investigate what causes the difference of the overall probability of failure, a fixed slip surface is reanalysed by 3 MCS methods. The assumed slip circle here is the critical failure circle selected by the deterministic analysis in Section 3.1.2.

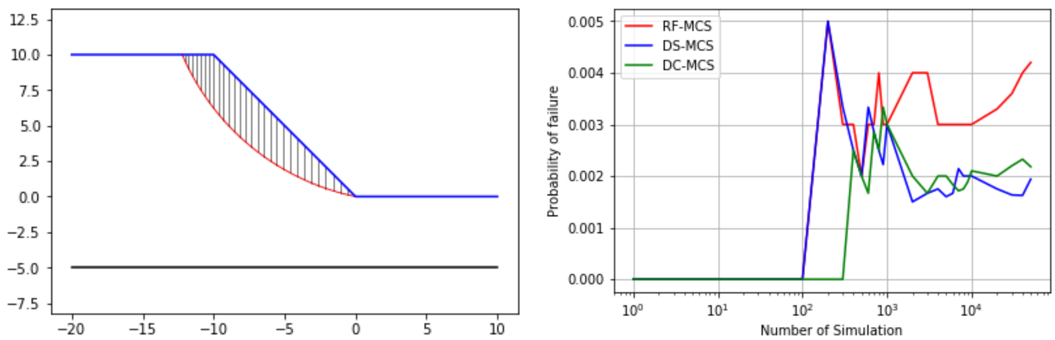

FIGURE 4.11: Slip circle geometry (left) and corresponding convergence of probability of failure (right)

Method	P_f(-)	$\mu_{FS_{min}}$	$\sigma_{FS_{min}}$	$COV_{FS_{min}}$	k(-)
RF-MCS (50,000)	4.2×10^{-3}	1.2359	0.0988	0.0799	-
DS-MCS (50,000)	2.1×10^{-3}	1.2358	0.0913	0.0739	2.0
DC-MCS (50,000)	2.0×10^{-3}	1.2354	0.0914	0.0740	2.1

TABLE 4.8: Results of 3 different methods from fixed failure circle

Results have shown that the probability of failure P_f calculated by RF-MCS method for this single circle is larger than that derived by DS-MCS method and DC-MCS method. This trend is consistent with the that from the overall probability of failure.

The effect of varying the density of mesh points was investigated at last and the results are shown in Figure 4.12. Table 4.9 summarised the statistical results. It can be observed the overall probability of failure calculated by RF-MCS method increased with the increasing density of the mesh points. However, the resultant difference is smaller compared with that from the slope with only cohesion.

Mesh density of RF-MCS	P_f(-)	$\mu_{FS_{min}}$	$\sigma_{FS_{min}}$	$COV_{FS_{min}}$
$5 * 5$	4.86×10^{-3}	1.2317	0.0994	0.0807
$10 * 10$	4.86×10^{-3}	1.2292	0.0979	0.0796
$30 * 30$	5.05×10^{-3}	1.2273	0.0972	0.0792
$60 * 60$	5.23×10^{-3}	1.2271	0.0969	0.0790

TABLE 4.9: Influence of mesh density on the statistical response

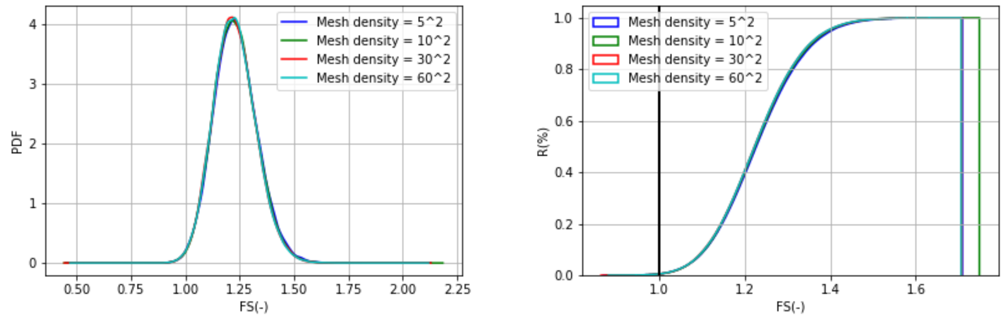

FIGURE 4.12: Distribution of F_{min} for mesh density; PDF (left) and CDF (right)

For direct MCS method, the critical failure circle selected by probabilistic approach and deterministic approach is almost same (Table 4.10). This is same as RF-MCS method when the correlation between potential slip circles are high. And the difference between the system probability of failure calculated by the search algorithm in probabilistic approach and the probability of failure calculated from the fixed deterministic critical failure circle by probabilistic approach is very small (Table 4.11). Figure 4.13 shows the convergence of the probability of failure by DS-MCS method and DC-MCS method from 2 different approaches.

Critical failure circle	x coordinate (m)	y coordinate (m)	radius (m)
Deterministic	3.444	16.667	17.019
Probabilistic (DS-MCS)	2.333	15.556	15.730
Probabilistic (DC-MCS)	2.333	14.444	14.632

TABLE 4.10: Critical failure circle selected by direct MCS method

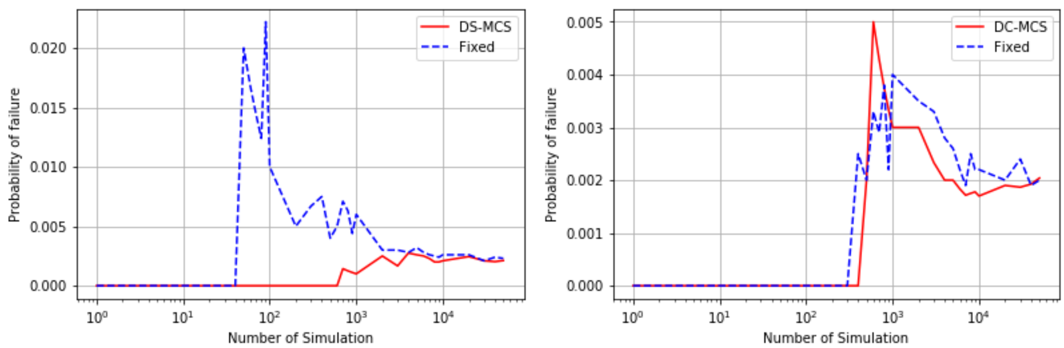

FIGURE 4.13: Probability of failure derived from 2 approaches; DS-MCS method (left) and DC-MCS method (right)

Approach	RF-MCS	DS-MCS	DC-MCS
Search (50,000)	5.5×10^{-3}	2.3×10^{-3}	2.0×10^{-3}
Fixed (50,000)	4.2×10^{-3}	2.1×10^{-3}	2.0×10^{-3}

TABLE 4.11: Probability of failure from different approach

However, the system probability of failure calculated by direct MCS method is still smaller than that from RF-MCS method. Combined with the findings from the previous case for the slope with only cohision, it can draw the general conclusion:

The main cause of the difference in the probability of failure P_f from 3 MCS methods is the fundamental definition of the system probability of failure of a slope or the methodology used by the proposed RF-MCS method and direct MCS method to calculate the system probability of failure.

4.3 Discussion

The influence of the level of mesh density was tested when investigated what causes the difference of the results from RF-MCS method and direct MCS method. Four level of mesh density was considered. P_f from RF-MCS method increased with finer meshes which is opposite to RFEM (probability of failure decreased with smaller random field mesh sizes). This increasing trend decreased by increasing the mesh density. For the slope with only cohesion, this trend decreased from 11% to 6.5%. For the c-ϕ slope, this trend decreased from 3.7% to 3.4%. This means that the calculated probability of failure will reach convergence by increasing the mesh density. However, the current setting of the laptop used cannot satisfy further finer meshes.

4.4 Summary

This chapter compared the accuracy and efficiency of RF-MCS method with direct MCS method. The comparison is mainly based on the probability of failure and the computational time. 2 different types of slope was analysed: a undrained clay slope with only cohesion and a c-ϕ slope. Different results have been found from 3 MCS methods. Parametric studies have been carried out to find out where the difference came from. Some findings can be drawn after the analysis:

1. Difference in the probability of failure from RF-MCS method and direct MCS method results from how the random values assigned onto each potential slip circle. There is a slight difference in the result between DS-MCS method and DC-MCS method which can be neglected.

2. The difference of the system probability of failure calculated by 3 MCS methods decreases with the decreasing mesh density of the random field in RF-MCS method. This degree of reduction is more significant for the slope with only cohesion than the c-ϕ slope.

3. RF-MCS method spends much more computational time than direct MCS method. Because, for RF-MCS method, the random field is generated first and then the random values are assigned onto each potential slip circle by linear interpolation. The results reach convergence after repeating multiple times. For direct MCS method, the random fields can be generated with the same amount as RF-MCS method. But the random values are directly assigned onto each potential slip surface which save much the computational efforts.

4. The random field for RF-MCS method is generated before assigning the slip circles. It keeps constant and each potential slip circle only draw the random values from it by linear interpolation. However, the random field for direct MCS method is "circle dependent". The random values generated are influenced by the geometry of the circle. More specifically, it depends on the coordinate of midpoints of each slice of the circle. So, it differs from circle to circle.

5. For the slope with only cohesion, 3 MCS methods calculate different results for the system probability of failure and the probability of failure for a single slip surface. For the system probability of failure, the result from RF-MCS method is larger than that from direct MCS method. However, opposite result has derived when it deals with a single slip surface.

6. For the c-ϕ slope, RF-MCS method calculates larger value of probability of failure than direct MCS method both for the system probability of failure and the P_f from a single slip surface.

7. The main cause of the difference in the probability of failure P_f from 3 MCS methods is the fundamental definition of the system probability of failure of a slope or the methodology used by the proposed RF-MCS method and direct MCS method to calculate the system probability of failure.

Chapter 5

Parametric study of 3 different Monte Carlo methods

In order to further investigate the influence of the spatial variability of soil properties, a series of parametric studies are performed in this chapter to investigate the application of 3 methods to different cases. The parametric studies aim to identify cases that 3 methods derive similar numerical results or to what extent the results behave similar trend. The test scenarios include the slope angle, autocorrelation distance, coefficient variation of strength parameters and cross-correlation between cohesion and friction angle.

5.1 Study based on a undrained clay slope ($\phi = 0$)

The geometry of four slopes are shown in Figure 5.1. The height of the slope is keep constant as 5 m. The slope angle β^* is equal to 26.6°, 45°, 55° and 63.5° for the four different slopes. Other input soil and domain parameters are given in Table 5.1.

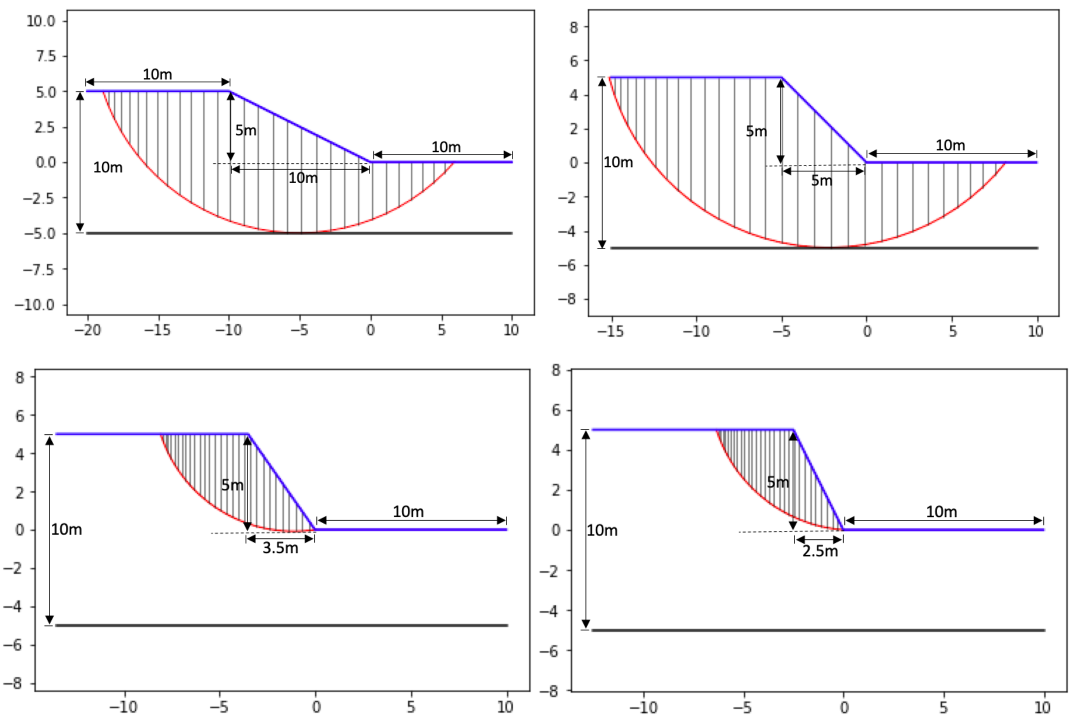

FIGURE 5.1: Slope geometry for different slope angles β^* from top left to bottom right: (a) β^*= 26.6°, (b) β^*= 45°, (c) β^*= 55°, (d) β^*= 63.5°

Parameter	Value	Unit
Cohesion (c)(COV=0.3)	23	(kPa)
Unit weight (γ)	20	(kN/m^3)
Density of random field mesh	60*60	(-)
Horizontal autocorrelation distance (θ_h)	20	(m)
Vertical autocorrelation distance (θ_v)	2	(m)

TABLE 5.1: Initial input parameters for the undrained slope

5.1.1 Pre-analysis

Because the computational time of Random Field - Monte Carlo Simulation method (RF-MCS method) has been largely influenced by the iteration times, this section aims to identify the adequate number of iterations needed to make the probability of failure reach convergence.

Figure 5.2 shows the convergence of probability of failure with the increasing iteration times. The results are derived from the undrained slope when the slope angle β^*= 26.6°. All the other parameters keep constant as given in Table 5.1, only the vertical autocorrelation distance θ_v varying from 1 m to 4 m.

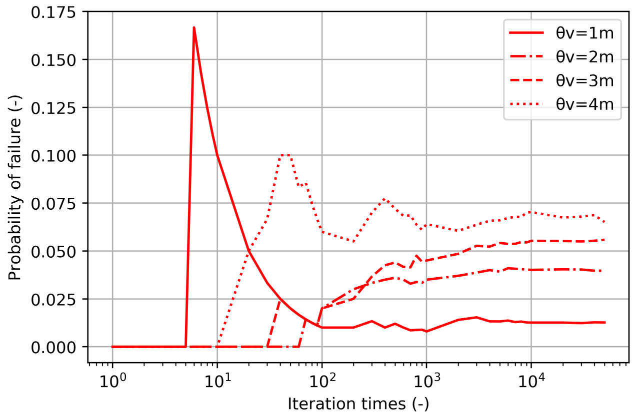

FIGURE 5.2: Convergence of probability of failure vs. iteration times

It can be observed 4,000 iterations are sufficient to guarantee the convergence of the probability of failure. Therefore, all the rest analysis for the undrained slope with only cohesion will be tested 4,000 iterations.

5.1.2 Influence of slope angle

The factor of safety FS of the slope decreases with the increasing slope angle β^*. Therefore, the slope angle is also considered as an influential factor in the probability of failure of the slope. This section uses 3 methods to analyze four different slopes in probabilistic approach. The factor of safety FS of these four slopes from deterministic analysis are 1.356, 1.299, 1.260 and 1.173, respectively. Figure 5.3 shows the results derived from 3 methods. The probability of failure are calculated by the basic parameters given in Table 5.1.

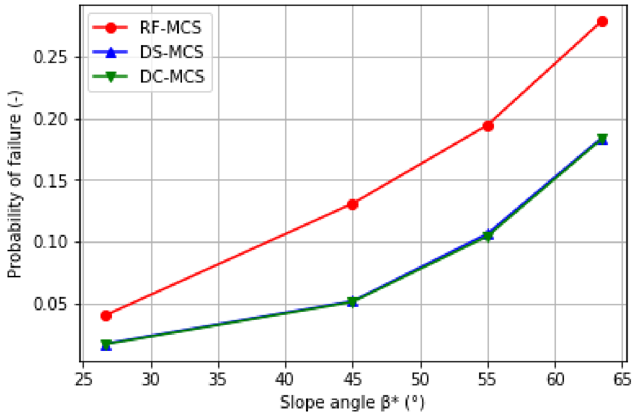

FIGURE 5.3: Probability of failure from 3 different methods vs. slope angle

The results indicate that the probability of failure of the undrained slope increases by increasing the slope angle. And this increasing trend keeps constant for all 3 methods.

5.1.3 Influence of autocorrelation distance

This section tests the influence of the autocorrelation distance on the probability of failure of the undrained slope. According to (El-Ramly et al., 2002), the reasonable horizontal autocorrelation distance fluctuates between 10 $\sim$ 40m, and 1 $\sim$ 3 m in the vertical direction. However, some extreme cases are also taken into consideration in the following analysis.

Thus, the horizontal autocorrelation distance θ_h is chosen as 2 m, 5 m, 10 m, 20 m, 30 m, 40 m, 80 m and 200 m. And the vertical autocorrelation distance θ_v keeps constant as 2 m when investigate the influence of the horizontal autocorrelation distance θ_h.

Also, the horizontal autocorrelation distance θ_h keeps constant as 20 m when investigate the vertical autocorrelation distance θ_v. θ_v is set to be 0.5 m, 1 m, 2 m, 3 m, 4 m, 20 m and 200 m in the analysis.

Figure 5.4 shows the influence of the autocorrelation distance on the probability of failure of the undrained slope. It can be observed that the probability of failure increased with the increasing autocorrelation distance both in horizontal and vertical direction for all 3 methods. This increasing trend tends to be more gentle as the slope becomes more steep. And the probability of failure is more sensitive to the vertical autocorrelation distance θ_v than the horizontal autocorrelation distance θ_h.

Here introduce another definition, the worst-case autocorrelation distance. (Fenton and Griffiths, 2003) defined the worst-case autocorrelation distance as the critical autocorrelation distance that gives the maximum probability of failure for the slope.

When slope angle β^*= 26.6°, the worst-case autocorrelation distance occured when θ_h equals to 80 m and θ_v approaches infinity for RF-MCS method. For direct MCS method, this increasing trend kept constant by increasing the autocorrelation distance both in horizontal and vertical direction. This means that the worst-case autocorrelation distance all approaches infinity.

When slope angle β^*= 45°, 55° and 63.5°, the increasing trend only existed within the range of reasonable autocorrelation distance for all 3 methods. When autocorrelation distance exceeded the reasonable range, the probability of failure will keep constant while further increase the autocorrelation distance.

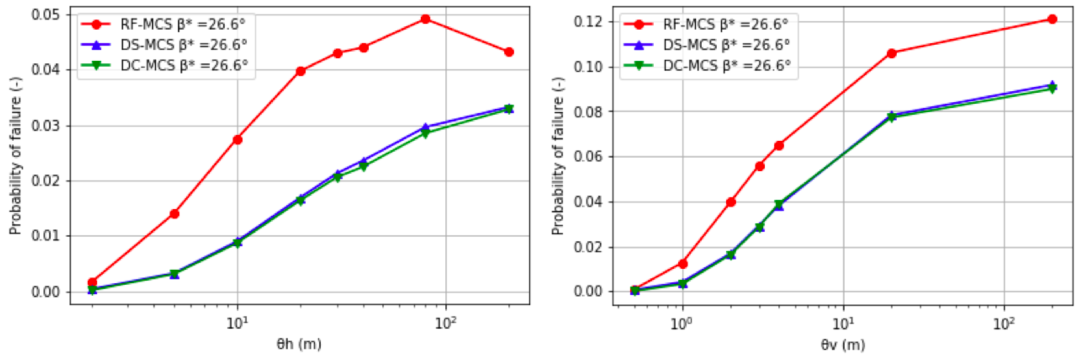

((a) β^{*}= 26.6°)

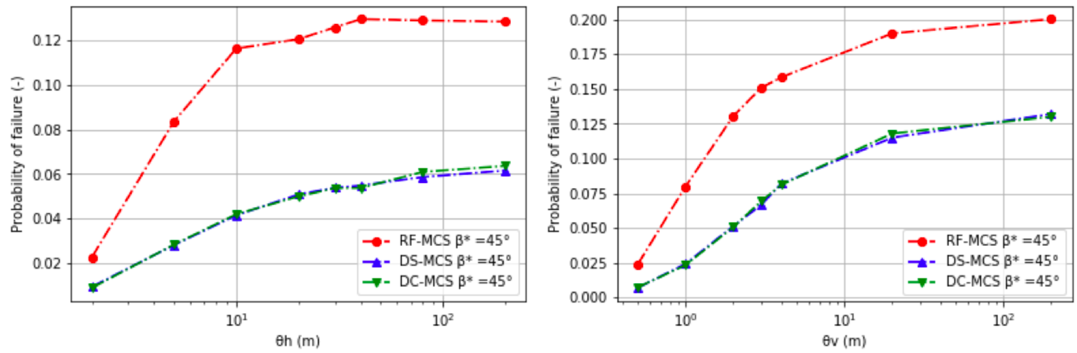

((b) β^{*}= 45°)

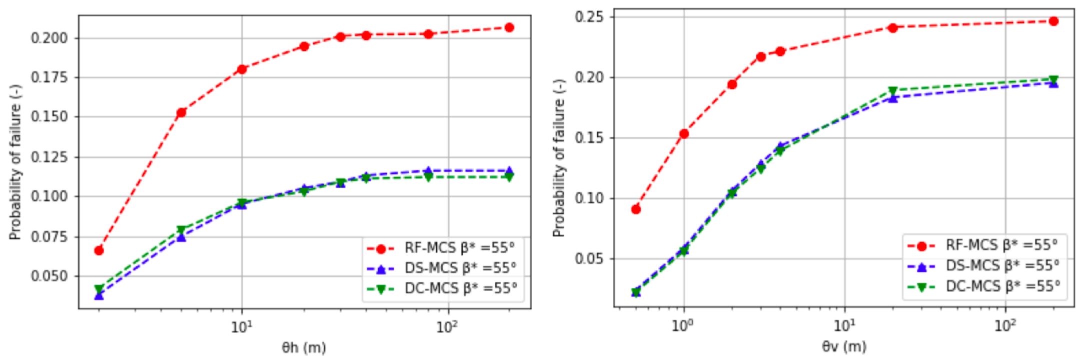

((c) β^{*}= 55°)

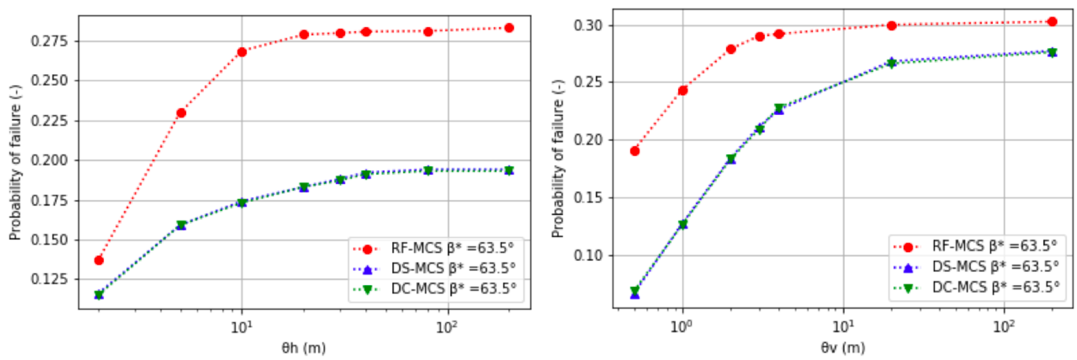

((d) β^{*}= 63.5°)

FIGURE 5.4: Probability of failure from 3 different methods vs. auto-correlation distance; Influence of θ_h (left) and θ_v (right)

5.1.4 Influence of coefficient of variation of strength parameters

To test the influence of the coefficient of variation of cohesion c on the probability of failure of the undrained slope, the COV of cohesion c is chosen as 0.2, 0.3, 0.4, 0.5 and 0.6 for four different slopes.

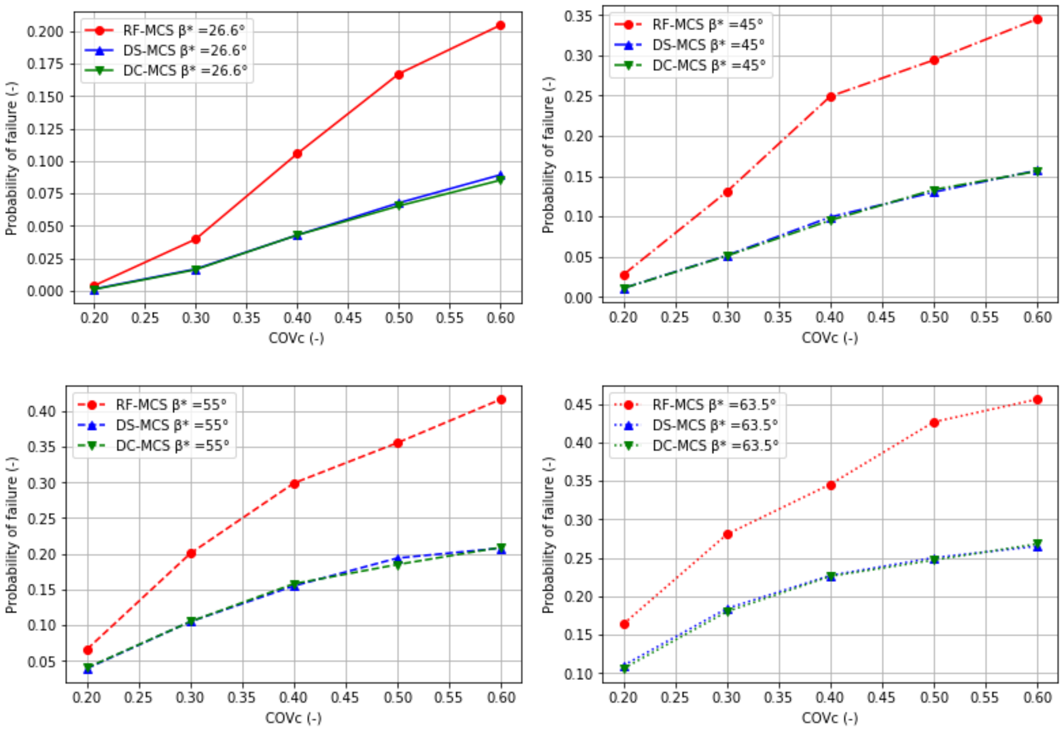

FIGURE 5.5: Probability of failure from 3 different methods vs. coefficient of variation; from top left to bottom right: (a) $\beta^*= 26.6°$, (b) $\beta^*= 45°$, (c) $\beta^*= 55°$, (d) $\beta^*= 63.5°$

Figure 5.5 shows the probability of failure from 3 different methods. As it can be observed, the probability of failure increased with the increasing COV of cohesion c for all four different slopes. The value of probability of failure corresponding to COV equals to 0.1 is too small, so it doesn't show in the plot.

5.2 Study based on a c-ϕ slope

The geometry of three c-ϕ slopes chosen for the analysis are shown in Figure 5.6. The height of the slope is keep constant as 10 m. The slope angle β^* is equal to 45°, 55° and 63.5° for the three different slopes. Other input soil and domain parameters are given in Table 5.1.

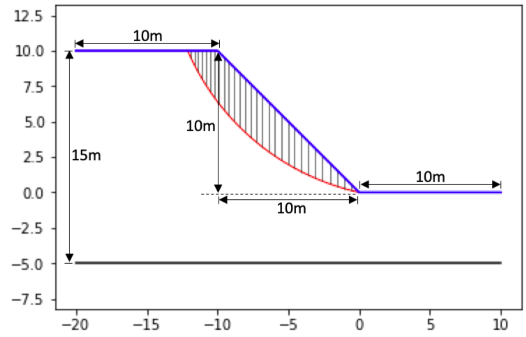

(a)

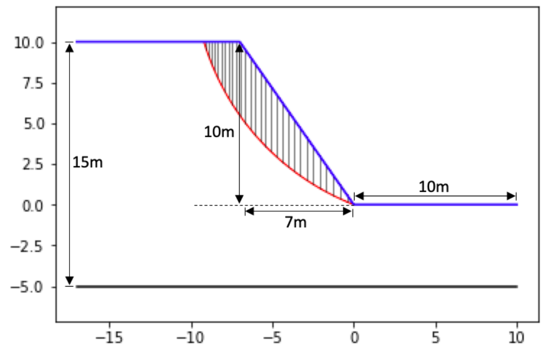

(b)

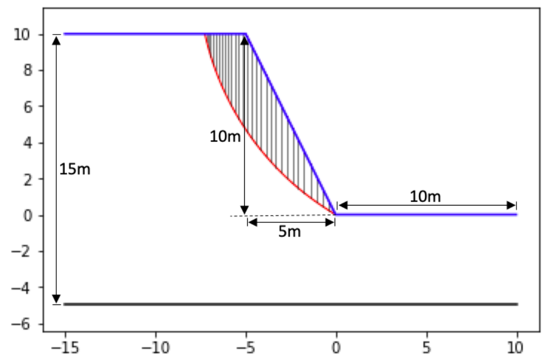

(c)

FIGURE 5.6: Slope geometry for different slope angles β^*: (a) $\beta^*= 45°$, (b) $\beta^*= 55°$, (c) $\beta^*= 63.5°$

Parameter	Value	Unit
Cohesion (c)(COV=0.3)	10	(kPa)
Friction angle (ϕ)(COV=0.2)	30	$(\circ)$
Unit weight (γ)	20	(kN/m^3)
$\rho_{c\phi}$	-0.5	(-)
Density of random field mesh	60*60	(-)
Horizontal autocorrelation distance (θ_h)	20	(m)
Vertical autocorrelation distance (θ_v)	2	(m)

TABLE 5.2: Initial input parameters for the c-ϕ slope

5.2.1 Pre-analysis

This section aims to identify the adequate number of iterations needed to render the probability of failure reach convergence for the c-ϕ slope.

Figure 5.7 shows the convergence of probability of failure with the increasing iteration times. The results are derived from the c-ϕ slope when the slope angle β^*= 45 °. All the other parameters keep constant as given in Table 5.2, only vertical autocorrelation distance θ_v varying from 1 m to 4 m.

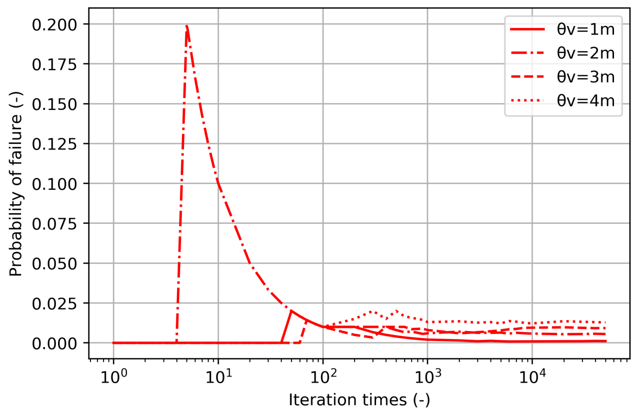

FIGURE 5.7: Convergence of probability of failure vs. iteration times

It can be observed 2,000 iterations are sufficient to guarantee the convergence of the probability of failure. Therefore, all the rest analysis for the c-ϕ slope will be tested 2,000 iterations.

5.2.2 Influence of slope angle

Like undrained slope, the factor of safety of the c-ϕ slope also influenced by the slope angle. The factor of safety FS of these three slopes from deterministic analysis are 1.204, 0.993 and 0.849, respectively. Figure 5.8 shows the results derived from 3 methods. The probability of failure are calculated by the basic parameters given in Table 5.2. $k1$, $k2$ in the figure indicate the relative difference of probability of failure P_f from 3 different methods. It is calculated by the P_f from RF-MCS method divided by the P_f from DS-MCS method and DC-MCS method. It equals to 1.0 when all 3 methods calculate the same probability of failure.

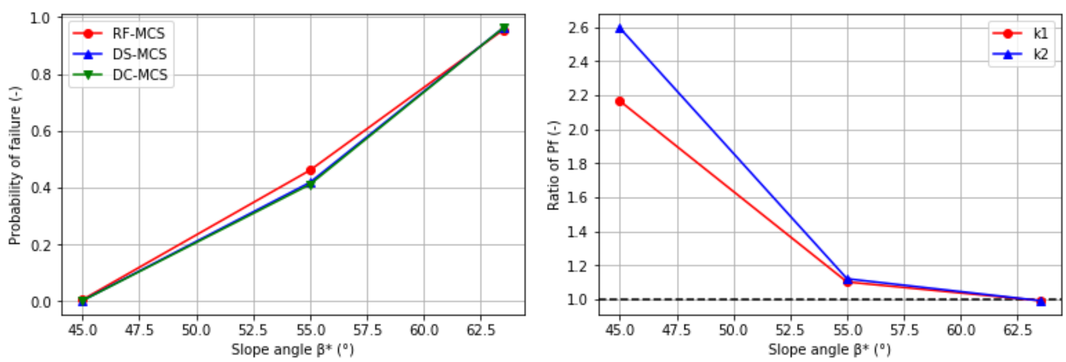

FIGURE 5.8: Probability of failure from 3 different methods vs. slope angle (left); Ratio of the probability of failure from 3 different methods vs. slope angle (right)

It can be observed that the probability of failure increased with the increasing slope angle. The difference of results between 3 different methods disappeared when the slope angle β^* larger than 62.5 °.

5.2.3 Influence of autocorrelation distance

Figure 5.9 shows the influence of the autocorrelation distance on the probability of failure of the c-ϕ slope. Unlike the undrained slope, the results didn't behave the same increasing trend for different slope angles. Instead, different results can be observed for three different slope angles.

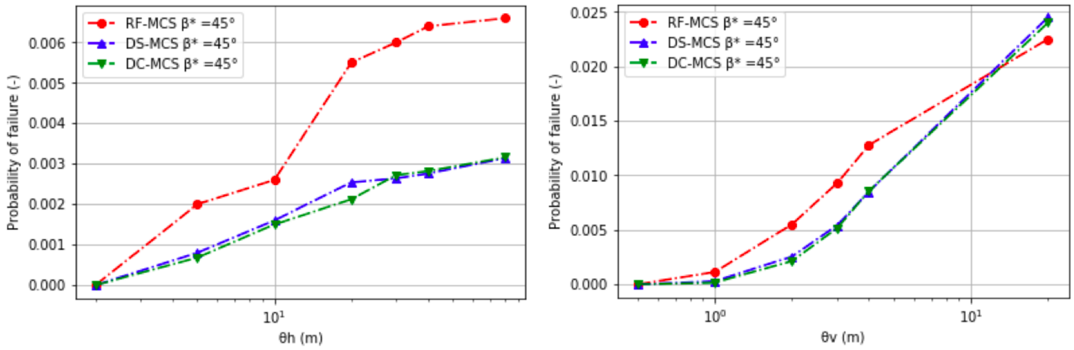

((a) β^*= 45°)

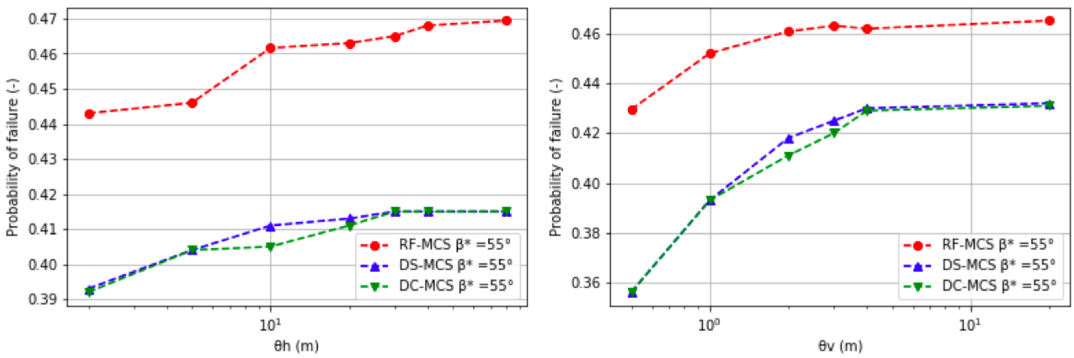

((b) β^*= 55°)

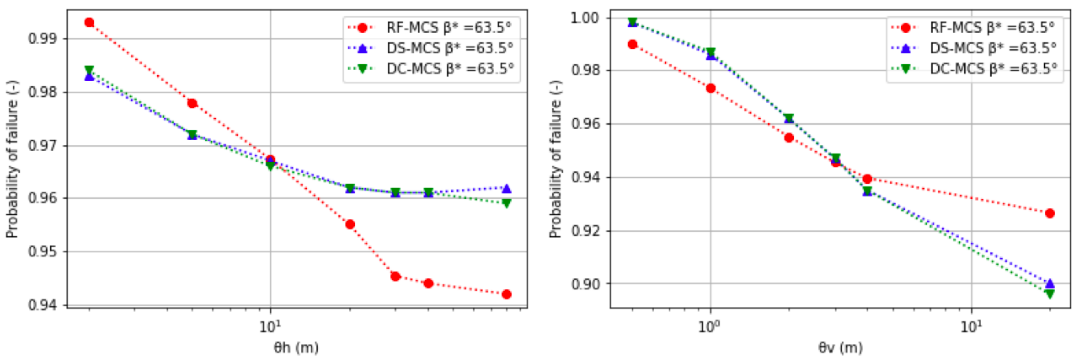

((c) β^*= 63.5°)

FIGURE 5.9: Probability of failure from 3 different methods vs. autocorrelation distance; Influence of θ_h (left) and θ_v (right)

When slope angle β^*= 45°, the probability of failure kept increasing with the increasing autocorrelation distance both in horizontal and vertical direction for all 3 methods. And the probability of failure is more sensitive to the vertical autocorrelation distance θ_v than the horizontal autocorrelation distance θ_h.

When slope angle β^*= 55°, the probability of failure increased with the increasing autocorrelation distance both in horizontal and vertical direction. But this increasing trend only existed within the range of reasonable autocorrelation distance for all 3 methods.

When slope angle β^*= 63.5°, the probability of failure decreased by increasing the autocorrelation distance both on horizontal and vertical direction. This indicated that the worst-case autocorrelation distance smaller than the reasonable range of the autocorrelation distance.

The overall trend of the probability of failure is similar with the results from the slope considering spatial variability of undrained cohesive strength and unit weight (Javankhoshdel, Luo, et al., 2017).

5.2.4 Influence of coefficient of variation of strength parameters

To test the influence of the coefficient of variation of cohesion c and friction angle ϕ on the probability of failure of the c-ϕ slope, the COV of cohesion c is chosen as 0.1, 0.2, 0.3, 0.4, 0.5 and 0.6 and the COV of friction angle ϕ is set to be 0.1, 0.2 and 0.3 for three different slopes. The COV of friction angle ϕ keeps constant as the value given in Table 5.2 when testing the influence of the COV of cohesion c, and vice versa.

Figure 5.10 shows the probability of failure from 3 different methods. The results didn't behave the same increasing trend as the one shown in the undrained slope. Instead, different results can be observed for three different slope angles.

When slope angle β^*= 45°, the probability of failure decreased first and kept increasing as the COV of cohesion c varying from 0.1 to 0.6. But the COV of the friction angle ϕ has a positive relationship with the probability of failure.

When slope angle β^*= 55°, the probability of failure decreased by increasing the COV of cohesion c and the friction angle ϕ. And this decreasing trend kept constant as the value of COV increased.

When slope angle β^*= 63.5°, the probability of failure decreased by increasing the COV of cohesion c and the friction angle ϕ. And the decreasing trend tends to be stronger as the value of COV increased.

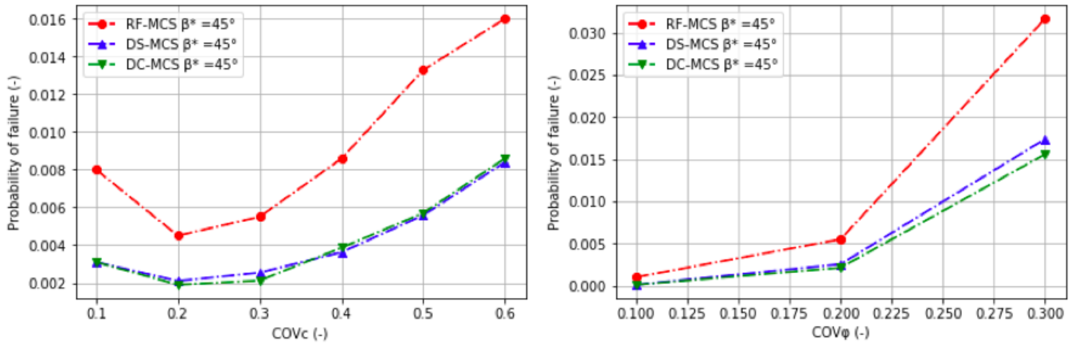

((a) β^*= 45°)

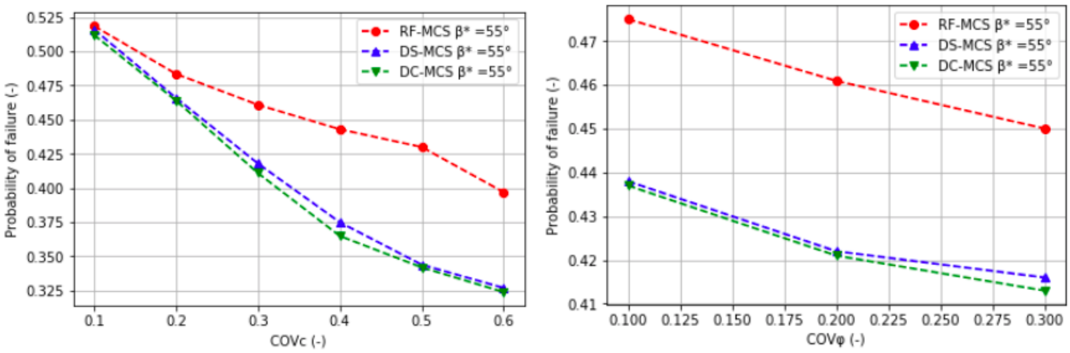

((b) β^*= 55°)

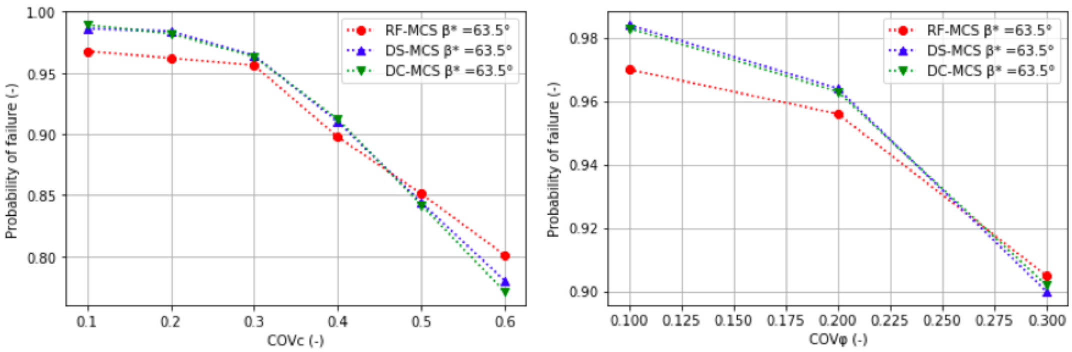

((c) β^*= 63.5°)

FIGURE 5.10: Probability of failure from 3 different methods vs. coefficient of variation; COV of cohesion c (left) and friction angle ϕ (right)

5.2.5 Influence of correlation coefficient

To test the influence of the cross-correlation between c and ϕ, all the other parameters keep constant as given in Table 5.2 and $\rho_{c\phi}$ varying from -0.7 to 0.7. The slope chosen for the analysis is the one with the slope angle β^*= 45°.

The effect of varying the cross correlation between c and ϕ on the simulation results are summarised in Table 5.3. Figure 5.11 shows the overall probability of failure calculated from 3 MCS methods against the cross correlation.

$\rho_{c\phi}$	RF-MCS	DS-MCS	DC-MCS	k1	k2
-0.7	0.0004	0.0002	0.0002	2.00	2.00
-0.5	0.0052	0.0025	0.0025	2.08	2.08
-0.25	0.0163	0.010	0.0086	1.63	1.90
0	0.038	0.0204	0.0218	1.86	1.74
0.25	0.0544	0.0341	0.032	1.60	1.70
0.5	0.0716	0.0476	0.0472	1.50	1.52
0.7	0.0864	0.0597	0.0587	1.45	1.47

TABLE 5.3: Influence of correlation coefficient on the probability of failure

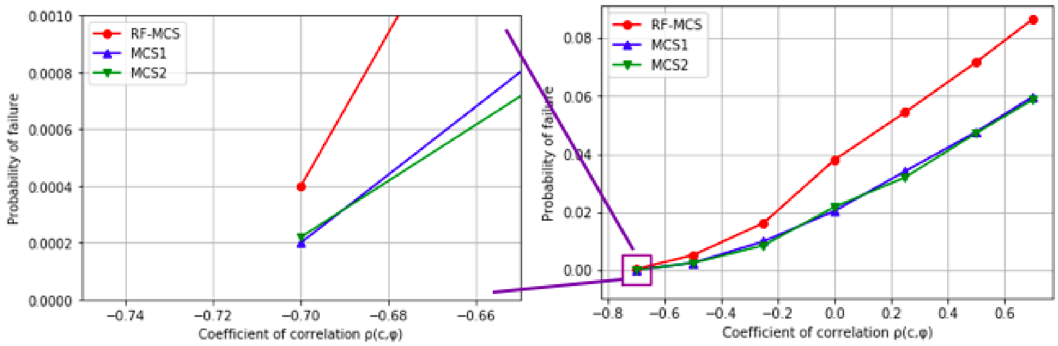

FIGURE 5.11: Influence of the cross correlation on the probability of failure

Results have shown that the difference between 3 MCS methods becomes lower when the correlation coefficient between c and ϕ increases. Thus, the assumption of positive relationship between c and ϕ will give higher results if the actual cross-correlation is negative.

5.3 Discussion

For all the tested scenarios, the difference of the calculated probability of failure between RF-MCS method and direct MCS method still existed. But the difference tend to be smaller by increasing the slope angle which means the probability of failure will increase. For the c-ϕ slope analyzed, the difference of results between 3 different methods disappeared when the slope angle β^* larger than 62.5°. However, the probability of failure corresponding to this critical slope angle was much greater than the acceptable value for engineering design.

For all 3 methods, the calculated probability of failure P_f behave similar trend by increasing different variables. And this trend was obviously manifested for the influence of autocorrelation distance. The probability of failure varied the most within the reasonable range of autocorrelation distance.

5.4 Summary

This chapter performed a wide range of parametric study using 3 different MCS methods. 2 different types of slopes were analysed: a undrained clay slope with only cohesion and a c-ϕ slope. Different results have been found from different cases with the application of these 3 methods. Some findings can be drawn after the analysis:

1. Probability of failure increased with the increasing slope angle both for the undrained slope with only cohesion and the c-ϕ slope. For the c-ϕ slope, the probability of failure calculated from 3 MCS methods get closer with the increasing slope angle.

2. For the influence of the autocorrelation distance, the probability of failure of the undrained slope with only cohesion increased with the increasing autocorrelation distance on both horizontal and vertical direction. The increasing trend tends to be gentle by increasing the slope angle. And the vertical autocorrelation distance θ_v is more sensitive than the horizontal autocorrelation distance θ_h. For the c-ϕ slope, the probability of failure from 3 analyzed slope behaved different trends.

3. For the influence of the coefficient of variation, the probability of failure of the undrained slope with only cohesion increased with the increasing value of COV. And this increasing trend keeps constant as the slope angle increases. For the c-ϕ slope, different slope angles behave different trends of the probability of failure.

4. For the influence of the correlation coefficient between c and ϕ, the probability of failure increases with the increasing value of $\rho_{c\phi}$. And the difference between 3 methods gets smaller by increasing the value of $\rho_{c\phi}$.

Chapter 6

Conclusions and recommendations

6.1 Conclusions

This study proposes three different MCS methods, which can consider the spatial variability of soil properties in probabilistic LEM analysis. Three different MCS methods have been tested in terms of accuracy and efficiency. The analysis is based on two types of slopes: the undrained slope with only cohesion and the c-ϕ slope. What causes the difference in the results from three methods has been investigated. In the end, parametric studies have been performed to test the robustness of these three methods. The report is written in the structure to answer the following research questions:

How to assign random field values onto each potential slip circle in three different MCS methods?

When formulating the probabilistic LEM model for these three MCS methods, a combination of Cholesky decomposition and midpoint method is used to generate random fields. The difference between RF-MCS method and direct MCS method is how to assign the random field values onto each potential slip circle. For direct MCS method, the correlation structure used in the Cholesky decomposition procedure depends on the coordinates of the midpoint of each slice base from each potential slip circle. The random field values are generated and directly assigned onto each potential slip circle. For RF-MCS method, the random field generation is irrelevant with the generation of the potential slip circle. The correlation structure depends on the rectangular mesh-grid whose domain matches the geometry of the slope. The random field values are generated and then map onto the rectangular mesh-grid. The value at the midpoint of each slice base is derived by linear interpolation from the mesh-grid.

How does the proposed RF-MCS method compared with two direct MCS methods in terms of accuracy and efficiency?

Based on the two types of slopes analyzed, the system probability of failure P_f calculated by RF-MCS method is more than twice as large as that by the direct MCS method. This difference implies that how the random fields are generated and how the random field values are assigned to each potential slip surface can significantly influence the statistical outcomes. For actual engineering practice, it is unacceptable that the relative difference between the results obtained by different methods exceeds 200%. The results from new proposed RF-MCS method are closer to the results given in the relevant literature. And considering the fundamental definition of the system probability of failure of a slope, RF-MCS method is more preferable to direct MCS method. However, RF-MCS method needs longer computational time to yield accurate results. Because the system probability of failure P_f requires multiple realisations to reach convergence. Instead, direct MCS method only needs one realisation to produce a decent result.

The parametric studies of two types of slopes show different results. For the undrained slope with only cohesion, the slope angle, autocorrelation distance and the COV of cohesion all have similar effects on P_f. That is, the P_f has a positive relationship with each corresponding variable. However, for the c-ϕ slope, there is the worst-case parameter that gives the highest probability of failure for different slope angles.

How is the robustness of 3 different MCS methods in different situations?

In different test scenarios, the results of the RF-MCS method and the direct MCS method shows the same growth trend while large difference still exist. The results indicate sensitivity analysis has nothing to do with using different methods and a combination of three methods is more efficient for future parameter studies.

There are also some other conclusions can be drawn in this study:

- For RF-MCS method, P_f derived by by combining the critical deterministic slip circle and the random fields is incorrect, and underestimates the system probability of failure of a slope. When the correlation between different potential slip circles increases, the difference between the P_f of the fixed slip circle and the system probability of failure of a slope decreases.

- For direct MCS method, since the methodology used to calculate the system probability of failure is different from RF-MCS method, there is no difference between the P_f of the deterministic slip circle and the system probability of failure of the slope.

- For RF-MCS method, the combination of LEM and random fields can visualise various failure mechanisms against the distribution of random fields. Various failure mechanisms caused by the inherent spatial variability of soil properties can not be manifested by the deterministic analysis. Instead of analyzing the fixed deterministic critical failure circle, the program can locate the probabilistic critical failure circle by the search algorithm. The critical slip circle always passes through areas with relatively low soil properties, which means that the failure mechanism tends to find weaker areas on slopes.

- For RF-MCS method, P_f increased with finer meshes which is opposite to RFEM (probability of failure decreased with smaller random field mesh sizes). This increasing trend decreased by increasing the mesh density. This means that the calculated probability of failure will reach convergence by increasing the mesh density.

6.2 Recommendations

- Because sensitivity analysis has nothing to do with using different methods, it is recommended to combine the 3 MCS methods for future parameter study. RF-MCS method can produce more accurate results but direct MCS method is more efficient. When choosing to use one of these methods, additional attention is required.

- In the process of formulating the probabilistic LEM model, the basic deterministic model has been well verified by the commercial software D-Geo stability and the results given in the literature. However, the probability of failure calculated by the proposed RF-MCS method is different from the result given by (Cho, 2009) and (Jiang et al., 2015). Both authors used Karhunen-Loève Expansion combined with Latin hypercube sampling (LHS) to generate random fields. Instead, this study used Cholesky decomposition in combination with standard normal sampling in the process of random fields generation. In future research, more work can be done to find out the reasons for this difference.

- All the analyses have done in this study are based on a single-layered slope. Various failure mechanisms have been observed when the correlation between different potential slip circles is small. The deterministic critical failure surface approaches the probabilistic critical failure surface when the correlation between different potential slip circles is high enough. These findings can be further validated by extrapolated the single-layered slope model to a multi-layered slope.

- This study demonstrates the influence of spatial variability of soil properties on the probabilistic outcomes. Two types of slopes investigated in this study using all 3 methods, namely the undrained slope with only cohesion and the cohesive and frictional c-ϕ slope, show significantly different results. Another important soil parameter, unit weight γ, remained constant throughout the entire study. Therefore, the influence of spatial variability of unit weight γ can be investigated in future research. For example, the cross-correlated c-γ slope, the cross-correlated ϕ-γ slope and the extreme slope with only friction ϕ.

- All the analyses in this study are limited to the two-dimensional random fields. Although it has provided an in-depth understanding of the application of uncertainty in slope stability analysis, and has shown the importance of the spatial variability of soil properties in probabilistic analysis approach, a three-dimensional random fields would be preferable which can better characterise the soil properties in reality.

Bibliography

Ang, Alfredo H-S and Wilson H Tang (1984). "Probability concepts in engineering planning and design, vol. 2: Decision, risk, and reliability." In: *JOHN WILEY & SONS, INC., 605 THIRD AVE., NEW YORK, NY 10158, USA, 1984, 608*.

Bishop, Alan W (1955). "The use of the slip circle in the stability analysis of slopes". In: *Geotechnique* 5.1, pp. 7–17.

Bromhead, Eddie (1992). *The stability of slopes*. CRC Press.

Cao, Zijun, Yu Wang, and Dianqing Li (2017). *Probabilistic approaches for geotechnical site characterization and slope stability analysis*. Springer.

Cho, Sung Eun (2007). "Effects of spatial variability of soil properties on slope stability". In: *Engineering Geology* 92.3-4, pp. 97–109.

– (2009). "Probabilistic assessment of slope stability that considers the spatial variability of soil properties". In: *Journal of geotechnical and geoenvironmental engineering* 136.7, pp. 975–984.

Chowdhury, RN and DW Xu (1995). "Geotechnical system reliability of slopes". In: *Reliability Engineering & System Safety* 47.3, pp. 141–151.

Cornell, C Allin (1967). "Bounds on the reliability of structural systems". In: *Journal of the Structural Division* 93.1, pp. 171–200.

Fellenius, Wolmar (1936). "Calculation of stability of earth dam". In: *Transactions. 2nd Congress Large Dams, Washington, DC, 1936*. Vol. 4, pp. 445–462.

Fenton, Gordon A and DV Griffiths (2003). "Bearing-capacity prediction of spatially random c φ soils". In: *Canadian geotechnical journal* 40.1, pp. 54–65.

Griffiths, DV and Gordon A Fenton (2004). "Probabilistic slope stability analysis by finite elements". In: *Journal of Geotechnical and Geoenvironmental Engineering* 130.5, pp. 507–518.

Griffiths, DV, Jinsong Huang, and Gordon A Fenton (2009). "Influence of spatial variability on slope reliability using 2-D random fields". In: *Journal of geotechnical and geoenvironmental engineering* 135.10, pp. 1367–1378.

Hassan, Ahmed M and Thomas F Wolff (1999). "Search algorithm for minimum reliability index of earth slopes". In: *Journal of Geotechnical and Geoenvironmental Engineering* 125.4, pp. 301–308.

Javankhoshdel, Sina and Richard J Bathurst (2014). "Simplified probabilistic slope stability design charts for cohesive and cohesive-frictional (c-ϕ) soils". In: *Canadian Geotechnical Journal* 51.9, pp. 1033–1045.

Javankhoshdel, Sina, Ning Luo, and Richard J Bathurst (2017). "Probabilistic analysis of simple slopes with cohesive soil strength using RLEM and RFEM". In: *Georisk: Assessment and Management of Risk for Engineered Systems and Geohazards* 11.3, pp. 231–246.

Ji, Jian, HJ Liao, and Bak Kong Low (2012). "Modeling 2-D spatial variation in slope reliability analysis using interpolated autocorrelations". In: *Computers and Geotechnics* 40, pp. 135–146.

Jiang, Shui-Hua et al. (2015). "Efficient system reliability analysis of slope stability in spatially variable soils using Monte Carlo simulation". In: *Journal of Geotechnical and Geoenvironmental Engineering* 141.2, p. 04014096.

Jonkman, SN et al. (2015). "Probabilistic design: Risk and reliability analysis in civil engineering". In: *Lecture Notes CIE4130. Delft University of Technology*.

Kulhawy, Fred H (1993). "On the evaluation of static soil properties". In: *Stability and performance of slopes and embankments II*. ASCE, pp. 95–115.

Li, Chun-Ching and Armen Der Kiureghian (1993). "Optimal discretization of random fields". In: *Journal of engineering mechanics* 119.6, pp. 1136–1154.

Li, Dian-Qing et al. (2014). "Effect of spatially variable shear strength parameters with linearly increasing mean trend on reliability of infinite slopes". In: *Structural safety* 49, pp. 45–55.

Low, BK, S Lacasse, and F Nadim (2007). "Slope reliability analysis accounting for spatial variation". In: *Georisk* 1.4, pp. 177–189.

Phoon, Kok-Kwang and Fred H Kulhawy (1999). "Characterization of geotechnical variability". In: *Canadian geotechnical journal* 36.4, pp. 612–624.

El-Ramly, H, N R Morgenstern, and D M Cruden (June 2002). "Probabilistic slope stability analysis for practice". In: *Canadian Geotechnical Journal* 39.3, pp. 665–683. DOI: 10.1139/t02-034.

Sivakumar Babu, GL, Amit Srivastava, and D SN Murthy (2006). "Reliability analysis of the bearing capacity of a shallow foundation resting on cohesive soil". In: *Canadian Geotechnical Journal* 43.2, pp. 217–223.

Spencer, E (1967). "A method of analysis of the stability of embankments assuming parallel inter-slice forces". In: *Geotechnique* 17.1, pp. 11–26.

Sudret, Bruno and Armen Der Kiureghian (2000). *Stochastic finite element methods and reliability: a state-of-the-art report*. Department of Civil and Environmental Engineering, University of California ...

Taylor, Donald Wood (1937). "Stability of earth slopes". In: *J. Boston Soc. Civil Engineers* 24.3, pp. 197–247.

Van den Eijnden, AP and MA Hicks (2011). "Conditional simulation for characterizing the spatial variability of sand state". In: *Proc. 2nd Int. Symp. Comp. Geomech., Croatia*, pp. 288–296.

Vanmarcke, EH (1983). *Random fields: analysis and synthesis*.

Vanmarcke, Erik H (1977). "Probabilistic modeling of soil profiles". In: *Journal of the geotechnical engineering division* 103.11, pp. 1227–1246.

Appendix A

Appendix

In order to highlight the first main difference between RF-MCS and the direct MCS (mentioned in **??**), 4 different fixed slip circles are reanalysed by 3 MCS methods. The chosen slip circles are varying in the sliding length (For convenience' sake, 4 testing cases will be named as "very deep", "deep", "medium" and "shallow" circle according to their sliding length). 50,000 random fields have been generated for each single slip surface.

Figure A.1 shows the geometry of different slip circle and the convergence of probability of failure from 3 different methods. Table A.1 ∼ Table A.4 gives the corresponding analysis results. The last column k in the table indicate the relative difference of probability of failure P_f from different methods. It is calculated by the P_f from RF-MCS divided by the P_f from DS-MCS and DC-MCS.

Figure A.2 shows the value of P_f ratio with the varying sliding length. It can be observed the value of k1, k2 doesn't follow a linear relationship with the increasing sliding length. This can prove that the random field value is somehow "circle dependent".

In order to further demonstrate this phenomenon, the correlation matrix that is used to define the correlation relationship between the midpoint of each slice base are shown in Figure A.3. It can be clearly observed that the correlation matrix of DS-MCS and DC-MCS changed with the varying sliding length. This can further influence the random values (the cohesion value c here in this section) generated because the correlation matrix will be used in the Cholesky decomposition process.

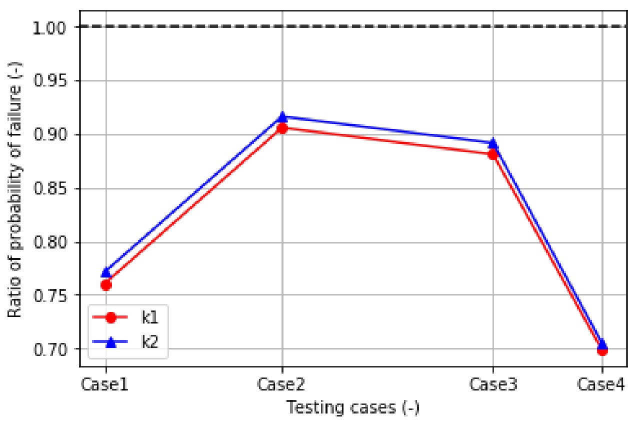

FIGURE A.2: P_f ratio from 3 methods with different sliding depth

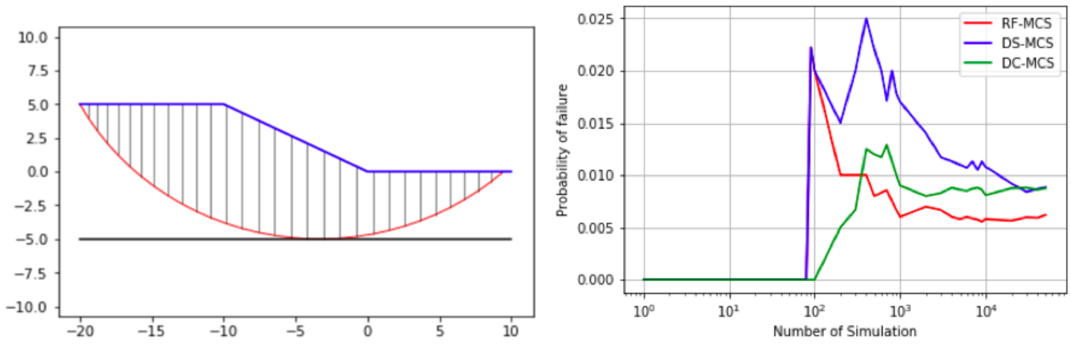

(Case4 (very deep circle): Sliding length = 34.48m)

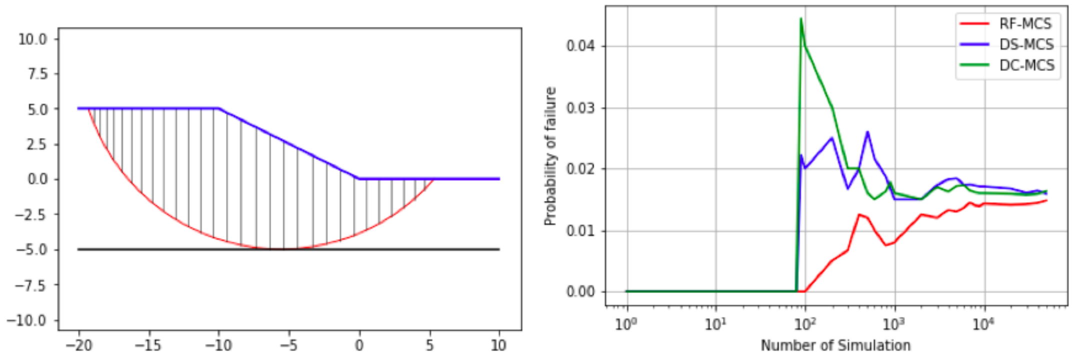

(Case3 (deep circle): Sliding length = 30.57m)

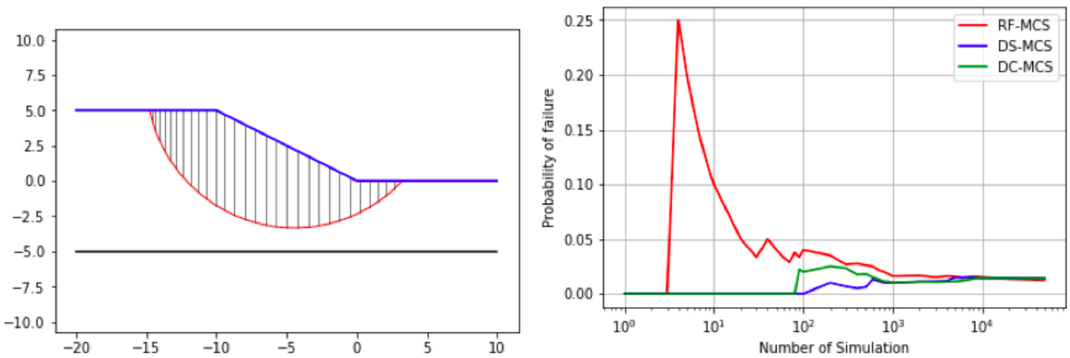

(Case2 (medium circle): Sliding length = 22.98m)

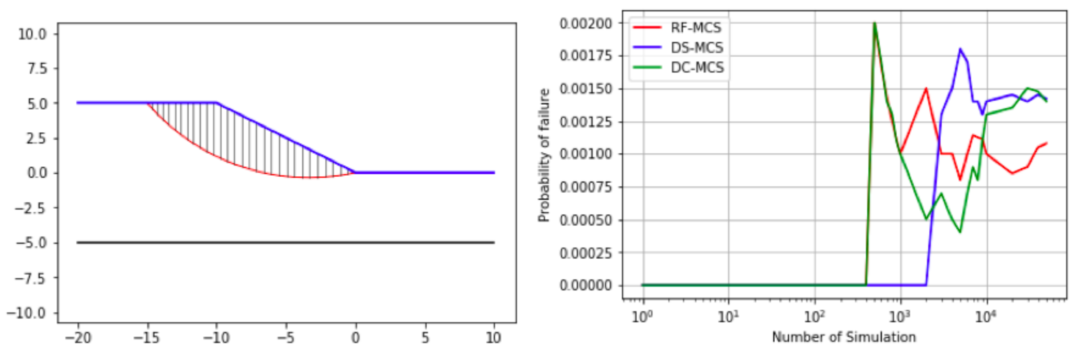

(Case1 (shallow circle): Sliding length = 16.60m)

FIGURE A.1: Slip circle geometry (left) and corresponding convergence of probability of failure (right)

Method	P_f(-)	$\mu_{FS_{min}}$	$\sigma_{FS_{min}}$	$COV_{FS_{min}}$	k(-)
RF-MCS (50,000)	6.2×10^{-3}	1.4616	0.2171	0.1486	-
DS-MCS (50,000)	8.84×10^{-3}	1.4635	0.2297	0.1569	1.43
DC-MCS (50,000)	8.76×10^{-3}	1.4639	0.2303	0.1573	1.42

TABLE A.1: Results of 3 different methods from fixed very deep failure circle

Method	P_f(-)	$\mu_{FS_{min}}$	$\sigma_{FS_{min}}$	$COV_{FS_{min}}$	k(-)
RF-MCS (50,000)	1.48×10^{-2}	1.4167	0.2203	0.1555	-
DS-MCS (50,000)	1.68×10^{-2}	1.4153	0.2264	0.1600	1.13
DC-MCS (50,000)	1.66×10^{-2}	1.4158	0.2271	0.1604	1.12

TABLE A.2: Results of 3 different methods from fixed deep failure circle

Method	P_f(-)	$\mu_{FS_{min}}$	$\sigma_{FS_{min}}$	$COV_{FS_{min}}$	k(-)
RF-MCS (50,000)	1.27×10^{-2}	1.4873	0.2590	0.1741	-
DS-MCS (50,000)	1.40×10^{-2}	1.4856	0.2595	0.1747	1.10
DC-MCS (50,000)	1.39×10^{-2}	1.4853	0.2614	0.1760	1.09

TABLE A.3: Results of 3 different methods from fixed medium failure circle

Method	P_f(-)	$\mu_{FS_{min}}$	$\sigma_{FS_{min}}$	$COV_{FS_{min}}$	k(-)
RF-MCS (50,000)	1.08×10^{-3}	1.8382	0.3585	0.1950	-
DS-MCS (50,000)	1.42×10^{-3}	1.8382	0.3655	0.1988	1.31
DC-MCS (50,000)	1.4×10^{-3}	1.8398	0.3663	0.1991	1.30

TABLE A.4: Results of 3 different methods from fixed shallow failure circle

For the RF-MCS, the random field is generated first and the correlation matrix keeps constant for all the potential slip circles since the absolute distance between the mesh points didn't change for each realisation. Figure A.4 shows the correlation matrix used in the RF-MCS which is different from that in the DS-MCS and DC-MCS.

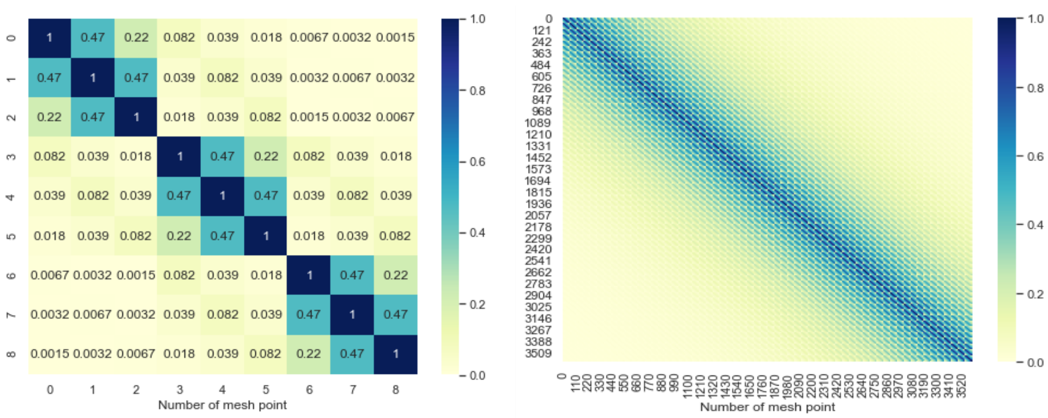

FIGURE A.4: Schematic visualization of the correlation matrix of RF-MCS; Number of mesh point 3×3 (left) and 60×60 (right)

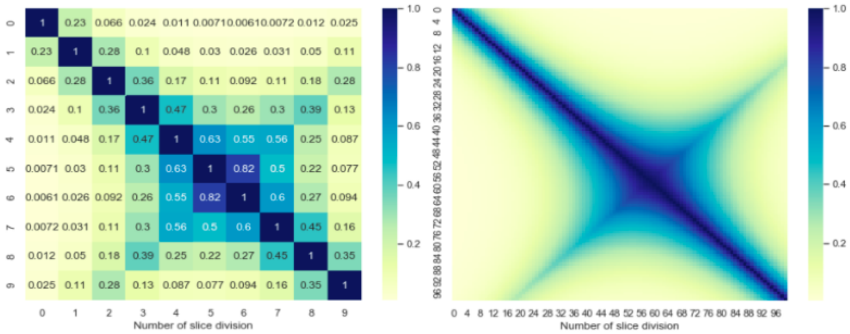

(Very deep: Sliding length = 34.48m)

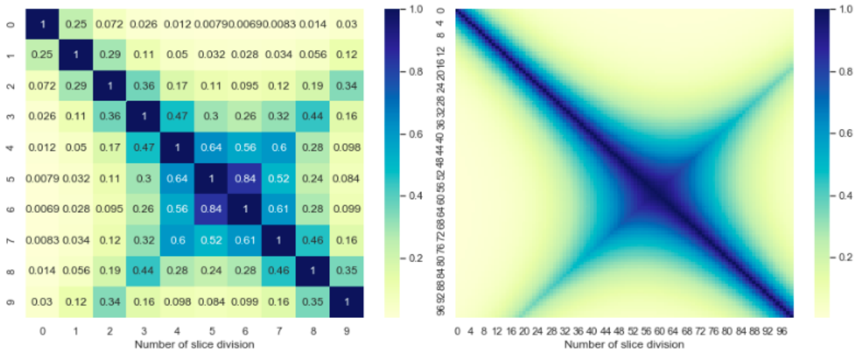

(Deep: Sliding length = 30.57m)

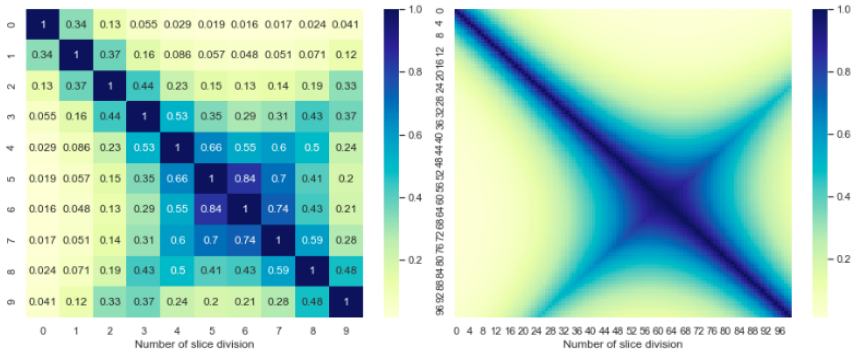

(Medium: Sliding length = 22.98m)

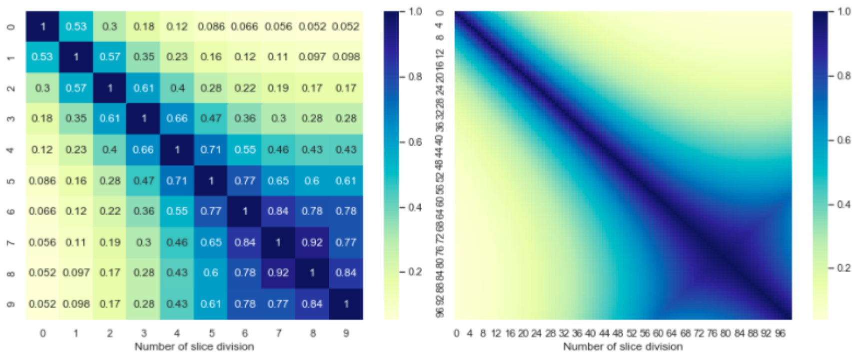

(Shallow: Sliding length = 16.60m)

FIGURE A.3: Schematic visualization of the correlation matrix of different slip circles; Number of slice division 9 (left) and 100 (right)